

Recirculating components to the deep boundary current of the northern North Atlantic

M.S. McCARTNEY

Woods Hole Oceanographic Institution, Woods Hole, MA 02543, USA

Abstract – The meridional overturning system of the North Atlantic is conventionally thought of as transporting warm water ($\theta \geq 4^\circ\text{C}$) to high latitudes and cold water to low latitudes. The northern cold water sources for this system are dense overflows from the Nordic Seas and less dense water from the Labrador Sea (LSW). The overflow components are carried westward by a deep northern boundary current (DNBC) that is shown here actually to begin southeast of the overflow regions. The DNBC lies along the southern side of a system of islands and submarine ridges that divides the Nordic Seas from the subpolar basins. The overflows act to increase the transport of the DNBC, and this transport is further increased through the entrainment of warm waters. Once inside the Labrador Sea, the DNBC is joined by LSW before continuing south to low latitudes as a cold, deep western boundary current (DWBC). However, published transport estimates are larger than can be explained by warm water entrainment alone, thus indicating entrainment also of recirculating cold components, the subject of this paper. Their sources are shown to be the LSW and cold abyssal waters originating from the southern hemisphere. The LSW is entrained downward into the denser part of the DNBC and laterally into the upper part of the DWBC, whereas the cold abyssal waters are supplied by an eastern-intensified northward flow in the eastern Atlantic (that serves as the initial source of the DNBC) and by a similar northward flow in the western Atlantic. The meridional overturning system described includes recirculations and poleward transports of cold water in addition to the components described by the conventional system. The cold abyssal waters in both the eastern and western basins have relatively low levels of oxygen and high concentrations of silicate reflecting their southern origin, but their influence in the northwestern Atlantic is somewhat obscured by strong recirculating cyclonic gyres in the Newfoundland and Labrador Basins. This influence is detected by a deep silicate maximum extending poleward from the mid-latitude western Atlantic through the two gyres with eastern concentration and recirculating back (diluted) toward the south in the DWBC within the respective basins. Such a maximum also extends northward through the Irminger Basin into the DNBC, but there is an ambiguity as to whether this is a direct extension of the signal from the south in the western basin, or if it comes from the mid-latitude eastern basin by way of westward flow through the Charlie-Gibbs Fracture Zone; it is perhaps a consequence of both. Estimates of the volume transports of the various recirculating cold components indicate that they supply about as much water to the deep boundary currents as do the combined cold water sources in the north.

CONTENTS

1.	Introduction	284
1.1	The motivation for this study	284
1.2	Paper outline	288
1.3	Comments on water mass terminology	290
1.4	A comment on inference of deep circulation from geological observations	291
2.	The Involvement of Labrador Sea Water in the Subpolar Circulation	291
2.1	Subpolar circulation schematics	291
2.2	Labrador Sea Water in the Deep Western Boundary Current	294
2.3	Labrador Sea Water in the Deep Northern Boundary Current	295
2.4	A new subpolar circulation schematic	298
3.	The Circulation of Mid-latitude Deep and Bottom Water in the Subpolar Basins	299
3.1	Eastern basin Antarctic Bottom Water and Lower Deep Water	318
3.1.1	The initiation of the Deep Northern Boundary Current in the eastern basin	318
3.1.2	Deep flow at mid-latitude	318
3.1.3	Deep flow in the Iberian and West European Basins	325
3.1.4	Quantification of the Deep Northern Boundary Current at the Rockall Plateau	330
3.1.5	Deep flow in the Iceland Basin	337
3.1.6	Deep flow at the Charlie-Gibbs Fracture Zone	344
3.2	Western basin Antarctic Bottom Water and Lower Deep Water	352
3.2.1	Silicate distribution in the Newfoundland, Labrador and Irminger Basins	352
3.2.2	Geostrophic shear in the Newfoundland and Labrador Basins	365
4.	Conclusions	376
5.	Acknowledgements	379
6.	References	379
7.	Appendix	383

1. INTRODUCTION

1.1 The motivation for this study

The dense overflows from the Nordic Seas¹ feed a dramatic Deep Northern Boundary Current (DNBC) along the system of ridges, subcontinents and islands that extends from the continental slope off Scotland and the Shetland Islands in the east to the coast of Labrador in the west as shown in Fig.1. The *Erika Dan* Expedition of 1962 produced particularly vivid images of the DNBC colorfully presented by WORTHINGTON and WRIGHT (1970). The DNBC turns southward at the coast of Labrador, and from there to the equator is conventionally referred to as a Deep Western Boundary Current (DWBC). The DWBC flow is accompanied by Labrador Sea Water (LSW, TALLEY and McCARTNEY, 1982), and the combined flow of dense overflow water and LSW is responsible for conveying polar and subpolar water mass characteristics to mid-latitudes.

Considerable efforts have been made for over thirty years to map and quantify the DNBC and DWBC at high latitudes. Early estimates of volume transport combined geostrophic shear with

¹For simplicity I adopt HURDLE's (1986) name "Nordic Seas" for the combined Iceland, Norwegian, Barents and Greenland Seas (instead of WORTHINGTON's (1970) somewhat ambiguous usage of Norwegian Sea for the same purpose). A second simplification will be the use of "subpolar basins" as a collective name for the basins south of the Nordic Seas: the Iceland, Irminger and Labrador Basins and the Rockall Trough.

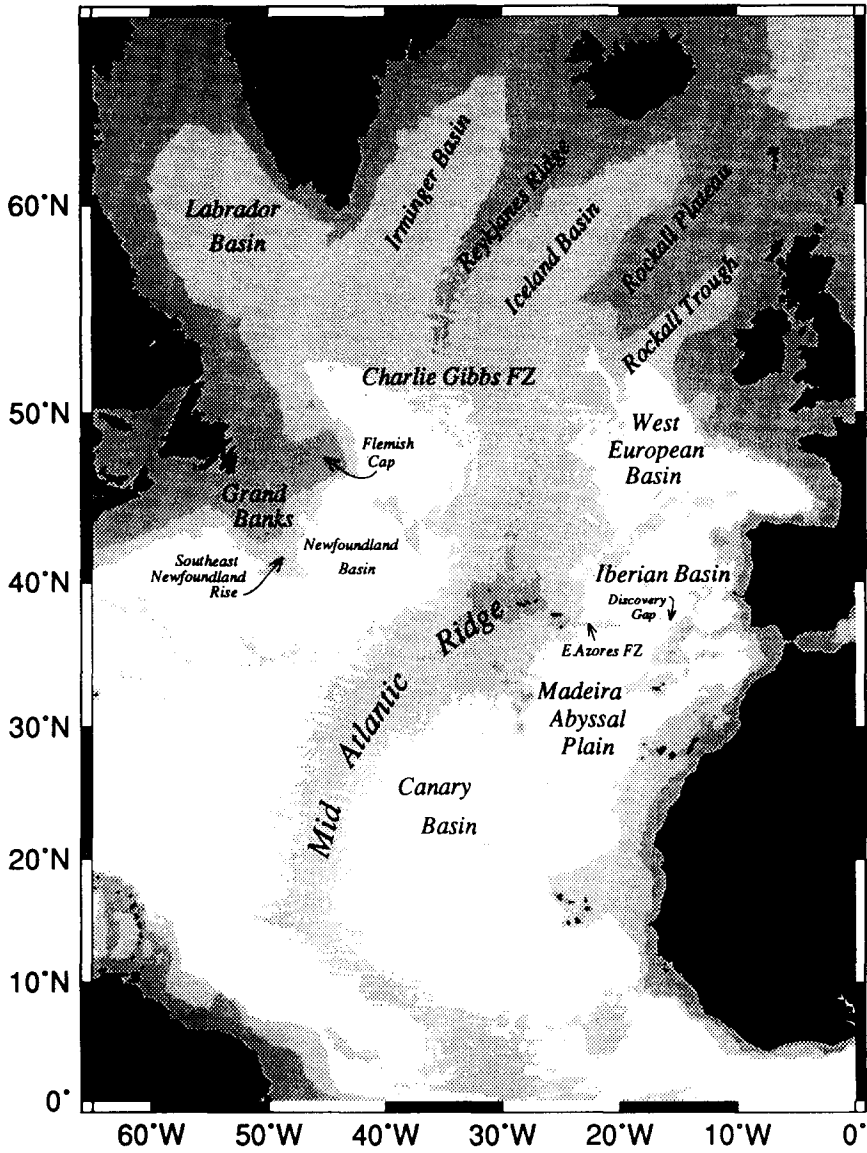


FIG. 1. Names of locations and principal bathymetric features referred to in this paper, bathymetric contours from "Etopo 5" data base obtained from the National Geophysical Data Center in 1989, with shading breaks indicating 4000m and 3000m.

reference level choices guided by water mass characteristics and Swallow float velocity determinations. In recent years the efforts have increasingly involved direct current measurements, and a clearer picture of the volume transport for specific flow elements is emerging. At this writing the latest image is from DICKSON, GMITROWICZ and WATSON (1990), repeated here as Fig.2. It includes transport measurements for the three primary overflows – through the Faroe Bank Channel, over the Iceland-Faroe Ridge, and through the Denmark Strait – and measurements of the transport of the resulting DNBC at two locations along the coast of Greenland. For the most part, the measurements summarized on Fig.2 are direct ones from current meter arrays, and represent robust results without some of the uncertainty that geostrophic estimates have (reference levels). The extensive array that yielded the $10.7 \times 10^6 \text{m}^3 \text{s}^{-1}$ estimate off eastern Greenland was reset (with some positioning differences), and the final long term average there has been recently computed by DICKSON (1991, personal communication) as $11.9 \times 10^6 \text{m}^3 \text{s}^{-1}$. Western boundary arrays at two locations between there and Denmark Strait yielded identical DNBC transports of only $5.0 \times 10^6 \text{m}^3 \text{s}^{-1}$, suggesting to Dickson that the DNBC loop around the Reykjanes Ridge into the northern Irminger Basin merges with the Denmark Strait overflow somewhat south of where it was placed on Fig.2. The measurements require explanation because the DNBC transports off southern Greenland are more than a factor of two larger than the sum of the overflows.

Part of the explanation for the largeness of the DNBC transports is the entrainment of warmer waters into the overflows, as discussed by WORTHINGTON (1970, 1976). This cannot be the whole explanation as is shown by the following calculation. The overflow temperatures² average 0°C , and therefore it transports zero heat (relative to 0°C). The DNBC average temperature is roughly 1°C . Mass conservation requires the overflows to have entrained $5.1 \times 10^6 \text{m}^3 \text{s}^{-1}$ (or $6.3 \times 10^6 \text{m}^3 \text{s}^{-1}$ using the final array transport) prior to reaching the location of the first measured DNBC transport along the east coast of Greenland, and an additional $2.6 \times 10^6 \text{m}^3 \text{s}^{-1}$ (or $1.4 \times 10^6 \text{m}^3 \text{s}^{-1}$ using the final array transport) by the time the DNBC reaches the south tip of Greenland. Heat conservation requires the corresponding mean temperatures of the entrained waters to be 2.1°C (or 1.84°C using the final array transport) and 1.73°C . If I have made a truly gross error in estimating the average temperature of the DNBC, and it is much warmer, say 2°C , the required entrained water temperatures increase to 4.2°C and 3.6°C . Even in this very extreme case, the temperatures barely qualify as “warm” entrainment. The large volume water mass of the thermocline in the immediate areas of the overflows is the Subpolar Mode Water (SPMW, McCARTNEY and TALLEY, 1982), and is warmer than 8°C for the eastern overflows, and warmer than 6°C in the area of the Denmark Strait. Only near southern Greenland does SPMW reach 4°C , with further cooling forming LSW near 3.5°C southwest of Greenland. The hydrography near the overflow sills is basically a two layer situation with the SPMW overlying the Norwegian Sea overflow waters (see Fig.3 of McCARTNEY and TALLEY, 1984, for examples). While entrainment from these warm waters is undoubtedly responsible for the initial modification of the overflows as they begin their descent from the overflow sills, the entrainment cannot be of warm water alone, otherwise the average temperature of DNBC would be warmer than observed. Hence colder components must also contribute to the downstream evolution of the DNBC transport and temperature, presumably entrained after the overflows have descended beneath the warm SPMW.

²All temperatures in this paper are potential temperatures.

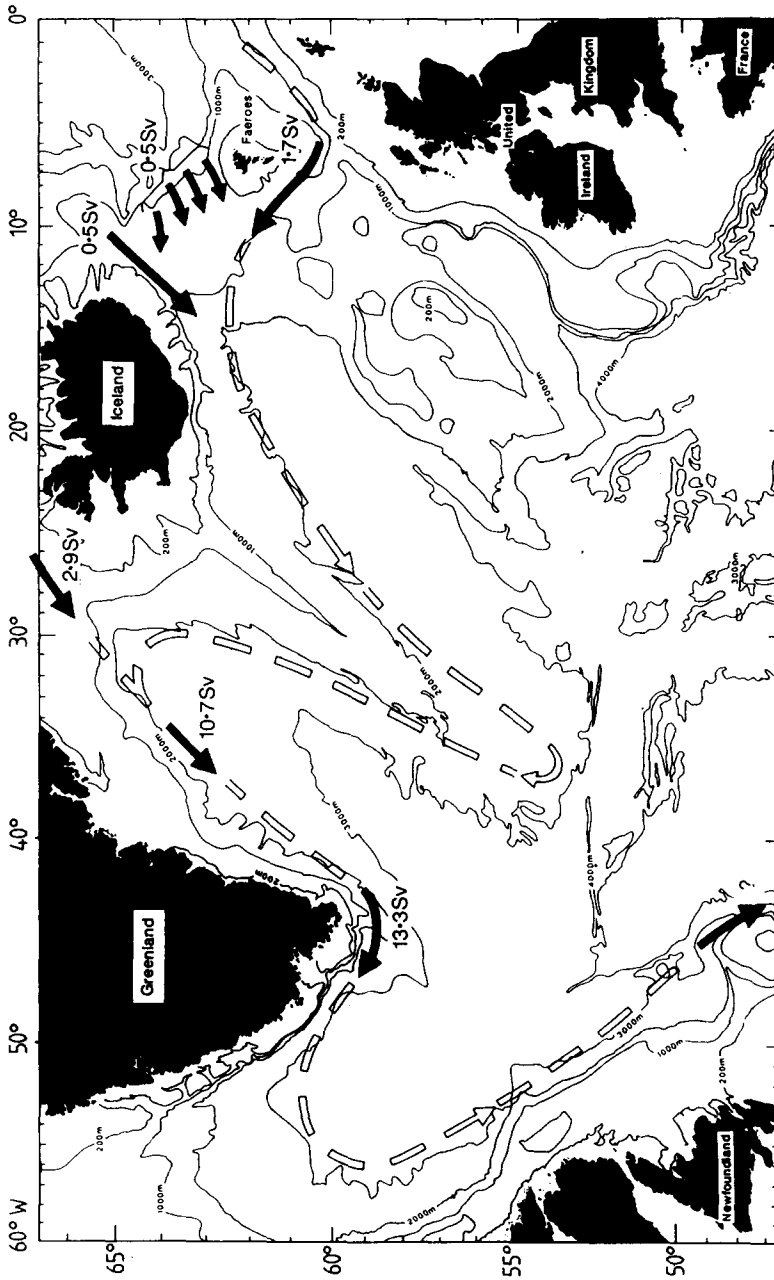


FIG. 2. The DICKSON, GMTROWICZ and WATSON (1990) schematic of the deep boundary current system of the northern North Atlantic Ocean. Numbers annotated by "Sv" are the volume transports in $10^6 \text{m}^3 \text{s}^{-1}$ of water denser than $\sigma_\theta = 27.8$. The $10.7 \times 10^6 \text{m}^3 \text{s}^{-1}$ is their own measurement; the other estimates are published measurements by: CLARKE (1984) at the south Cape of Greenland, ROSS (1984) at the Denmark Strait, MEINCKE (1983) at the Iceland-Faroe Ridge, and BORENÁS and LUNDBERG (1988) and SAUNDERS (1990) at the Faroe Bank Channel. Their chart is based on bathymetry from LAUGHTON and MONAHAN (1984).

1.2 Paper outline

I will discuss cold entrainment from two such deeper water masses in this paper on the basis of the sections located in Fig.3. In section 2 the circulation of LSW in the subpolar basins is described. It exhibits a cyclonic gyre circulation in which some of the southward transport of LSW in the DWBC in the Labrador Sea returns northward in the interior of the subpolar basins. The recirculating LSW impinges on the DNBC, and affects it in two ways. First, part of the northward flow of LSW is returned by the DNBC to the DWBC essentially unaltered in characteristics, a pure recirculation. Nonetheless, this recirculation may contribute to the large transport of the DNBC in Fig.2, for the core density of LSW into the DNBC is near $\sigma_\theta = 27.8$. Second, the remaining part of the northward flow of LSW into the DNBC is entrained into the dense overflows, contributing to the downstream evolution of the dense water component of the DNBC, as well as increasing the transport of that component.

In section 3 a northward flow of Antarctic Bottom Water (AABW) and Lower Deep Water (LDW) from mid-latitudes into the subpolar basins is described. In the eastern basin this flows onto the northern boundary and, turning westward, initiates the westward flowing DNBC along the south flanks of the Rockall Trough and Plateau. The water involved is as warm as 2.2°C , and is lower in oxygen and salinity but higher in nutrients than the eastern basin's dense overflows. The transport of this southern originating element of the DNBC is estimated at $1.9 \times 10^6 \text{m}^3 \text{s}^{-1}$. The DNBC begins, therefore, not with the easternmost dense overflow from the Faroe Bank Channel as shown in Fig.2, but with the northward flow of deep water in the eastern basin impinging on the northern boundary and turning west. This water of southern origin flows into the Iceland Basin and merges with the Faroe Bank Channel and Iceland-Faroe Ridge overflows; this combined DNBC flow loops around the Reykjanes Ridge to the Irminger Basin. In the eastern basin the northward flow of southern source waters is intensified to the east and traceable to as low a latitude as 32°N (SAUNDERS, 1987). South of there the northward flow is intensified along the east flank of the Mid-Atlantic Ridge which is the western boundary of the basin (McCARTNEY, BENNETT and WOODGATE-JONES, 1991). The mechanism causing this switch of boundaries is unknown; some ideas are discussed below.

In the western basin deep recirculation gyres associated with the Gulf Stream and the North Atlantic Current lead to meridionally sharp transitions from a strong to a dilute AABW characteristic. Dense overflow waters dominate the near bottom water north of 40°N in the western part of the western basin. A silicate maximum layer, with associated temperatures near 1.9°C derived from the AABW, penetrates north past Newfoundland into the Labrador Basin with eastern concentration; it recirculates into the DNBC and DWBC diluted with dense overflow waters. This layer is too dense to influence the eastern basin via the deepest passage through the Mid-Atlantic Ridge, the Charlie-Gibbs Fracture Zone (CGFZ), but may penetrate part way into the Irminger Basin. The strong deep shear of the recirculation gyres precludes meaningful estimation of the net northward transport of southern origin water in the western basin, as the net balance is a small difference between large opposing flows, and is very sensitive to reference level issues. A high-silicate layer intruding into the Irminger Basin at temperatures near 2.7°C is of ambiguous origin: it could come westward through the CGFZ as part of the southern originating contribution to the DNBC in the eastern basin or it could come from the northward flow in the western basin through the Labrador Basin just described. At this temperature, these two paths involve nearly indistinguishable water characteristics, thus the ambiguity.

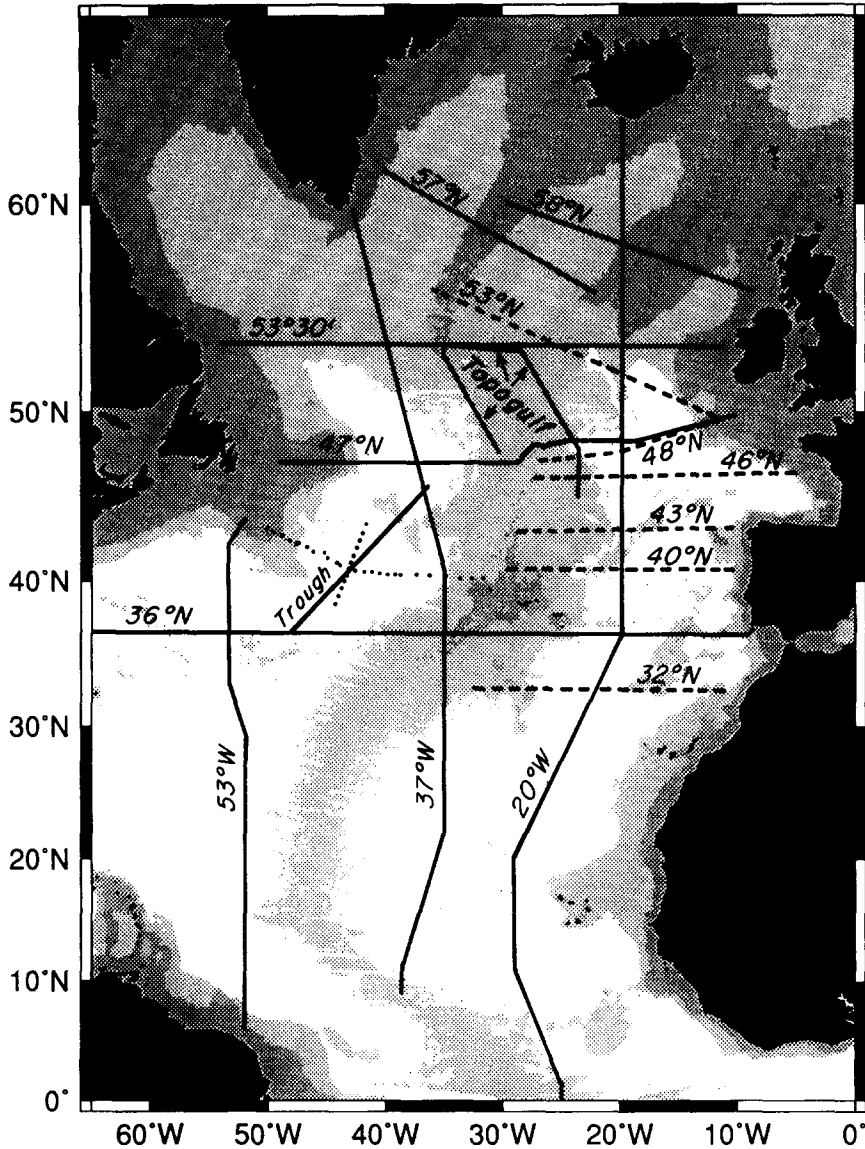


FIG.3. Locations of hydrographic sections superimposed on bathymetric contours of the North Atlantic from "Etopo 5" data base obtained from the National Geophysical Data Center in 1989, with shading breaks indicating 4000m and 3000m. The dashed sections are used in Fig.15. "Trough" is the section of Fig.23. "TOPOGULF" is the section of Fig.22. The dotted section pair are the sections of Figs 25 and 26.

1.3 Comments on water mass terminology

Terminology for abyssal water masses at mid-latitude in the North Atlantic is controversial. The dense overflows from the Nordic Seas and the dense waters crossing the equator from the South Atlantic are distinct and not in direct contact below about 1.8°C (WORTHINGTON and WRIGHT, 1970). I will follow the tradition of referring to the latter simply as Antarctic Bottom Water, even though the water crossing the equator is at a density value corresponding to the Circumpolar Deep Water, and, in fact, has a complex evolution along the western basin of the South Atlantic, with denser waters warming and upwelling into the density layer corresponding to the densest water at the equator. It is estimated (McCARTNEY, 1992; McCARTNEY and CURRY, 1992) that between 4 and 5 x 10⁶m³s⁻¹ of AABW crosses the equator in the western basin, and that of this net about 2 x 10⁶m³s⁻¹ diverts to the eastern basin through the Vema Fracture Zone near 11°N and continues north from there (McCARTNEY, BENNETT and WOODGATE-JONES, 1991). In both basins the AABW is a cold dense water of lower salinity, oxygen, and higher nutrient character than the northern dense overflows.

The AABW transport 4-5 x 10⁶m³s⁻¹ and the dense overflows' collective transport of 5-6 x 10⁶m³s⁻¹ (Fig.2) have nowhere to go but "up" – into the overlying lighter layers, and thus are a combined source totalling 9-11 x 10⁶m³s⁻¹ for deep water. The terminology problems are equally controversial for deep water. WRIGHT and WORTHINGTON (1970) used North Atlantic Deep Water (NADW) as a name for the high volume ridge (on volumetric θ -S diagrams) between 1.8°C and 4°C whose θ -S characteristics are common to all basins in their census. (They also have a useful review of the diverse nomenclature of this subject.) This NADW ridge is surrounded by the various water masses whose mixture must produce the high volume ridge: the overflow waters, the AABW, the Mediterranean water, the LSW, and the thermocline waters. The θ -S class in their census with the largest volume (per 0.1°C x 0.01 salinity) is the class 1.9°C-2°C and 34.89-34.90, near the cold end point of the NADW ridge, just warmer than the classes where the AABW and overflow waters are distinct.

McCARTNEY (1991) has examined the western basin circulation of the coldest NADW, 1.8°-2°C, and found that it is present as a transport mode in the mid-latitude DWBC from the Bahamas southward to the equator, and that it acquires its characteristics over the Sohm Abyssal Plain east of Bermuda by mixing of the net northward flow of AABW (colder than 1.8°C) with lighter waters recirculating in the deep anticyclone of the Gulf Stream recirculation. It is thus a mixture of AABW with waters brought to the Gulf Stream recirculation system by the DWBC north of that system (HOGG, PICKART, HENDRY and SMETHIE, 1986). In the eastern basin large contributions to the colder part of the NADW ridge are also indicated by the WRIGHT and WORTHINGTON (1970) basin census; this water represents the mixture of the eastern flow of AABW through the Vema Fracture Zone at 11°N with warmer water as it flows northward in the eastern basin. For both the eastern and western basins it seems misleading to continue to call this colder NADW component AABW. The southern source influence is apparent through the higher nutrients and lower salinity and oxygen in the colder NADW, but admixture of northern source water is necessary to give the observed characteristics. "Lower NADW" would be appropriate – but that has a specific prior usage dating from WÜST (1935). I have adopted the generic name Lower Deep Water (LDW) for the purposes of a shorthand notation (and not, hopefully, to add yet another name to the already too long name list relating to NADW!).

1.4 A comment on inference of deep circulation from geological observations

After the completion of this study, Ian McCave was kind enough to take it upon himself to inform and educate me about the vast literature on abyssal circulation inferred from various geological measurements. I cannot begin to do justice to this literature; McCave and Tucholke (1986) provide an overview that pulls together the diverse observations and produces a circulation scheme for the bottom currents of the North Atlantic. In particular, their scheme recognizes the eastern intensified northward flow of LDW in the eastern basin. However, it differs from the present scheme in that it has the eastward flow of AABW through the Vema Fracture Zone at 11° penetrating the eastern boundary and initiating the eastern intensified northward flow. It also has northern source water flowing southward to the Vema with western intensification in the eastern basin. Both these elements are contradicted by McCartney, Bennett and Woodgate-Jones (1991) and by the present study, in which Vema waters begin the northward flow with western intensification and only shift to eastern intensification north of 30°N . This flaw notwithstanding, the agreement between their bottom circulation inferred from sediment characteristics with the scheme developed in the present paper from hydrographic data is quite good. A particularly succinct and provocative summary of the northeastern North Atlantic from the geological based literature is from Lonsdale (1982):

“Rather than seeing the dominant feature of the region’s abyssal circulation to be the dispersal of Norwegian Sea Overflow, it may be more valid to consider a deep cyclonic circulation around the whole, complex margin of the northeastern Atlantic. The Overflow merely feeds and adds tracers to this circulation, a fundamental feature of the ocean’s dynamics that would probably exist even without any input of dense northern water (Ivers, 1975).”

Elsewhere in the same paper:

“There are other significant but less well understood flows, including northward currents that link into a generally cyclonic bottom circulation traceable around the entire basin margin from Biscay to the Charlie-Gibbs Fracture Zone.”

2. THE INVOLVEMENT OF LABRADOR SEA WATER IN THE SUBPOLAR CIRCULATION

2.1 Subpolar circulation schematics

Worthington (1970, 1976), who was involved in several of the early efforts in the region, twice reviewed the northern North Atlantic deep circulation system. His earlier study included a combined circulation and formation scheme, reproduced here as Fig. 4. The dense overflows occur at three locations: The Faroe Bank Channel (which connects to the Nordic Seas via the Faroe-Shetland Channel), the Iceland-Faroe Ridge, and the Denmark Strait. The DNBC (dashed contours) is indicated as beginning in the northeastern Iceland Basin with the confluence of the first two overflows, and is strongly steered by the Reykjanes Ridge before being joined by the Denmark Strait Overflow in the northeastern Irminger Basin; it then loops around Greenland and the northwestern Labrador Basin before turning south to become the DWBC. The numbers on the schematic are transports in $10^6\text{m}^3\text{s}^{-1}$, circled numbers indicate transports “measured” from geostrophic shear combined with Swallow Float based reference level velocities; the rest are indirect estimates from a regional box model. A fourth overflow, from the Faroe Bank Channel

to the Rockall Trough, occurs through a gap in the Wyville-Thomson Ridge (ELLETT and ROBERTS, 1973; SAUNDERS, 1990). It will not be included in the present treatment of the DNBC, as its impact in the Trough is on the warm water, about 4.5°C. A few remarks on this overflow are included in the Appendix.

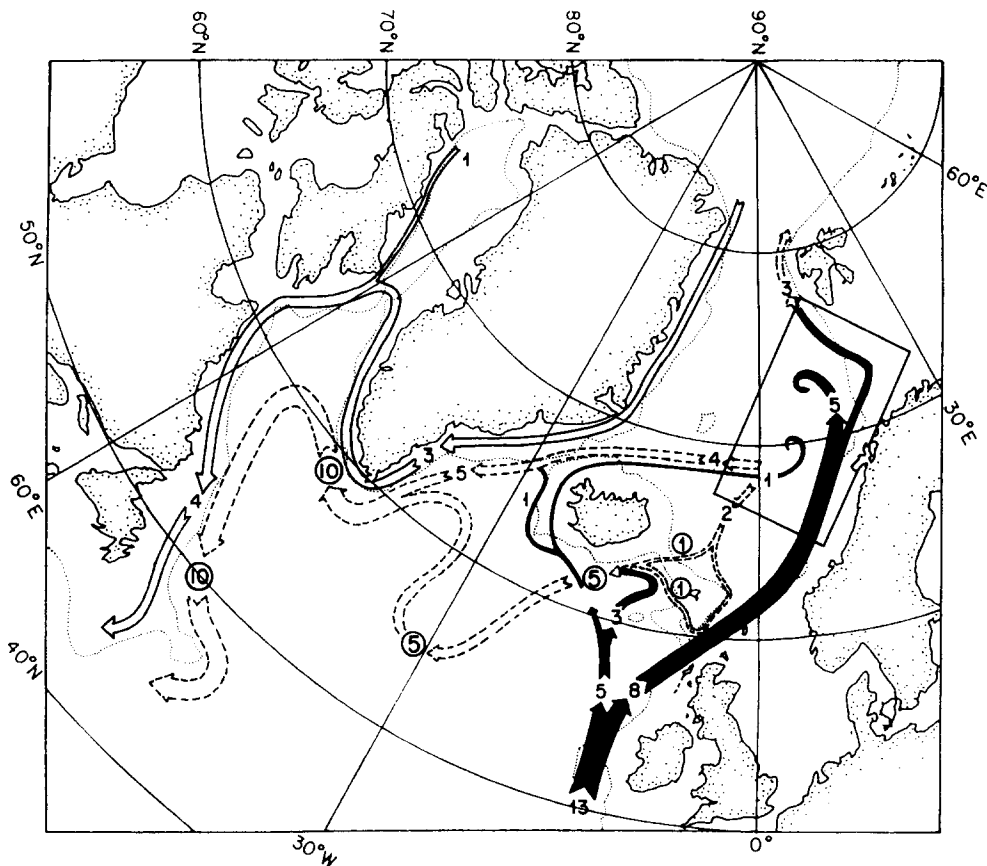


FIG.4. Water mass conversion paths (WORTHINGTON, 1970). Warm ($\theta > 4^{\circ}\text{C}$) currents are the black pathways, with the curved tips in the Norwegian Sea denoting sinking to form dense water. The unshaded pathways are cold but fresh and light waters that remain near the surface (East and West Greenland and Labrador Currents), while the dashed pathways are the dense overflows from the Norwegian Sea spilling over the sills at the Denmark Strait, the Iceland-Faroe Ridge, and the Faroe Bank Channel, and their subsequent circulation pathways as a DNBC transitioning to a DWBC in the Labrador Basin. Warm entrainment is indicated downstream of the overflow sills. The DNBC southward loop at 30°W is induced by the Reykjanes Ridge extending southwest from Iceland, the DNBC passing to the western basin through the CGFZ. Numbers are volume transport estimates in $10^6\text{m}^3\text{s}^{-1}$ of water colder than 4°C , without circles indicating indirect (mass balance) estimates, with circles indicating geostrophic estimates supported by short term Swallow float tracking.

WORTHINGTON (1970, 1976) recognized that entrainment of mass into the DNBC was needed to achieve consistency of the transport estimates and to allow the observed downstream evolution of the water mass characteristics. The need is most evident south of Iceland where the STEELE, BARRETT and WORTHINGTON (1962) measurements indicate the DNBC to have more than

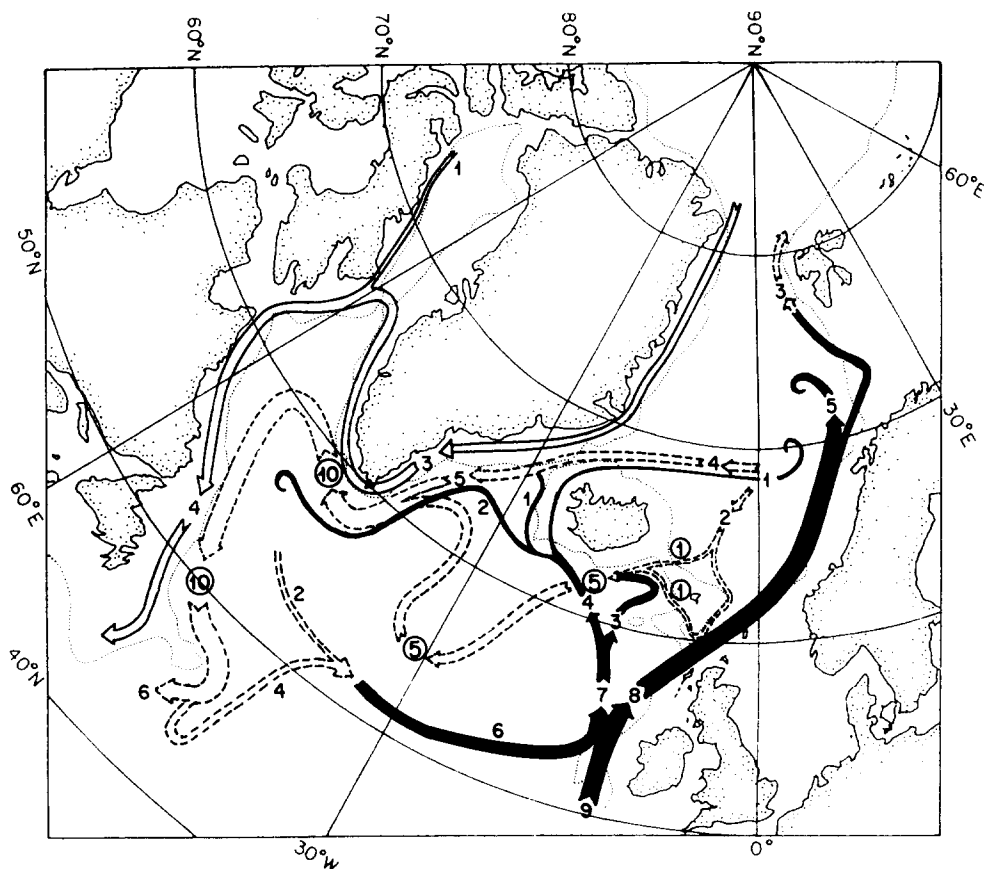


FIG.5. As Fig.4, with modifications inferred from the discussion by WORTHINGTON (1976). From McCARTNEY and TALLEY (1984).

doubled its transport relative to the nearby overflows. At that time the Denmark Strait Overflow had not been quantified, so WORTHINGTON (1969) estimated it at $4 \times 10^6 \text{ m}^3 \text{ s}^{-1}$ and assumed an entrainment there of $1 \times 10^6 \text{ m}^3 \text{ s}^{-1}$ to explain its downstream evolution of characteristics (MANN, 1969) and to account for the increase in DNBC transport from $5 \times 10^6 \text{ m}^3 \text{ s}^{-1}$ at the Reykjanes Ridge to $10 \times 10^6 \text{ m}^3 \text{ s}^{-1}$ at the south tip of Greenland. Thus at the south tip of Greenland, the DNBC is indicated as being composed of a mixture of $6 \times 10^6 \text{ m}^3 \text{ s}^{-1}$ of cold dense overflow water (average temperature 1°C , but excluding cold but relatively fresh and light waters of the East Greenland Current that do not sink as part of the DNBC) and $4 \times 10^6 \text{ m}^3 \text{ s}^{-1}$ of entrained warmer waters.

WORTHINGTON's (1976) second review had a more mid-latitude emphasis, and did not directly update Fig.4. He discussed the elements of layer-to-layer water mass exchange he believed to be occurring in the North Atlantic. McCARTNEY and TALLEY (1984) combined his text and graphical materials to provide an updated Fig.4, which is reproduced as Fig.5. There are two changes from the earlier scheme; it adds a small amount of LSW production, $2 \times 10^6 \text{ m}^3 \text{ s}^{-1}$, which is presumed to recirculate in the subpolar basin and upwell back into the thermocline. Secondly a significant part of the $10 \times 10^6 \text{ m}^3 \text{ s}^{-1}$ DWBC transport is assumed to recirculate and upwell within the subpolar basin rather than to continue south to subtropical latitudes. This reduction in DWBC transport was

derived from an early SWALLOW and WORTHINGTON (1961) estimate of DWBC transport of $6 \times 10^6 \text{m}^3 \text{s}^{-1}$ south of the Gulf Stream, which suggested to Worthington that not all the $10 \times 10^6 \text{m}^3 \text{s}^{-1}$ estimated off the coast of Labrador continues into the slope water to cross under the Gulf Stream at Cape Hatteras.

The small LSW production and its complete confinement in the north derives from two ideas of WORTHINGTON (1976). First: his estimates of transports west of 35°W all, in effect, use the core of the LSW as a level-of-no-motion (WORTHINGTON and VOLKMANN, 1965; SWALLOW and WORTHINGTON, 1969), so there is little calculated residual LSW flow, and no need to incorporate a major LSW circulation element. This use of LSW as a level-of-no-motion was first questioned by IVERS (1975), and later TALLEY and McCARTNEY (1982) described active participation by LSW both in the subpolar gyre circulation and in DWBC. Second, the LSW in the area of Worthington's gyre, east of Newfoundland, was observed to be much lower in salinity and higher in oxygen than that in the Gulf Stream recirculation gyre. He took this contrast as reflecting a separation of the circulation between the two regions at the level of the LSW. This contrast in LSW between the two regions, documented from 1958-1962 data, was absent in the 1972 data used by CLARKE, HILL, REINIGER and WARREN (1980). LSW production and characteristics are known to have dramatically varied in the intervening years (TALLEY and McCARTNEY, 1982; LAZIER, 1980), so the degree of separateness of the gyre circulation at the LSW level remains uncertain.

2.2 Labrador Sea Water in the Deep Western Boundary Current

Aspects of the circulation of Deep Water at mid- and low-latitudes call into question the smallness of Worthington's estimate of LSW production. TALLEY and McCARTNEY (1982) found that a western intensified southward influence of LSW exists to as low a latitude as 17°N . It is hard to imagine this as anything else but a participation of the LSW in the DWBC. Various studies of meridional heat flux agree in representing the meridional overturning cell that underlies the net poleward flux of heat at mid-latitude as having net southward flow throughout the Deep Water to water at least as warm as 4°C , with an amplitude of order $15 \times 10^6 \text{m}^3 \text{s}^{-1}$ (BRYDEN and HALL, 1980; ROEMMICH, 1980; WUNSCH, 1980; HALL and BRYDEN, 1982; WUNSCH and GRANT, 1982). Thus, Worthington's scheme is restricted to too cold a level – and his net flow of $7 \times 10^6 \text{m}^3 \text{s}^{-1}$ is too small by a factor of two. A significant net production of LSW is a key omission in Worthington's scheme. The flow of warm water into the subpolar latitudes, its cyclonic flow in the subpolar gyre, and its conversion to LSW as described in McCARTNEY and TALLEY (1982) provide a closure to the system. These interpretations led to a third version of the subpolar circulation scheme, reproduced in Fig.6 (McCARTNEY and TALLEY, 1984). It includes a larger input of warm water to the subpolar gyre than WORTHINGTON (1970, 1976) envisaged, which in turn allows a larger westward flow of warm water to the Labrador Sea for conversion to LSW, which then participates in the southward flow of the DWBC. Using observed temperatures of the principal flow elements and estimated heat fluxes at the sea surface in a box model, they estimated LSW production to be $7 \times 10^6 \text{m}^3 \text{s}^{-1}$ for a total meridional overturning of $14 \times 10^6 \text{m}^3 \text{s}^{-1}$.

McCARTNEY and TALLEY (1984) did not include transport estimates on the geographic schematic, Fig.6. It shows the warm water pathways suggested by WORTHINGTON (1970) and McCARTNEY and TALLEY (1982), general locales of the warm-to-cold water formation in the Nordic and Labrador Seas (curly tips on warm water pathways), the courses of the DNBC and DWBC, and two sites where significant localized warm water entrainment is required to evolve the dense cold overflows rapidly from their very cold character at the Nordic Seas' exit sills to their more moderate temperatures a short distance downstream in the DNBC. But it does not

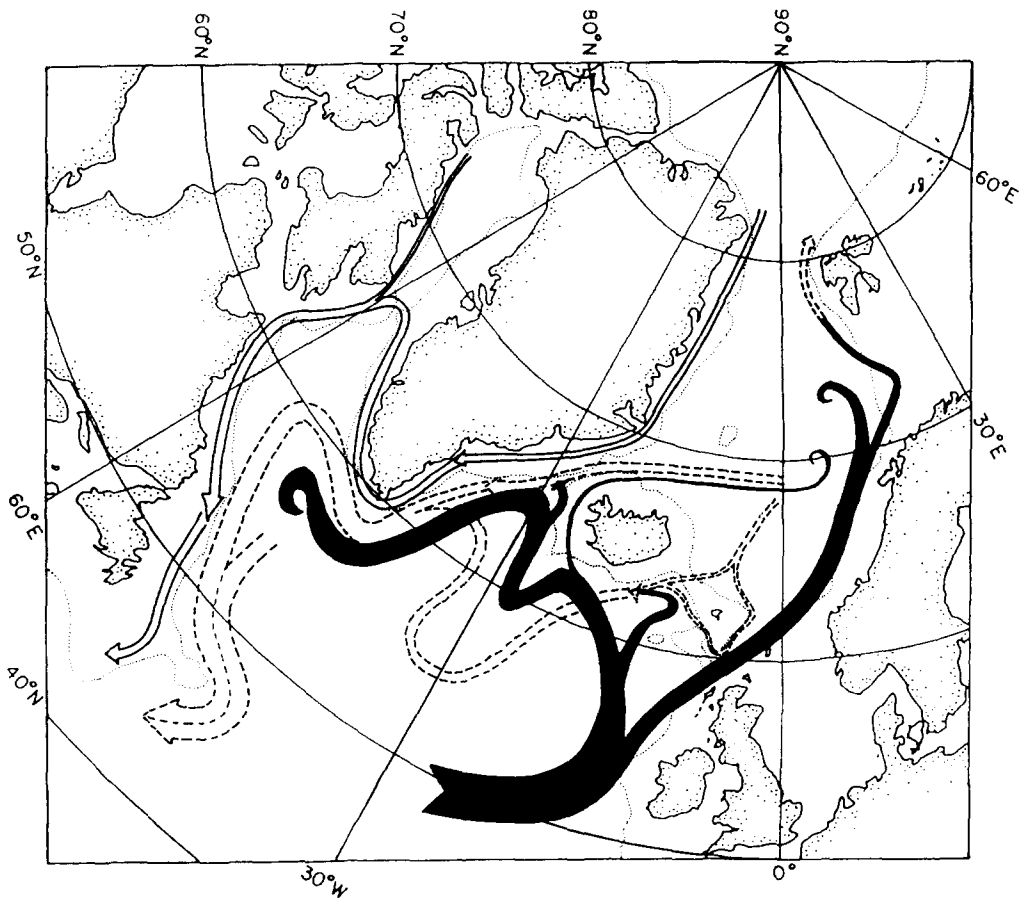


FIG.6. As Fig.4, with modifications suggested by the McCARTNEY and TALLEY (1982) and TALLEY and McCARTNEY (1982) description of Labrador Sea Water formation by cooling of cyclonically circulating warm water in the subpolar gyre. From McCARTNEY and TALLEY (1984).

include a schematic representation of any recirculating gyre component to the circulation of cold water, nor does it allow for some of the entrainment of water into the dense overflows being from such a recirculating component in the cold water, e.g. LSW. They did not realize the involvement of northward flow of LDW that is discussed below in Section 3. A new circulation schematic will be introduced below that rectifies some of these differences.

2.3 Labrador Sea Water in the Deep Northern Boundary Current

The possibility of entrainment from recirculating LSW into the dense overflows is examined in one of the special cases of a box model developed by McCARTNEY and TALLEY (1984, the "cold entrainment" case). Pure recirculations, in which the water moves without significant alterations or exchanges with other layers, need not be included in box models, heat flux calculations or consideration of the meridional overturning cell. But such flows are presumably included in a measurement of a DWBC or DNBC transport to an unknown degree – unless one measures across

an entire basin rather than just at the western boundary. McCARTNEY and TALLEY (1984) comment on the problem of such recirculations, noting that they play a prominent role in the STOMMEL and ARONS (1960) abyssal circulation theory. For example, in the latter authors' pie-shaped basin extending from the equator to the pole the DWBC transport near the pole is twice that of the polar source of dense water. A different factor would result for a basin with a lower latitude northern boundary. Thus the transports along the coast of Greenland in Fig.2, or the transports in Worthington's schemes, Figs 4 and 5, could include recirculating components and not reflect simply the net source strength (downwelling minus upwelling) north of that location. This is not the same thing as the entrainment of warm water into the DNBC shown in all three schematics. These represent downwelling from warm water to cold water, and mean that the net northern source of cold water is partly in the Nordic Seas and partly in the subpolar basins.

Charts of LSW characteristics (TALLEY and McCARTNEY, 1982) show evidence of recirculation of LSW within the subpolar basins. With the LSW source characteristics being low salinity and low potential vorticity, three primary paths away from the formation region in the Labrador Sea are noted, all deduced from tongues of LSW characteristics pointing away from the limited area of formation. These are the southward flow of the DWBC, eastward flow near 50°N (beneath and parallel to the eastward flow of the North Atlantic Current), and northeastward flow into the central Irminger Basin. These are evident in their potential vorticity chart, reproduced here as Fig.7. The second and third paths represent recirculations within the subpolar basin. The eastward flow bifurcates into northeastward flows into the Iceland Basin and Rockall Trough. Thus the LSW source supplies extrusions of young LSW extending northeast in each of the three deepest basins of the central and eastern subpolar North Atlantic. An interaction with deep waters occurs in each of these deep basins: with the Denmark Strait Overflow waters in the Irminger Basin, with the Faroe Bank Channel and Iceland-Faroe Ridge Overflows in the Iceland Basin, and with deep water in the Rockall Trough (to be discussed in the next section). These interactions are manifested by elevated LSW potential vorticity along the northwest side of each of the three basins (Fig.7). The LSW observations thus suggest that there is a recirculation of LSW within the subpolar basins, and that some part of that flow may be entrained into the dense overflows in the DNBC. There is no evidence for LSW passing over the sills into the Nordic Seas.

There are several aspects of the recirculation of LSW within the subpolar basins that affect the makeup of the DWBC. The interaction of the LSW with the dense overflows in the northeast means that some of the downstream modification of overflow waters, both in properties and in transport, is caused by entrainment of LSW rather than the warm water entrainment (warm and salty compared to LSW) explicit in the three circulation schemes. But the LSW is very much a mid-depth water mass in the northeast, and there can be no doubt that the initial evolution of the overflows, from the sills until the descending plumes reach the depth of the LSW, is wholly dominated by entrainment of warm water from the saline thermocline. There simply is no other water available to mix with initially. Where the water depth is less than 1200m at and downstream of the overflow sills, regional hydrography basically shows a two layer structure (TAIT, LEE, STEFANSSON and HERMAN, 1967; MÜLLER, MEINCKE and BECKER, 1979), with the thick layer of the local variety of Subpolar Mode Water (McCARTNEY and TALLEY, 1982) overlying the downstream evolving overflow waters.

Both the Faroe Bank Channel and Iceland-Faroe Ridge Overflows begin with very cold temperatures ($\leq 1.0^{\circ}\text{C}$) and with salinities near 34.9, but these overflows' interaction with warm thermocline water, principally SPMW, before they reach the depth range of the LSW, is so strong that the DNBC appears as a saline tongue $S \geq 35.0$ on subpolar basin property charts at and deeper than the depth range of the LSW (WORTHINGTON and WRIGHT, 1970, θ surfaces; IVERS, 1975,

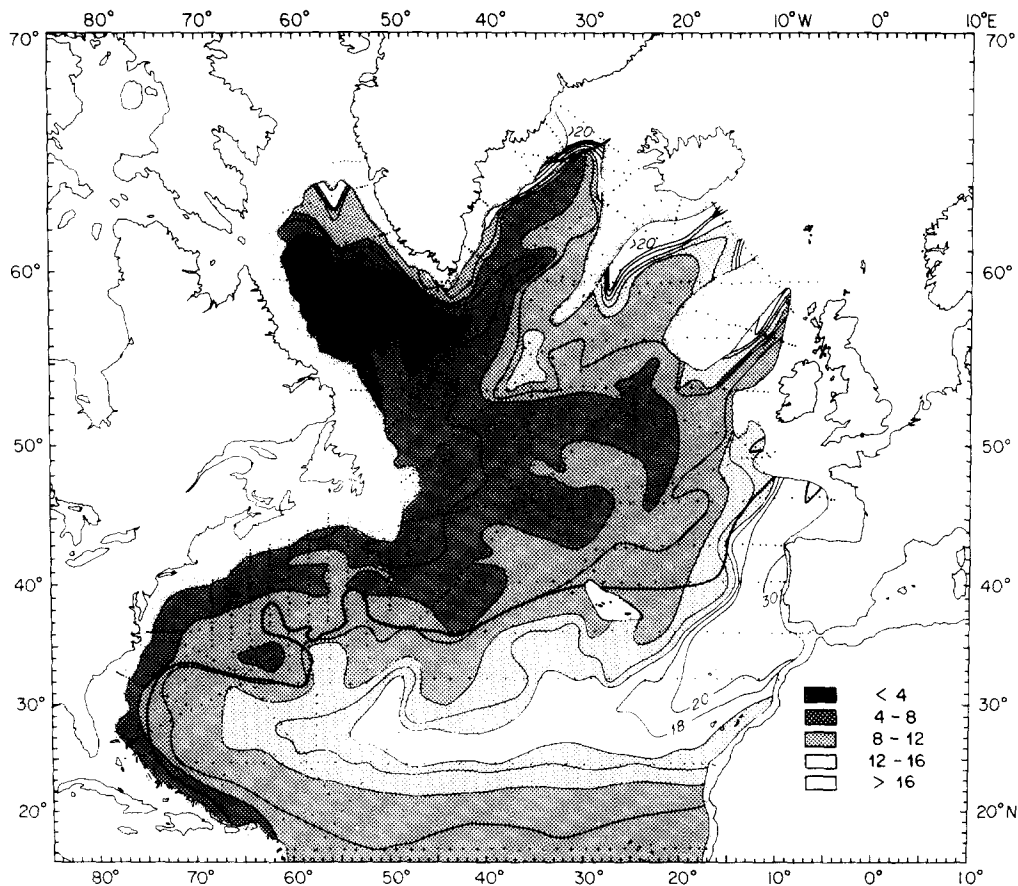


FIG. 7. Distribution of potential vorticity ($10^{-14}\text{cm}^{-1}\text{s}^{-1}$) at the core layer of the Labrador Sea Water, defined by the vertical minimum of potential vorticity, which is very nearly an isopycnal. The extra contour in the area of the Mediterranean outflow tongue marks the lateral limit of the potential vorticity minimum layer, and the contouring has been continued into the tongue on the same isopycnal as the Labrador Sea Water core. From TALLEY and McCARTNEY (1982).

neutral surfaces; SWIFT, 1984a, σ_2 surface; and HARVEY and THEODOROU, 1986, neutral surfaces). As the DNBC flows south along the eastern flank of the Reykjanes Ridge, the saline characteristic fades in intensity on these charts, which could reflect the admixture of LSW that flows northeast adjacent to the DNBC as well as denser deep water.

The situation for the Denmark Strait Overflow differs from that of the eastern Overflows. The charts of TALLEY and McCARTNEY (1982) show a more direct and stronger flow of LSW into the Irminger Basin than into the two eastern basins (Fig. 7). MANN's (1969) sections across the basin show the LSW at shallower levels than in the two eastern basins, so interaction between the LSW and the descending Overflow can occur over a larger depth range than for the eastern overflows. Near the Denmark Strait sill, these sections show a two layer structure similar to that in the two eastern basin overflows: the SPMW is somewhat colder (6.5°C versus 8.5°C compared to the overflow's temperature of $\leq 1^\circ\text{C}$) and fresher (35.15 versus 35.35 compared to the overflow's

salinity of about 34.92). The Denmark Strait Overflow does not gain salinity with its interaction with the warm water, either because of the smaller salinity difference or because it interacts more with the equally low-salinity LSW than with the warm water. By the time this Overflow reaches depths below the LSW, it appears as a fresh DNBC along the continental slope of east Greenland (western side of Irminger Basin) on TALLEY and McCARTNEY's property charts. This contrasts with the saline DNBC into which the eastern overflows evolve.

The other aspect of the involvement of the LSW with the DNBC is the pure recirculation of LSW. In hydrographic sections crossing the continental slope of Greenland (GRANT, 1968; MANN, 1969; WORTHINGTON and WRIGHT, 1970), LSW is observed sandwiched between the denser levels of the DNBC and the SPMW that is flowing to the Labrador Sea on a pathway similar to that of the DNBC in the western Irminger Sea and northern Labrador Sea. WORTHINGTON (1970, 1976) indicates the LSW in this three layer system to be a level-of-no-motion (with reversed shear above compared to below giving the same sign to the velocity of the upper and lower layers). IVERS (1975), on the other hand, shows all three strata moving in the same direction. His method anticipates that of REID (1986): a subjective determination is made station pair by station pair of the apparent flow direction based on tracer profiles and regional distributions, and combined with the observed shear distribution and overall mass balance for sections closed off by land. The IVERS (1975) treatment estimates larger dense water and SPMW transports in the DNBC than are derived from Worthington's level-of-no-motion – and of course there is also appreciable transport of LSW since it is no longer a level-of-no-motion.

PROVOST and SALMON (1986) illustrated their variational inverse method with an application to the 1966 C.S.S. *Hudson* data in the Labrador and southwestern Irminger Seas (GRANT, 1968). They gave results of a progression of inversions, with increasing dynamical constraints implemented. These support the Ivers flow pattern rather well. The CLARKE (1984) estimation of the flow field south of Greenland in 1978, of $13.3 \times 10^6 \text{ m}^3 \text{ s}^{-1}$ transport of water with $\sigma_\theta \geq 27.8$ on Fig. 2, included a velocity section showing maximum westward speeds in both the Subpolar Mode Water and dense overflow water exceeding 25 cm s^{-1} , and with a minimum speed less than 15 cm s^{-1} at the LSW layer. This is a geostrophic calculation referenced to current meters in the DNBC, but using traditional reference level arguments over part of the section. This distribution is remarkably similar to the estimated flow at the same location, from 1966 data, by IVERS (1975) and by PROVOST and SALMON (1986). Thus it appears that although the LSW is a level of minimum motion it is not one of no motion. The evidence of LSW participation in the flow of the DNBC is conclusive, such that LSW reaches $\sigma_\theta \geq 27.8$; the two DNBC transport estimates in Fig. 2 include transport of LSW that is recirculating back to the Labrador Sea, together with the dense overflow waters and water that has been entrained into them. CLARKE (personal communication, 1991) estimates that about $4.3 \times 10^6 \text{ m}^3 \text{ s}^{-1}$ of the $13.3 \times 10^6 \text{ m}^3 \text{ s}^{-1}$ DNBC transport south of Greenland is warmer than 3.0°C (but denser than $\sigma_\theta = 27.8$), and thus falls in the LSW layer ($3^\circ\text{-}4^\circ \text{C}$) of the present study.

2.4 A new subpolar circulation schematic

To recapitulate: in WORTHINGTON's (1970) original scheme (Fig. 4) the DNBC and DWBC transports are comprised of two elements: firstly the dense waters from the Nordic Seas spilling over the ridge system between Greenland and Scotland into the subpolar basins, and secondly warm waters from the thermocline that are entrained into the overflows. In his later scheme (Fig. 5), WORTHINGTON (1976) added a third component: a production of LSW (albeit small) joining the southward flow of the DWBC. This component does not continue to lower latitudes,

instead upwelling back into the warm water layer without recirculation interaction with the DNBC. The McCARTNEY and TALLEY (1984) scheme (Fig.6) increased the LSW component in the DWBC, to allow for a net LSW flow to lower latitudes, but did not include either a recirculating component of LSW, or entrainment of LSW into the dense overflow waters. The TALLEY and McCARTNEY (1982) LSW charts and the above discussion indicate two additional contributions the LSW may make to the DWBC and the DNBC. The boundary current transport can be larger by an amount that reflects the recirculating gyre component of the LSW circulation (with a compensating eastward and northward interior flow of LSW). There can be a "hidden" component of LSW in the DWBC: LSW entrained into the colder overflow waters, which increases the cold water transport and warms the temperature of the boundary current as does warm water entrainment, though less efficiently because of its lower temperature.

These considerations lead to a fourth version of the circulation schematic, shown in Fig.8. The single deep water layer ($\leq 4^{\circ}\text{C}$) of the older schematics is divided into a LSW layer (nominally between 3° - 4°C) and a lower NADW layer (nominally $\leq 3^{\circ}\text{C}$). The circulations of the resulting three layers are shown on separate charts, vertically offset in perspective view, and with the appropriate basin topography for each layer. The warm water circulation remains the same as in Fig.6; but to reduce the figure's complexity the superficial circulations of cold fresh light waters in the East and West Greenland and Labrador Currents are omitted. As before, left turning curved tips along the warm water path denote the entrainment of warm water into the descending dense overflows southeast and southwest of Iceland. The production of LSW is denoted by the curved tail between Greenland and Newfoundland in the warm layer, with the corresponding notched tail in the LSW layer denoting its arrival into that layer.

The LSW layer receives this net production of LSW and delivers part of it to mid-latitudes both as a component of the DWBC in the west, and also as a component of the subtropical anticyclone in the interior (eastward flow with the North Atlantic Current and subsequent southward flow in the subtropical gyre interior). The remainder of the net production is entrained from the interior circulation of LSW in the subpolar cyclone into the lower NADW layer. A recirculation of LSW is indicated by the closed loop of the LSW circulation: downward entrainment occurs along this loop, but some LSW returns to the Labrador Basin without descending into the lower NADW.

The lower NADW layer differs in two ways from WORTHINGTON's (1970) original (Fig.4). First is the entrainment of LSW into the dense overflows in addition to (and downstream of) the warm entrainments. Second, the southward flow in the DWBC across 50°N is partly balanced by a northward flow of LDW into the subpolar basin in the interior. In the eastern basin, this flow is concentrated along the eastern boundary and turns westward south of the Rockall Plateau to join the dense overflows in the Iceland Basin. Thus LDW from mid-latitudes is shown as flowing northwards into the northern boundary of the subpolar basin. The westward flow of the DNBC carries both northern source waters and these mid-latitude waters, both of which have been diluted by entrainment of warm water and LSW. The southward flow of dense water in the DWBC is thus larger than the combined overflows and entrained waters by the amount of northward flow of LDW in the interior, which represents a recirculating component to the overall boundary current system reminiscent of the recirculations first described in the STOMMEL and ARONS (1960) model for the abyssal circulation. Next, the evidence for this dense recirculation component is described.

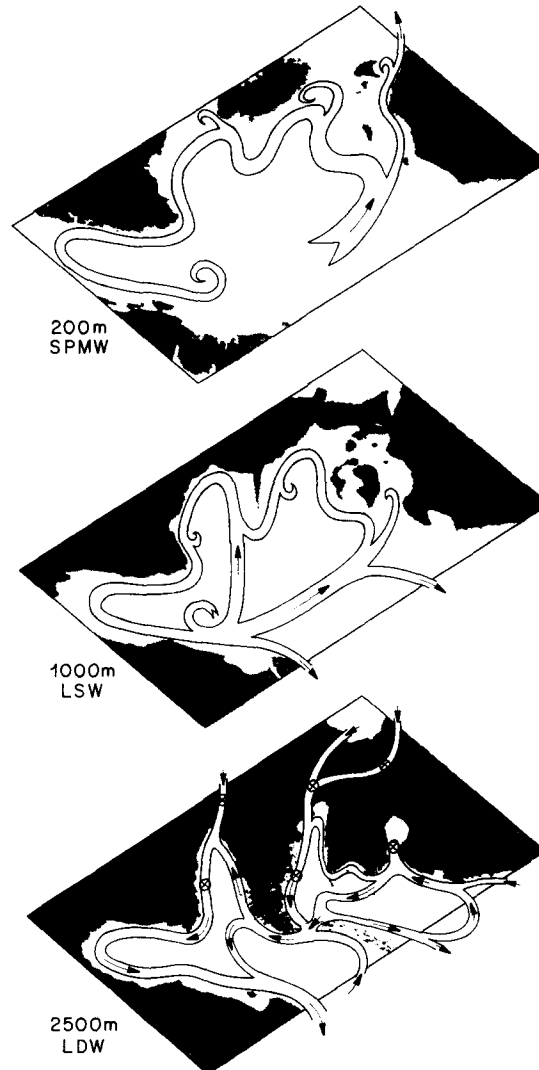


FIG.8. Circulation diagram combining that of Fig.6 with new elements introduced in the present paper, with three layers representing the total circulation. The warm water layer is dominated by the Subpolar Mode Water (SPMW, $\theta \geq 4^\circ\text{C}$), and is shown with the 200m isobath. Curved pointed tips show 3 sites for downward entrainment of SPMW into the lower deep water (LDW), and production of Labrador Sea Water (LSW). The LSW layer ($4^\circ\text{C} \geq \theta \geq 3^\circ\text{C}$) is shown with the 1000m isobath, and receives cooled SPMW in the Labrador Sea. The LSW layer includes a substantial cyclonic recirculation (as part of the subpolar gyre). Three sites for downward entrainment of LSW into the LDW are shown by curved pointed tips. The LDW layer ($\theta \leq 3^\circ\text{C}$) is shown with the 2500m isobath, with circled x's denoting the approximate sites of entrainment of SPMW and LSW from above. The DNBC and DWBC receive contributions from the dense overflows from the Nordic Seas, and, from the south, mid-latitude LDW derived from AABW, in addition to the entrained SPMW and LSW.

3. THE CIRCULATION OF MID-LATITUDE DEEP AND BOTTOM WATER IN THE SUBPOLAR BASINS

The influence of AABW on the deep water mass of the North Atlantic is perceived through its lower salinity and oxygen and higher silicate (WORTHINGTON and METCALF, 1961; METCALF, 1969; MANN, COOTE and GARNER, 1973) relative to the large volume of North Atlantic Deep Water which dominates the subthermocline water mass (WORTHINGTON and WRIGHT, 1970; WORTHINGTON, 1976), and particularly relative to the high salinity and very low silicate of the overflow waters. The AABW enters the North Atlantic crossing the equator into the western basin, where it spreads northwards in its interior (WÜST, 1933, 1935; WORTHINGTON and WRIGHT, 1970; MANTYLA and REID, 1983). The net AABW flow into the North Atlantic flow is estimated to be $4.5 \times 10^6 \text{ m}^3 \text{ s}^{-1}$ (McCARTNEY, 1992; McCARTNEY and CURRY, 1992). Figure 9 shows properties along a section³ near 53°W that follows the northward spreading route for the AABW between 20° and 30°N. At this longitude the strong AABW signatures, coldness, elevated silicate and high vertical gradients, weaken sharply at the southern edge of the deep Gulf Stream system which is shown as the deep isotherm bowl centered near station 280. In this same area, McCARTNEY (1991) has described the conversion of some of the AABW to LDW which then flows west with the deep Gulf Stream recirculation to the western boundary, where it joins the southward flow of the DWBC, contributing a transport mode at 1.9°C.

AABW flows from the western basin into the eastern basin through the Vema Fracture Zone at 11°N, and its influence extends northwards to about 30°N in the eastern basin as a western intensified flow against the eastern flank of the Mid-Atlantic Ridge (McCARTNEY, BENNETT and WOODGATE-JONES, 1991) and thereafter continuing northwards as an eastern intensified flow (SAUNDERS, 1987). Figure 10 shows properties along a section near 37°W that intersects the poleward flow of AABW. At mid-latitudes, as first illustrated by WÜST (1933), the AABW influence is stronger in the western basin than in the eastern basin. This can be seen by comparing the properties in the sections of Figs 9 and 10 as a function of latitude. In both sections the AABW is a cold high-silicate influence, but at a given latitude the western section shows the stronger influence. In both basins the most extreme AABW characteristics, at the bottom, fade northwards. The coldest AABW crossing the equator is about 0.6°C (McCARTNEY and CURRY, 1992) while at 25°N the coldest AABW is 1.60°C in the western basin (Fig.9) which approximately equals the temperature (1.66°C) of the coldest AABW immediately outside the Vema Fracture Zone at only 11°N in the eastern basins (Fig.10). At 25°N in the eastern basin the coldest water is 1.89°C, and has achieved the LDW definition discussed in the introduction.

The influence of the southern source (AABW) on the LDW is evident in Figs 9 and 10, keeping in mind that the two sections sample the regions that are dominated by the large volume classes of the WORTHINGTON and WRIGHT (1970) ridge, as discussed in the introduction. Farther north, the influence of the dense overflows can be seen. Figure 11 is a section through the western basin from southern Greenland to the Mid-Atlantic Ridge west of the Azores. The high silicate and low oxygen AABW influence is visible near the Ridge – but is much weaker than along the mid-latitude section at 53°W (Fig.9) and fades northward through the influence of the dense overflows.

³All sections in this paper are plotted with the same vertical distortion as the FUGLISTER (1960) Atlas: 500 to 1 (e.g. 200m depth equals 100km distance).

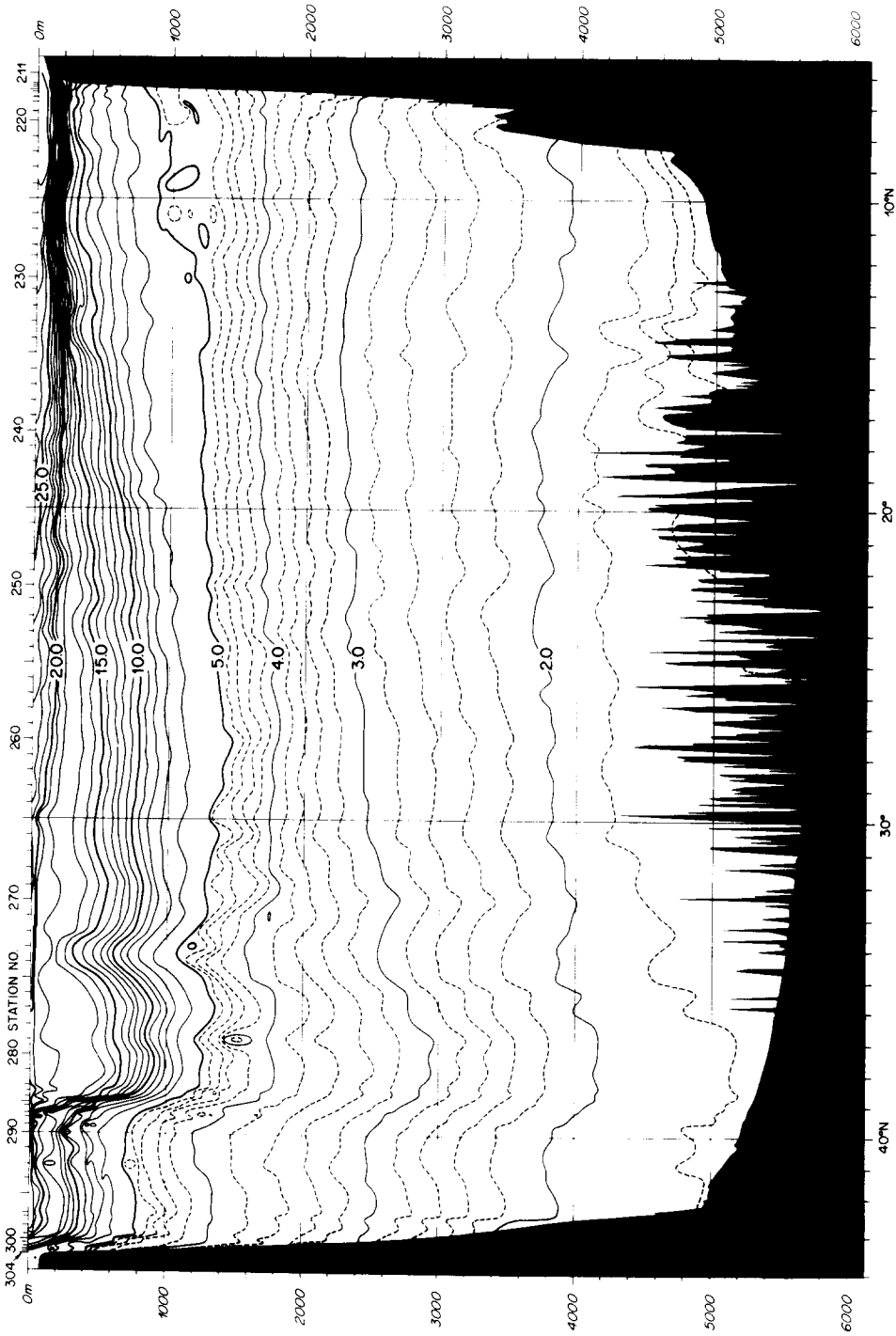


FIG.9a. Meridional section of potential temperature (°C) along the *Oceanus* 53°W transect (nominal longitude, see Fig. 3), April 1983. (KNAPP and STOMMEL, 1985).

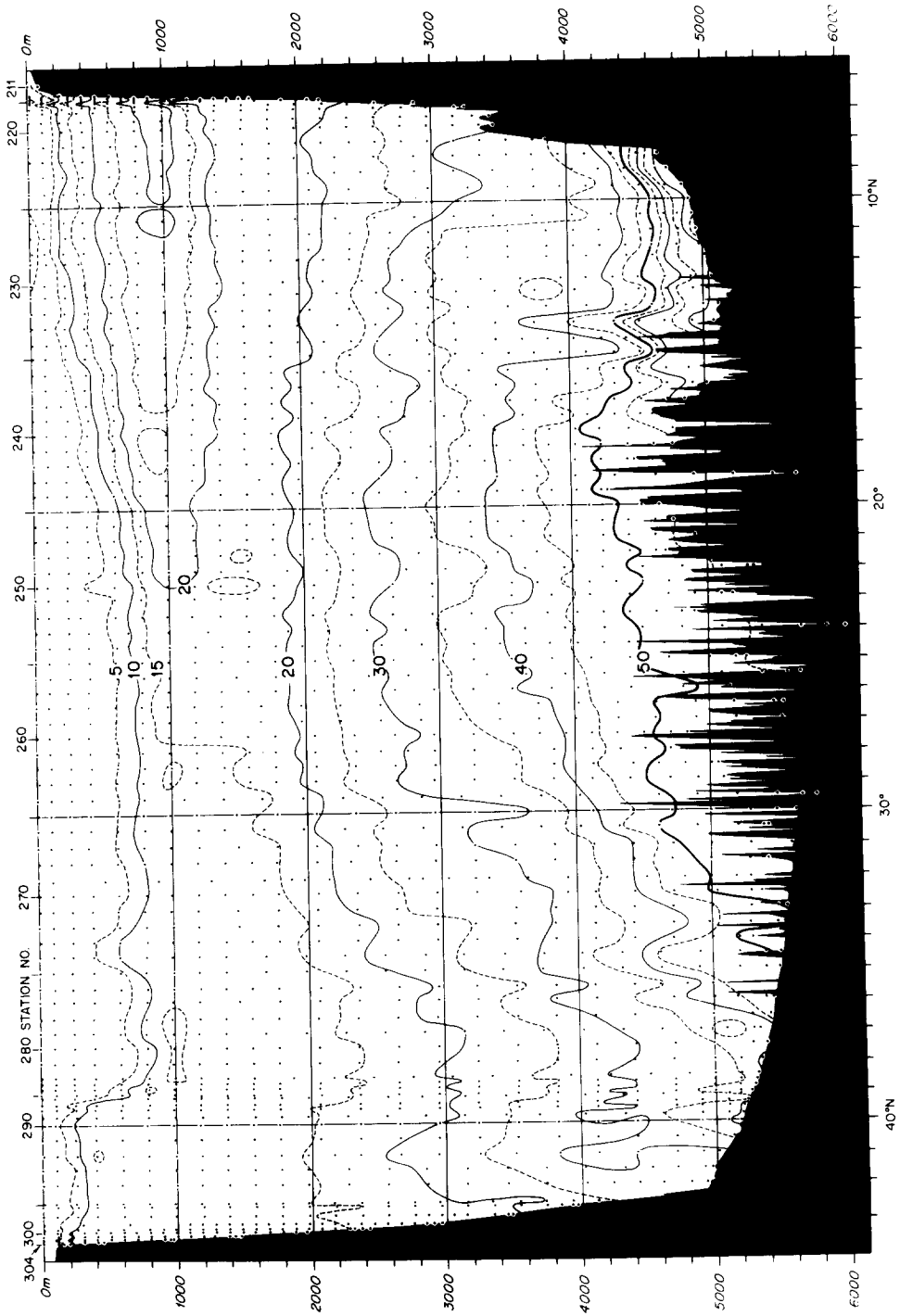


FIG.9b. Meridional section of silicate ($\mu\text{mol l}^{-1}$) at 53°W , as Fig.9a.

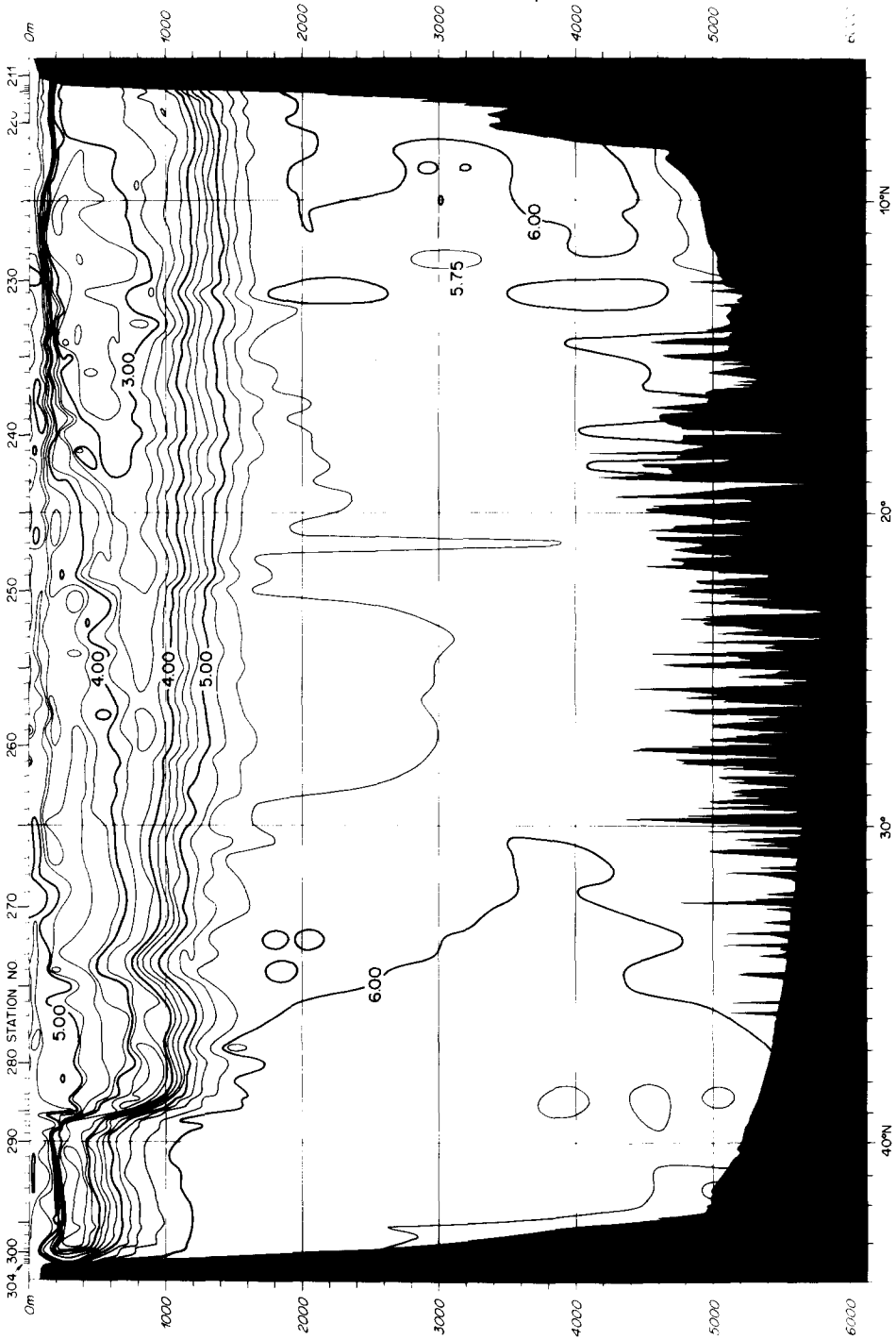


FIG.9c. Meridional section of oxygen (ml l⁻¹) at 53°W, as Fig.9a.

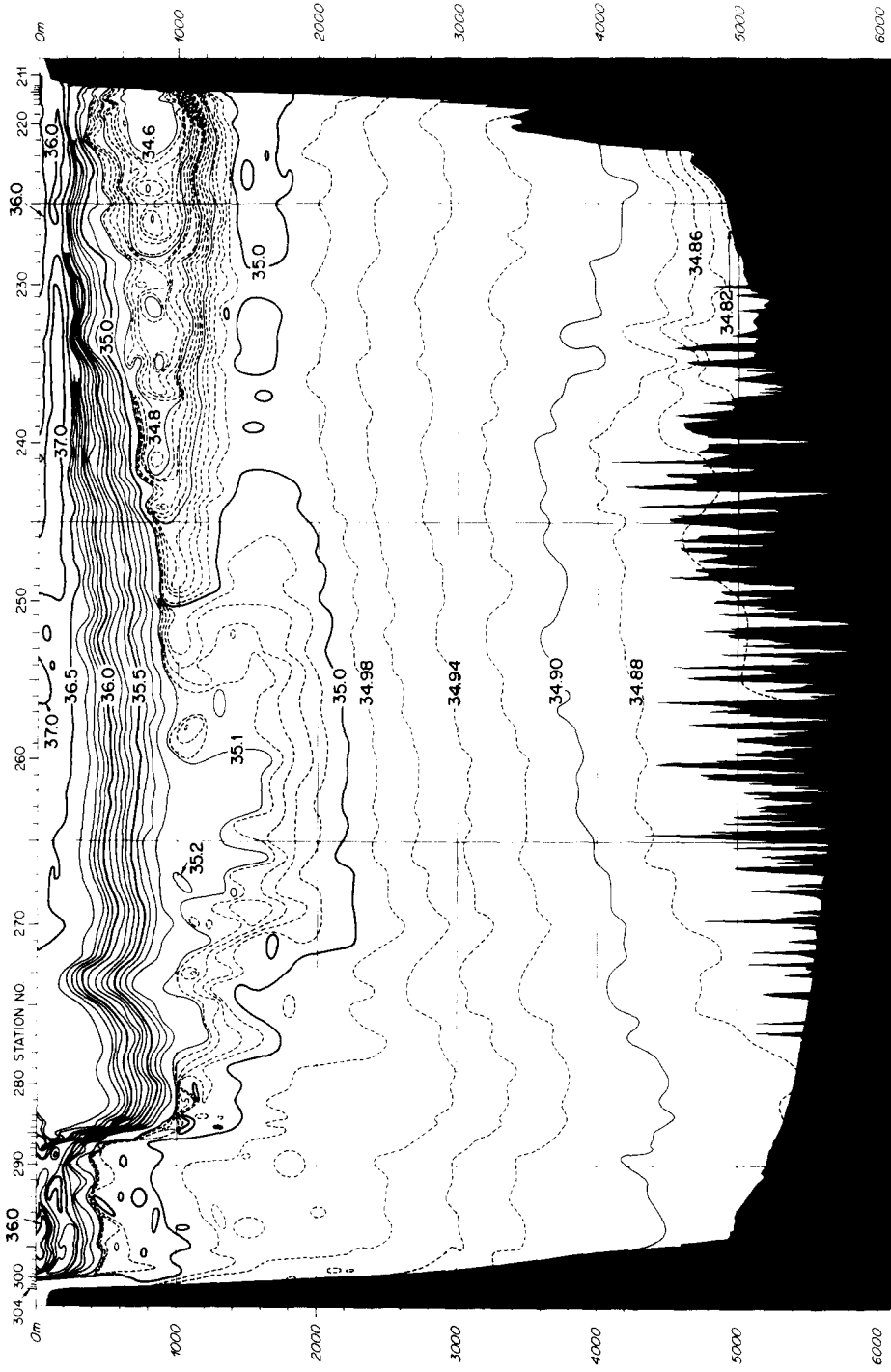


FIG.9d. Meridional section of salinity at 53°W, as Fig.9a.

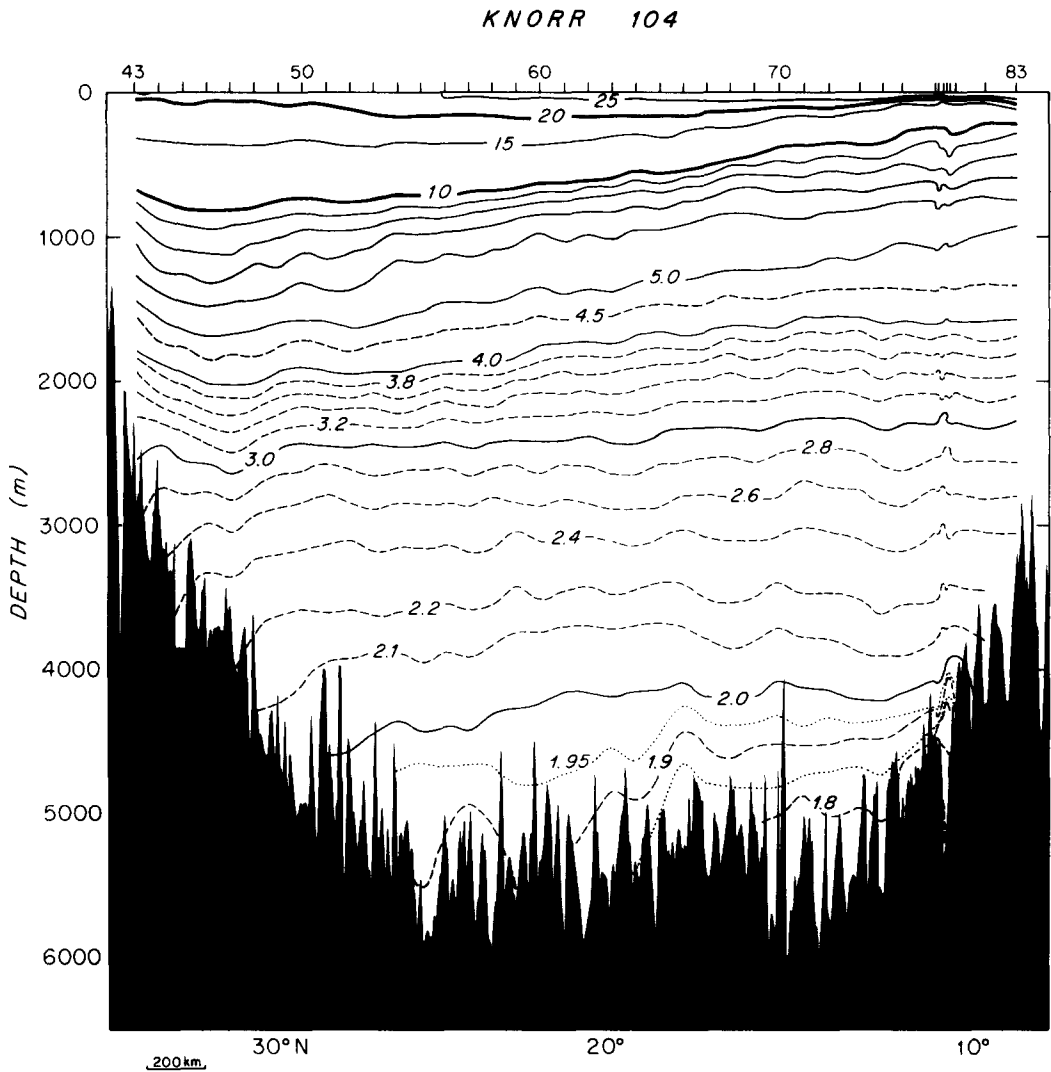


FIG.10a. Meridional section of potential temperature ($^{\circ}\text{C}$) along the low- and mid-latitude part of the *Knorr* 37°W transect (nominal longitude, see Fig.3) in August-September 1983 (McCARTNEY, BENNETT and WOODGATE-JONES, 1991).

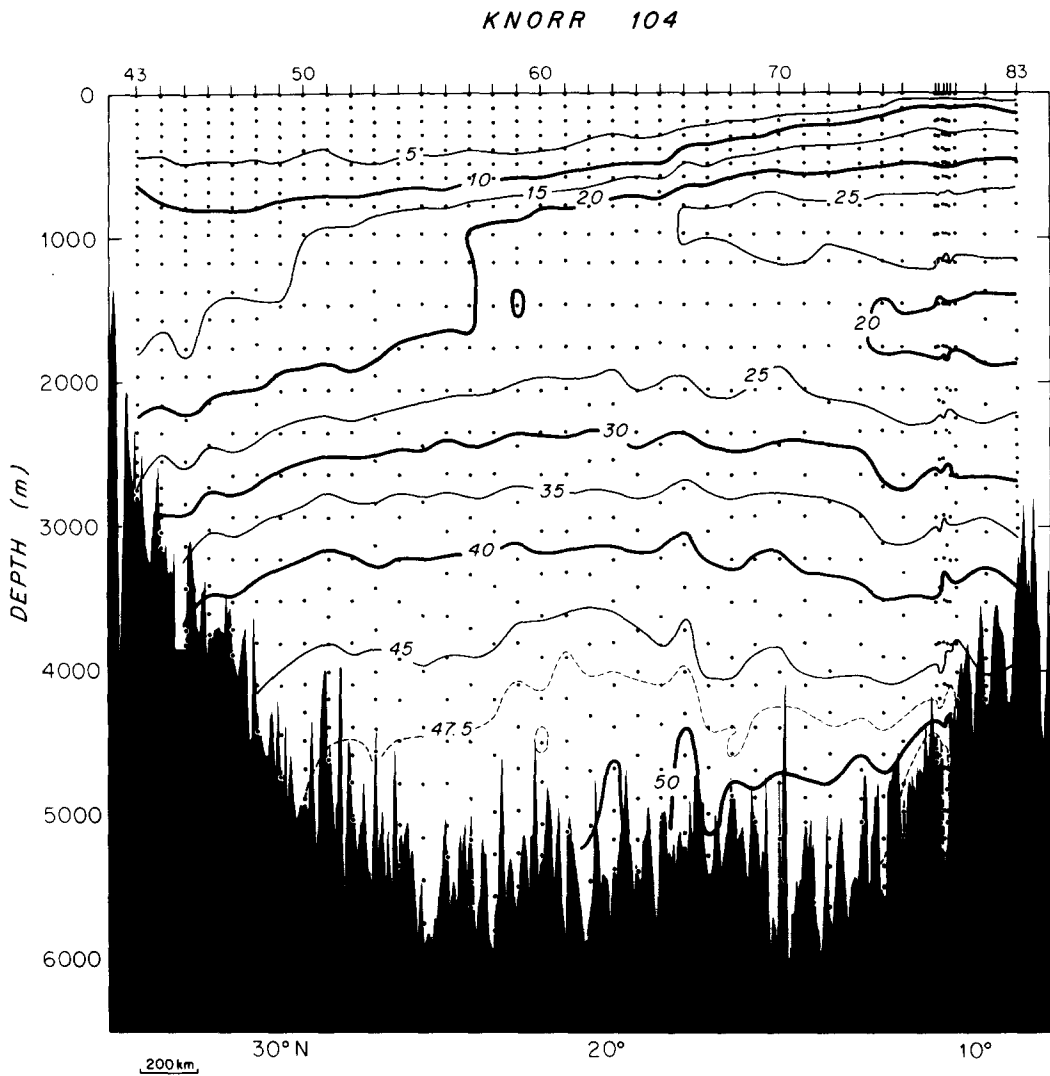


FIG.10b. Meridional section of silicate ($\mu\text{mol l}^{-1}$) at 37°W , as Fig.10a.

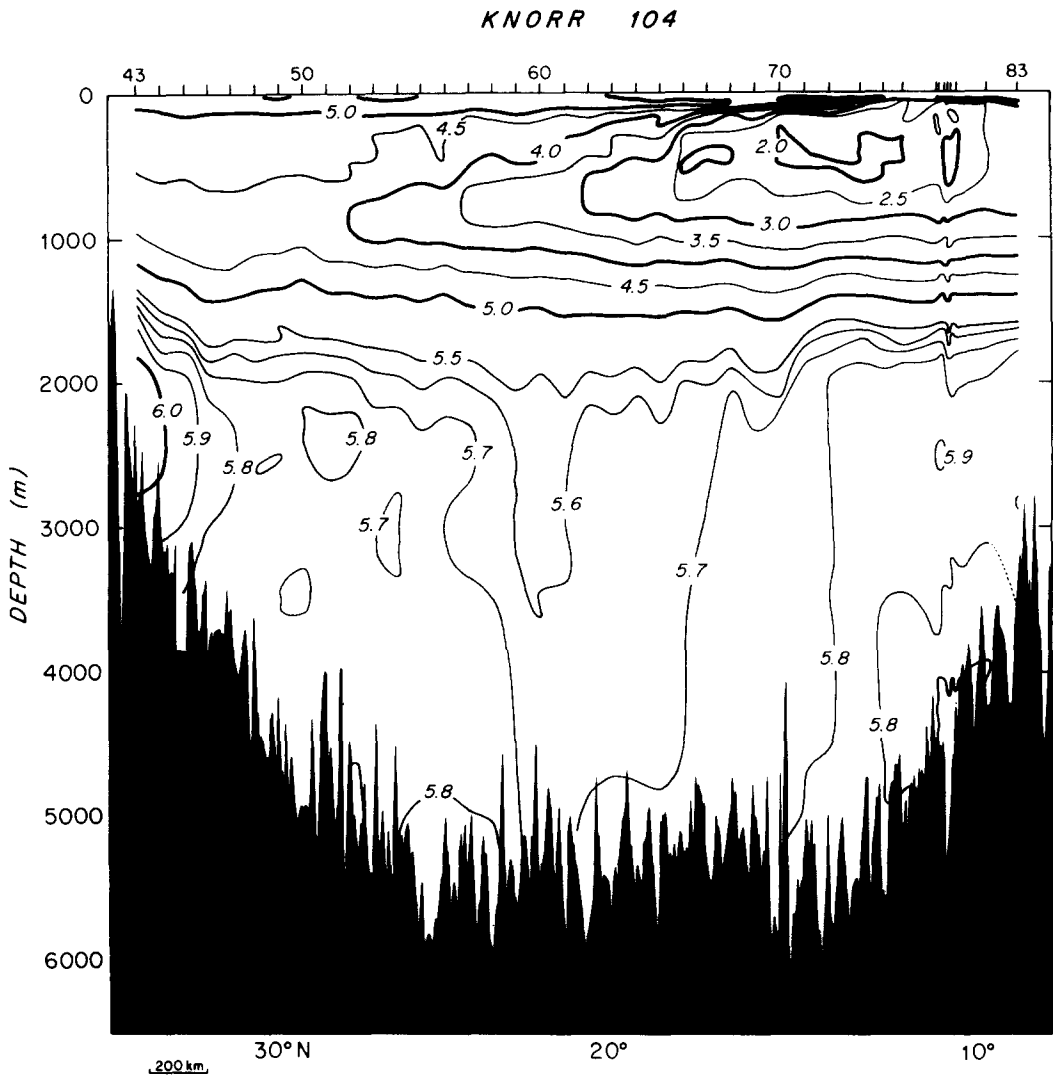


FIG.10c. Meridional section of oxygen (ml l⁻¹) at 37°W, as Fig.10a.

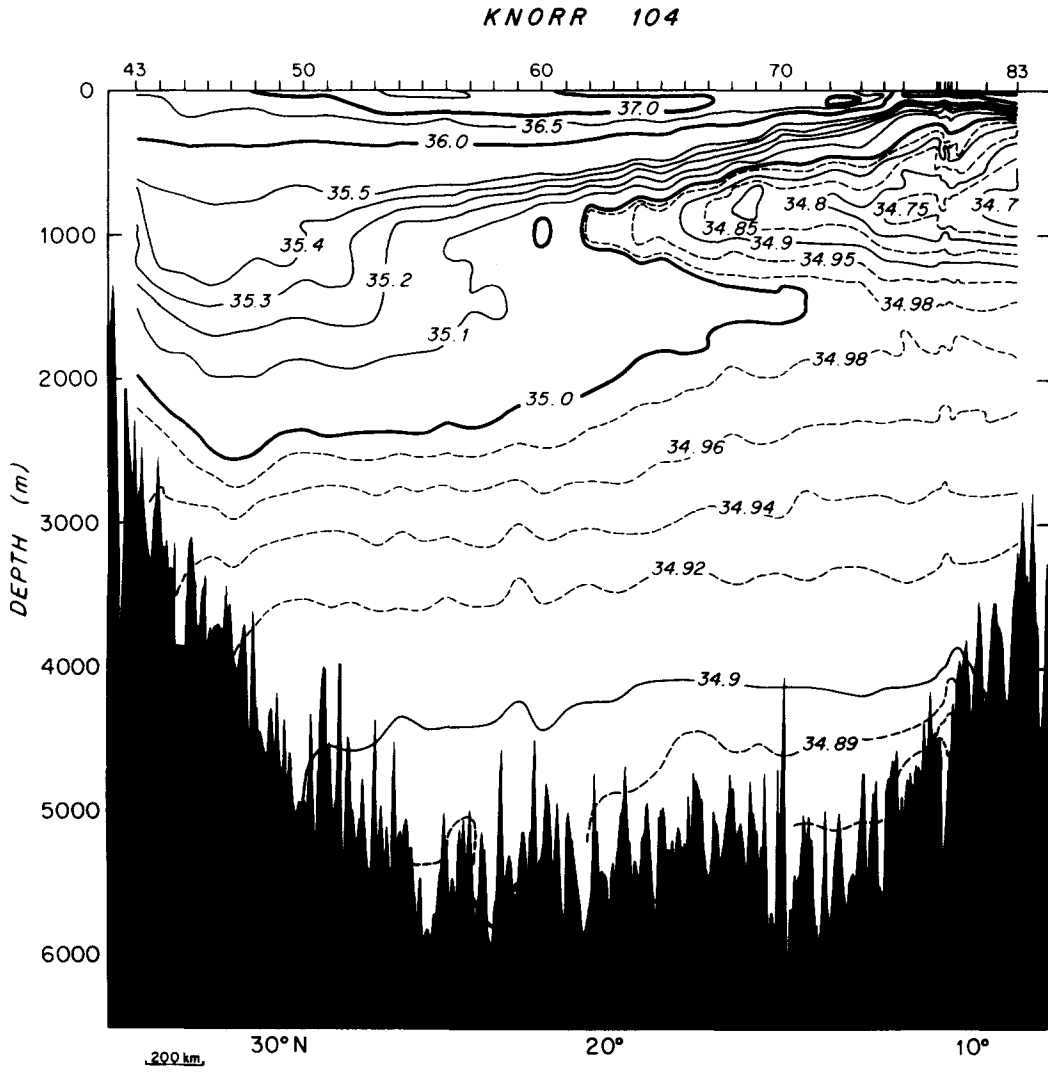


FIG.10d. Meridional section of salinity at 37°W, as Fig.10a.

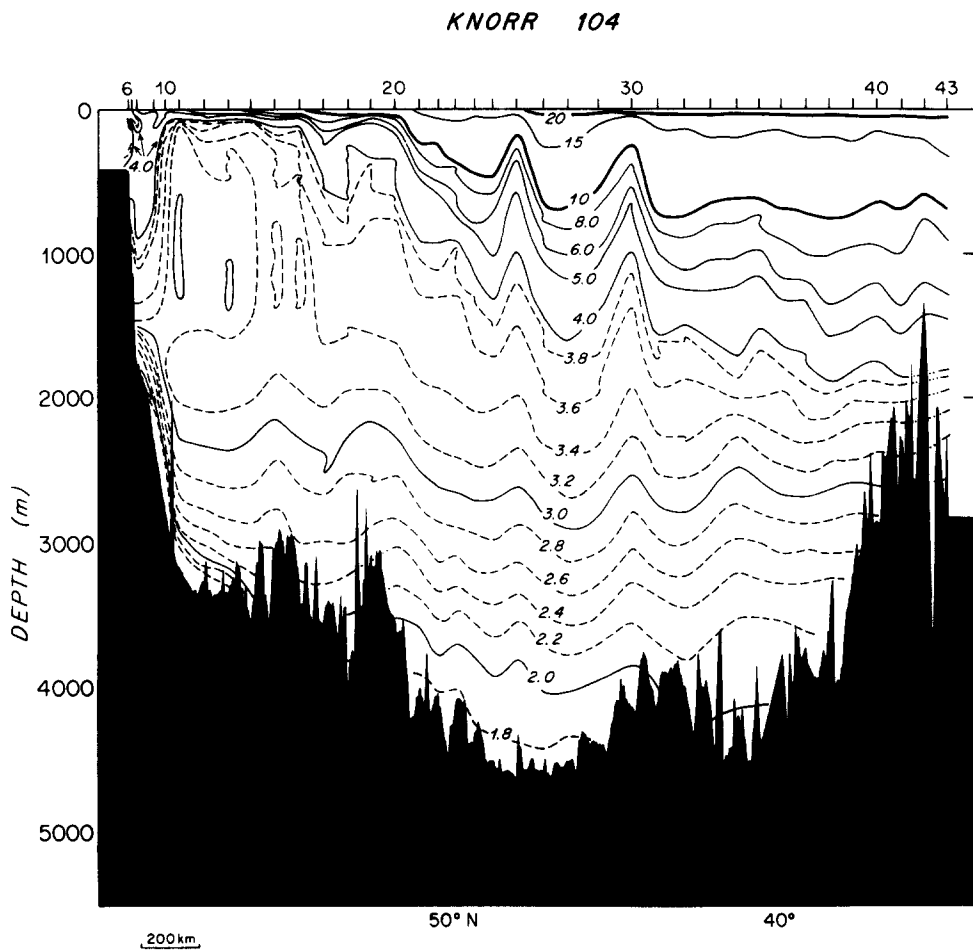


FIG. 11a. Meridional section of potential temperature (°C) along the subpolar part of the *Knorr* 37°W transect (nominal longitude, see Fig.3) in August 1983.

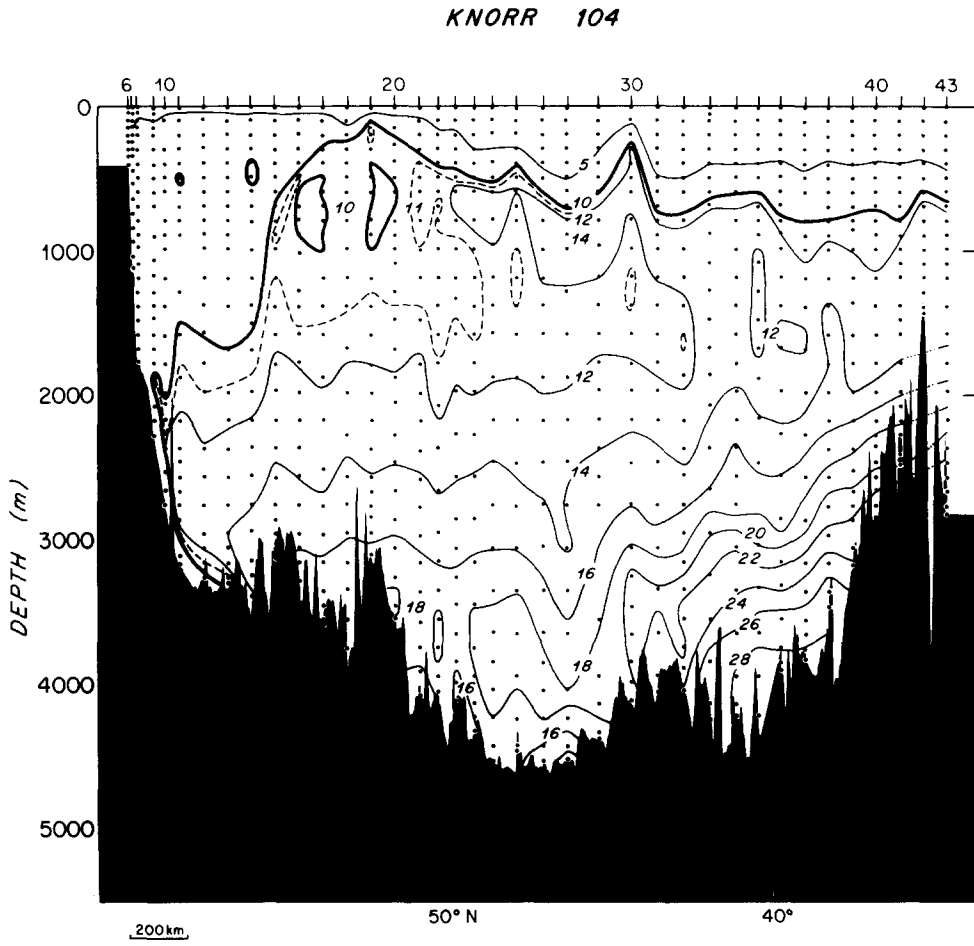


FIG.11b. Meridional section of silicate ($\mu\text{mol l}^{-1}$) at 37°W, as Fig.11a.

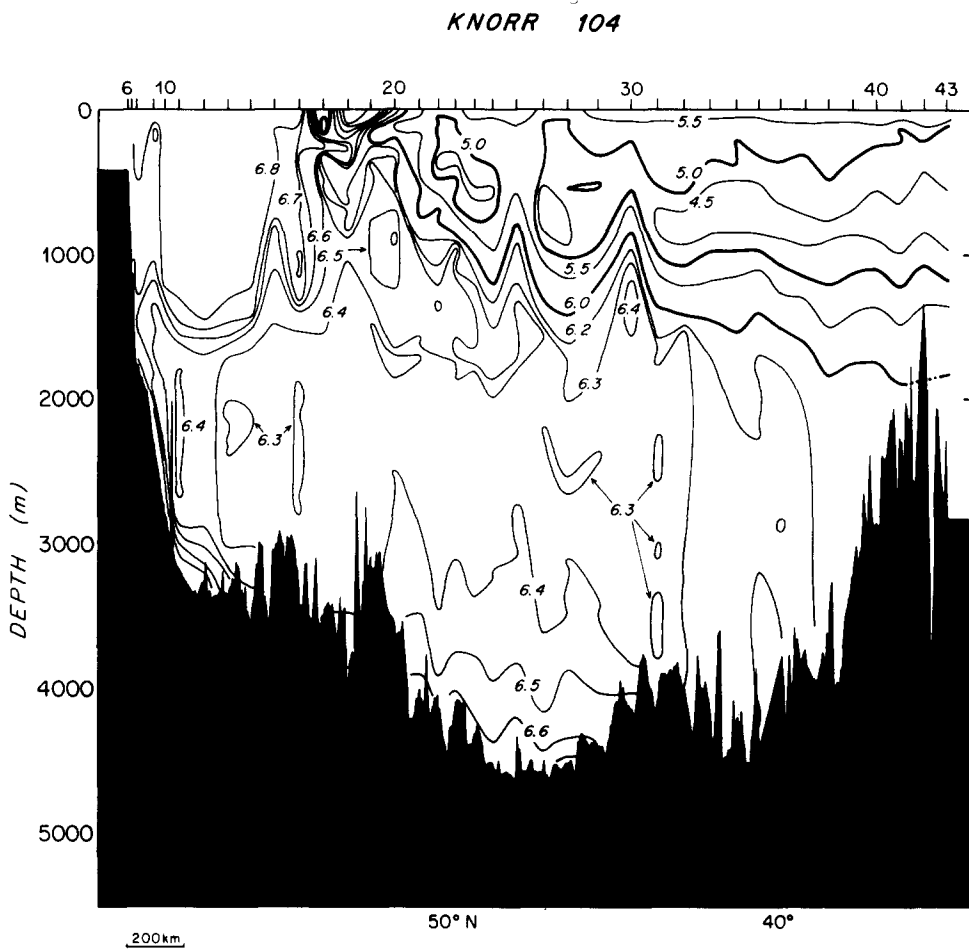


FIG.11c. Meridional section of oxygen (ml l⁻¹) at 37°W, as Fig.11a.

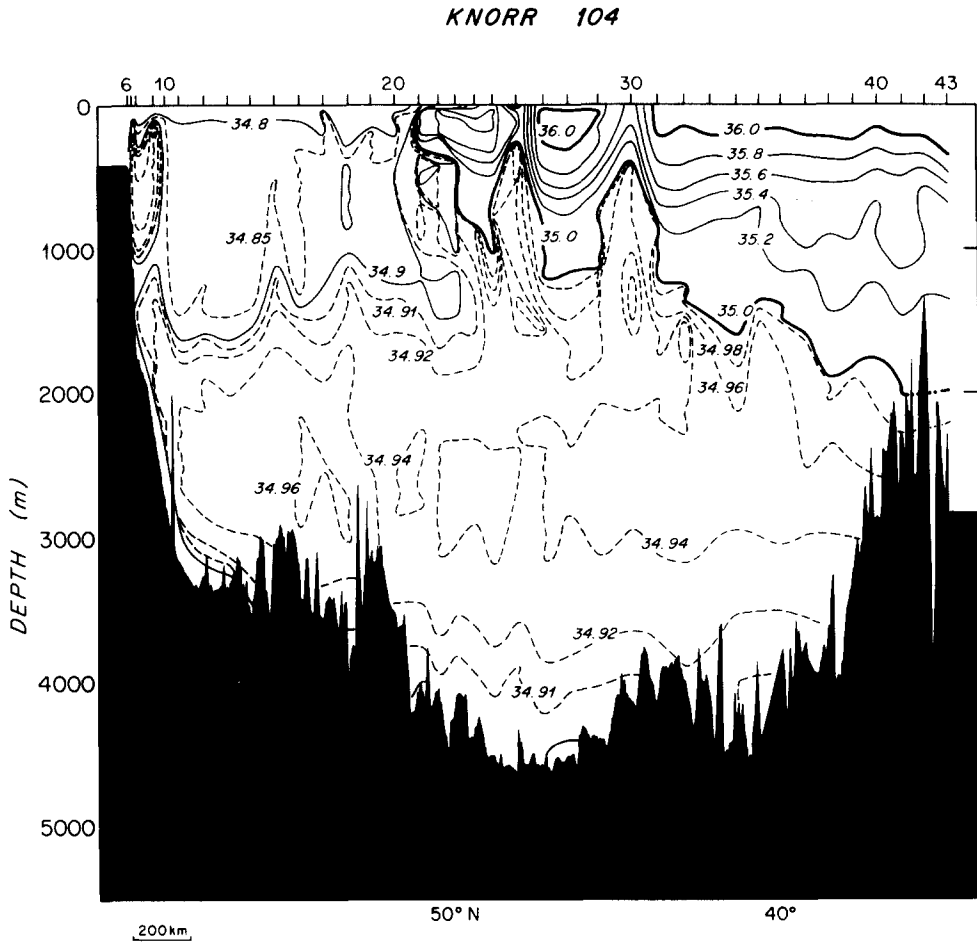


FIG.11d. Meridional section of salinity at 37°W, as Fig.11a.

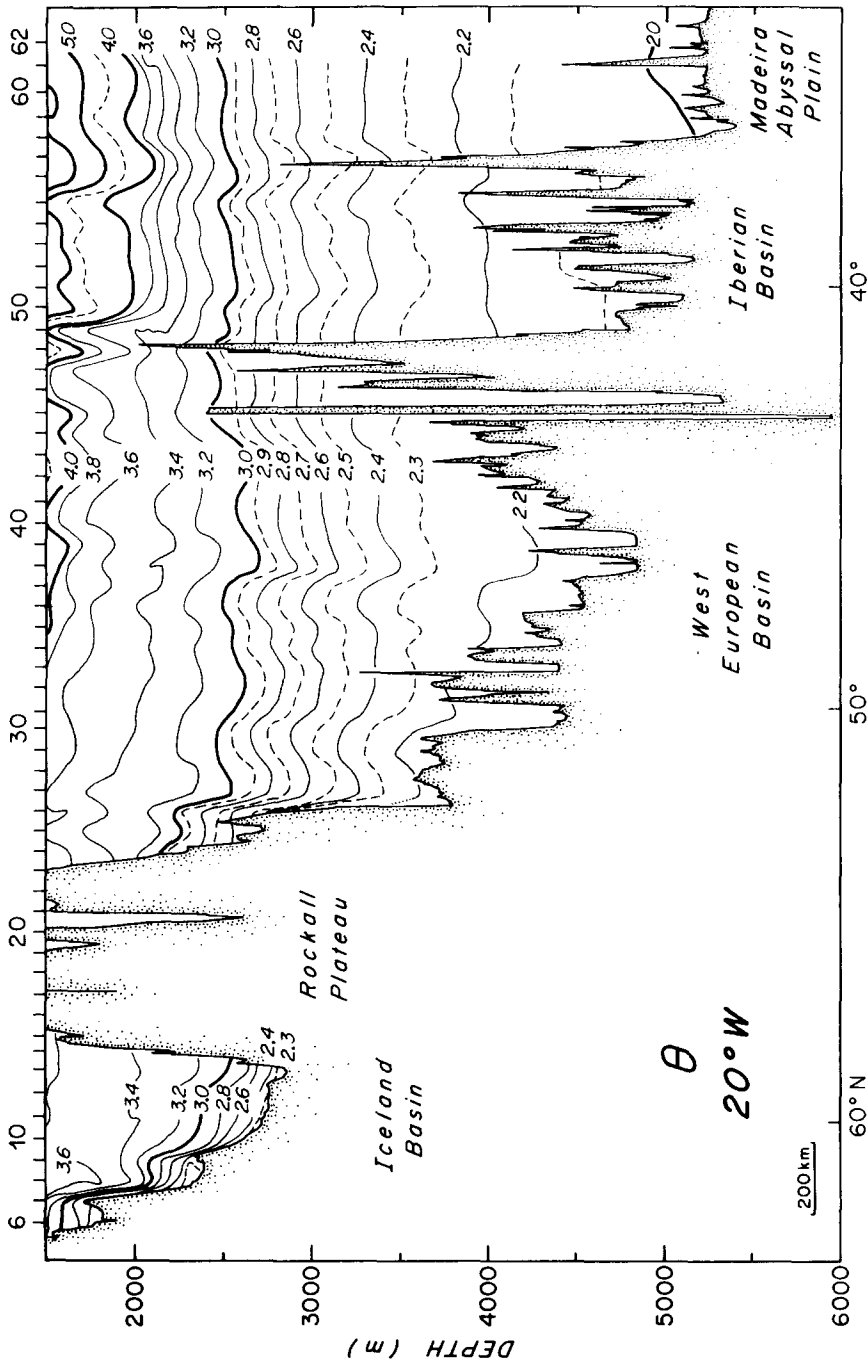


FIG. 12a. Meridional section of potential temperature (°C) along the subpolar part of the Oceanus 20°W transect (see Fig. 3) in July-August 1988 (TSUCHIYA, TALLEY and McCARTNEY, 1992).

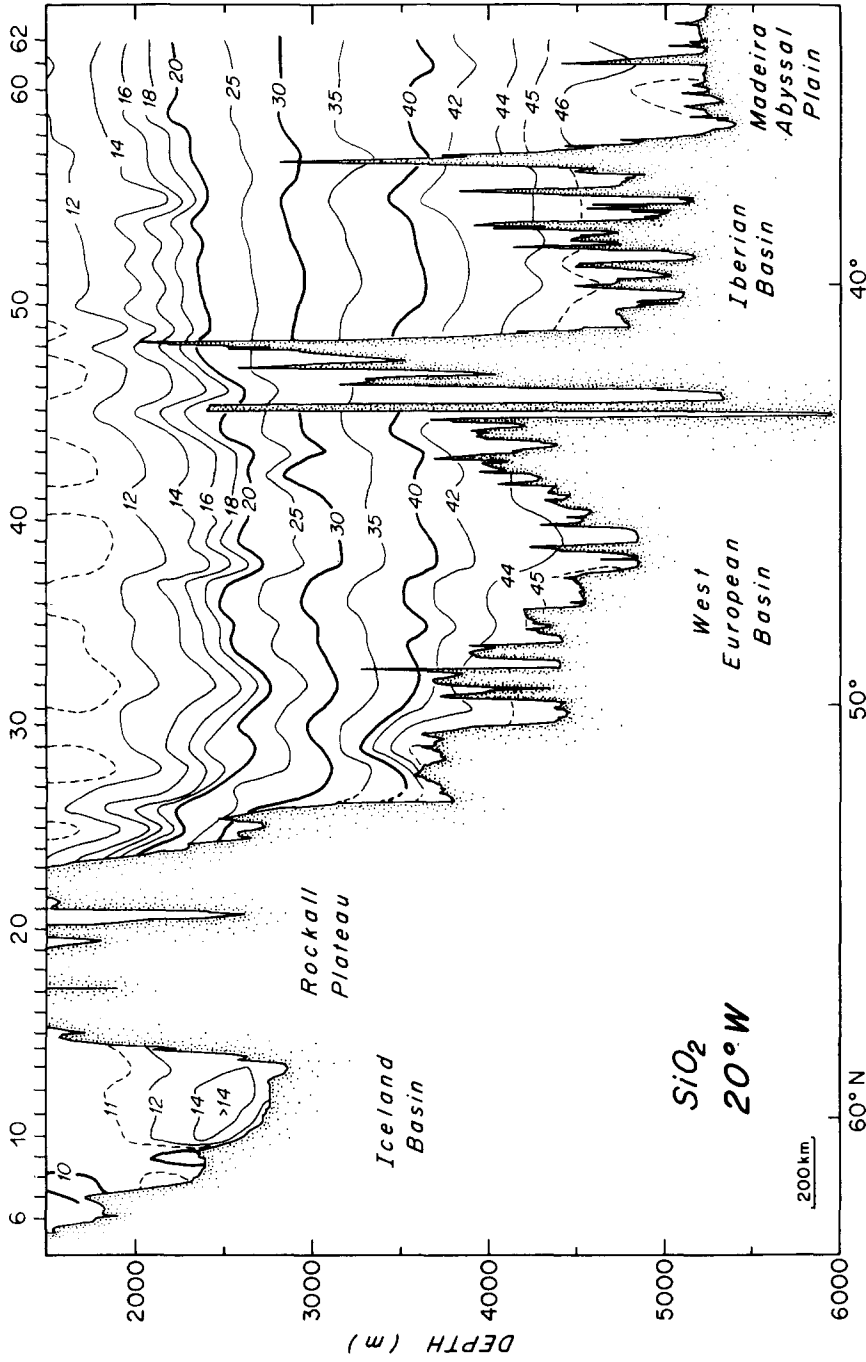


FIG.12b. Meridional section of silicate ($\mu\text{mol l}^{-1}$) at 20°W , as Fig.12a.

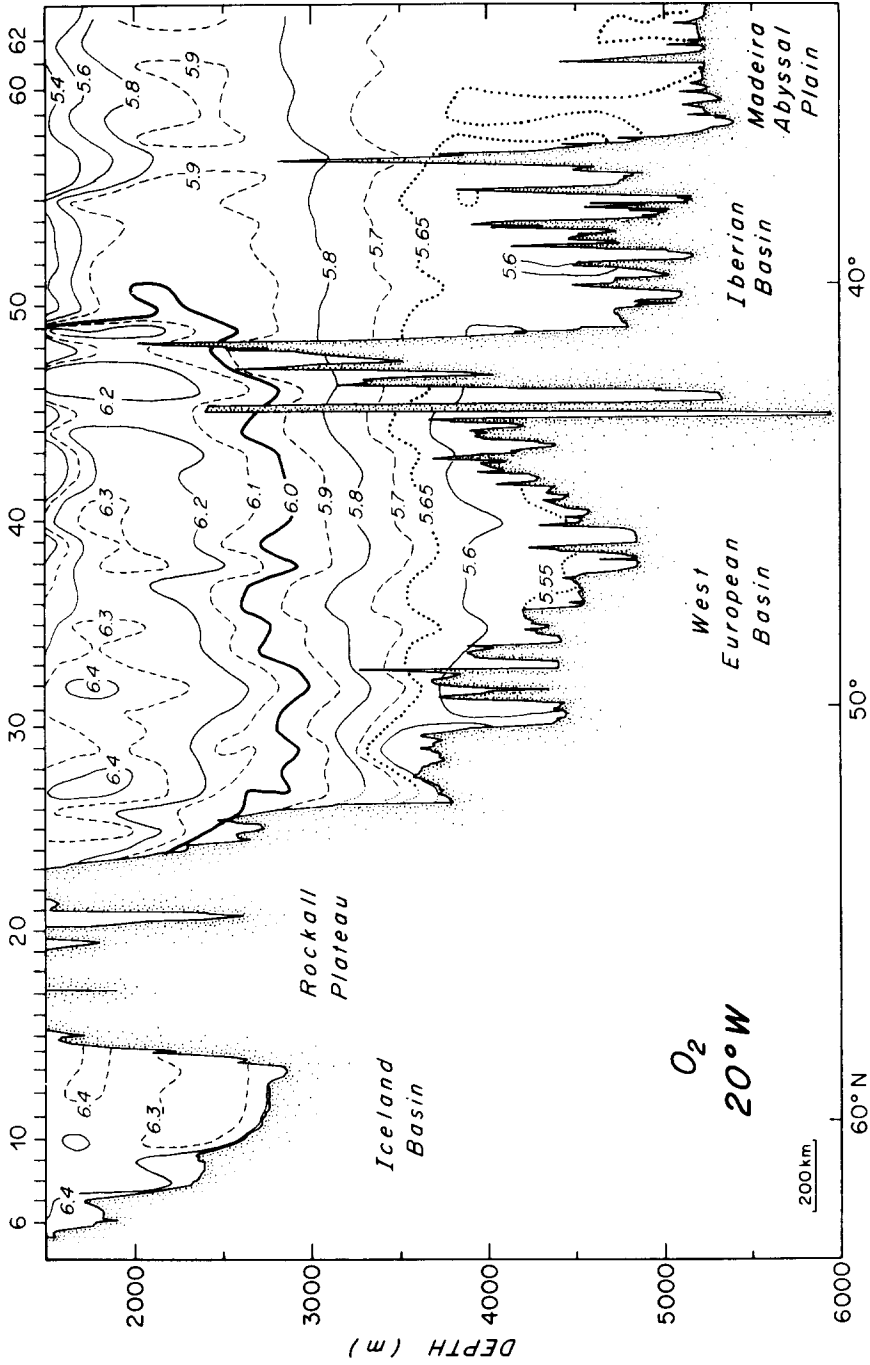


FIG. 12c. Meridional section of oxygen (ml l⁻¹) at 20°W, as Fig. 12a.

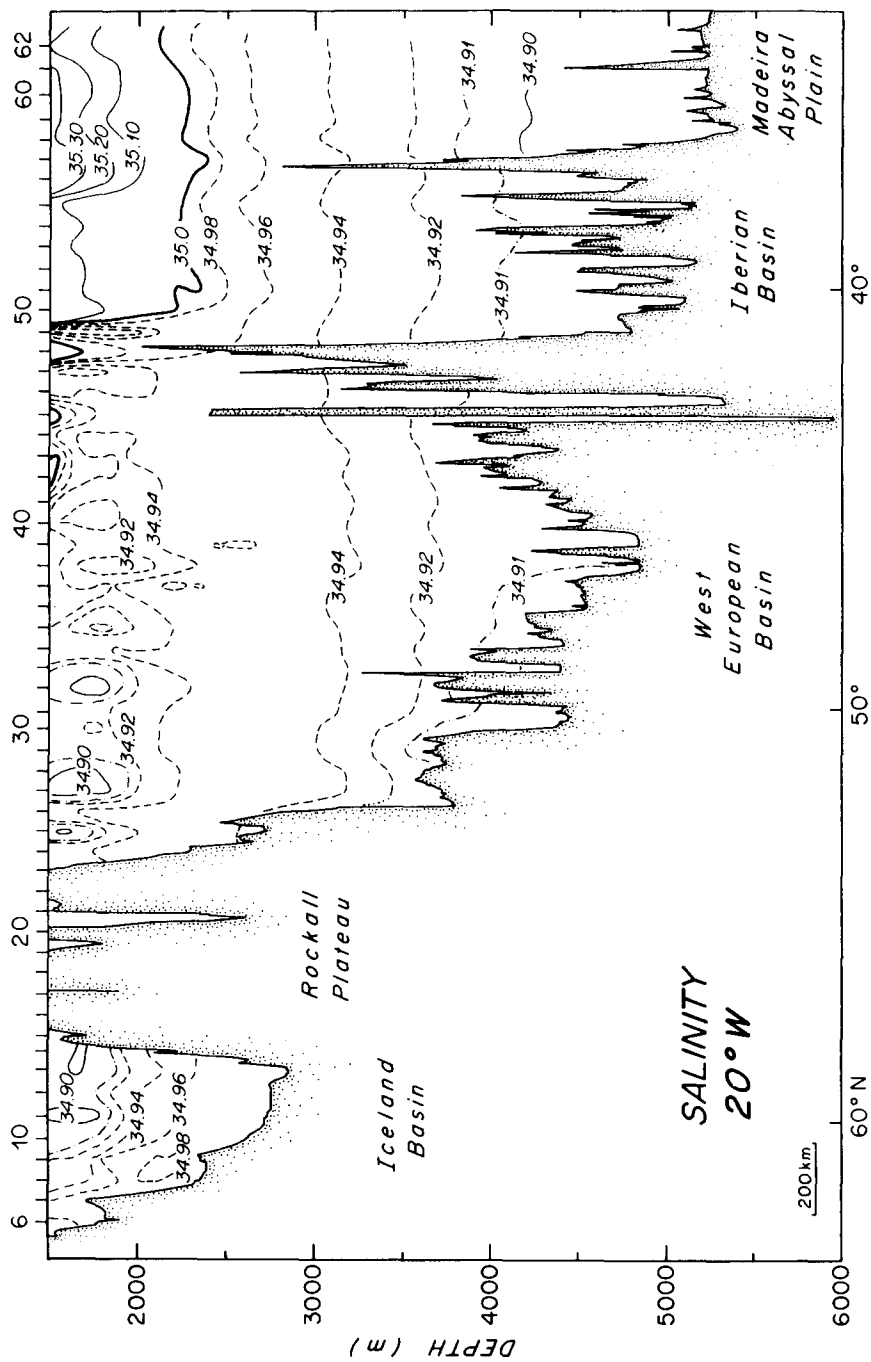


FIG.12d. Meridional section of salinity at 20°W, as Fig.12a.

A section in the eastern basin at 20°W running south from Iceland (Fig. 12) shows more substantial AABW influence – high silicate and oxygen – throughout the Western European Basin; the influence of the dense overflows is visible only in the northern Iceland Basin at the most northern part of the section. I will now describe the interaction of LDW with the dense overflows. First, is described the northward flow of LDW in the eastern basin and its involvement with DNBC, and then the corresponding flows in the western basin. The 3°C isotherm is again used as a nominal dividing surface within the deep water, as with Fig. 8, with LSW predominant above 3°C, and LDW and the dense overflows predominant below.

3.1 Eastern basin Antarctic Bottom Water and Lower Deep Water

3.1.1. The initiation of the Deep Northern Boundary Current in the Eastern Basin. Charts of near bottom silicate (WORTHINGTON and WRIGHT, 1971; MANTYLA and REID, 1983) show that in the western basin the 40 $\mu\text{mol l}^{-1}$ contour penetrates to about 37°N, the neighborhood of the Gulf Stream (see also Fig. 9). In the eastern basin the same contour penetrates to subpolar latitudes north of 50°N, into the Rockall Trough and onto the southern flank of the Rockall Plateau (Fig. 12). Charts of near bottom oxygen (MANTYLA and REID, 1983) show that the 5.8 ml l^{-1} oxygen contour penetrates to only 28°N in the western basin, but again reaches the Rockall area in the eastern basin. LDW thus penetrates northward to the Rockall area. The distribution of geostrophic shear sheds light on the northward flow path and what the flow at Rockall is. The Erika Dan section at 53°30'N (Fig. 13) shows two aspects of the LDW in the neighborhood of Rockall. The oxygen section (Fig. 13b) shows a thin layer of oxygen lower than 6 ml l^{-1} “draped” over the Rockall Plateau and Trough. (Val Worthington described this feature to me in 1975 as “the oxygen-eating ridge”.) It represents the lowest oxygen in the LDW system along this subpolar section. The potential temperature section (Fig. 13a) shows a clear boundary current shear signature through the rise of deep isotherms towards the Plateau (on both sides), and towards the continental slope forming the eastern boundary of the Trough. If there is a level-of-no-motion above this deep water, then a westward flowing DNBC results: this enters the Rockall Trough from the south at its eastern boundary, loops counter-clockwise out of the Trough to flow west round the south of the Plateau, then turns back north to the west of the Plateau. The orthogonal section at 20°W shows the shear signature (the steep rise of LDW isotherms towards the plateau) establishing the west flow south of the Plateau (Fig. 12a), the continuity of the relatively low oxygen of the DNBC with the LDW to the south (Fig. 12b), and the high silicate indicative of the LDW and AABW components of the water mass (Fig. 12c) (see also: TSUCHIYA, TALLEY and McCARTNEY, 1992). (Silicate determinations were made on a very few Erika Dan stations. Station 189 shows a silicate of 26 $\mu\text{mol l}^{-1}$ at the bottom bottle in the low-oxygen layer, Fig. 13b.) Together these basic data: the water mass characteristics indicative of southern origin, and the geostrophic signature of flow, are the basis for the addition of the DNBC component along the Rockall Plateau in Fig. 8. I will return to these two sections shortly and quantify the DNBC transport. But first I will outline the evidence that connects the high-silicate and low-oxygen water mass flowing west past the Plateau to the geostrophic flow of LDW and AABW at mid-latitudes. The idea of inflow to the Rockall Trough from the south, and its cyclonic tuning within the Trough have been discussed in two papers: ELLETT and MARTIN (1973), and LONSDALE and HOLLISTER (1979). The latter particularly focused on the shaping of the sediment drifts in the trough by the looping current, as well as noting the high silicate character of the water suggesting southern influence.

3.1.2. Deep flow at mid-latitude. McCARTNEY, BENNETT and WOODGATE-JONES (1991) discuss the distribution and circulation of AABW in the eastern basin between 10°N and 36°N,

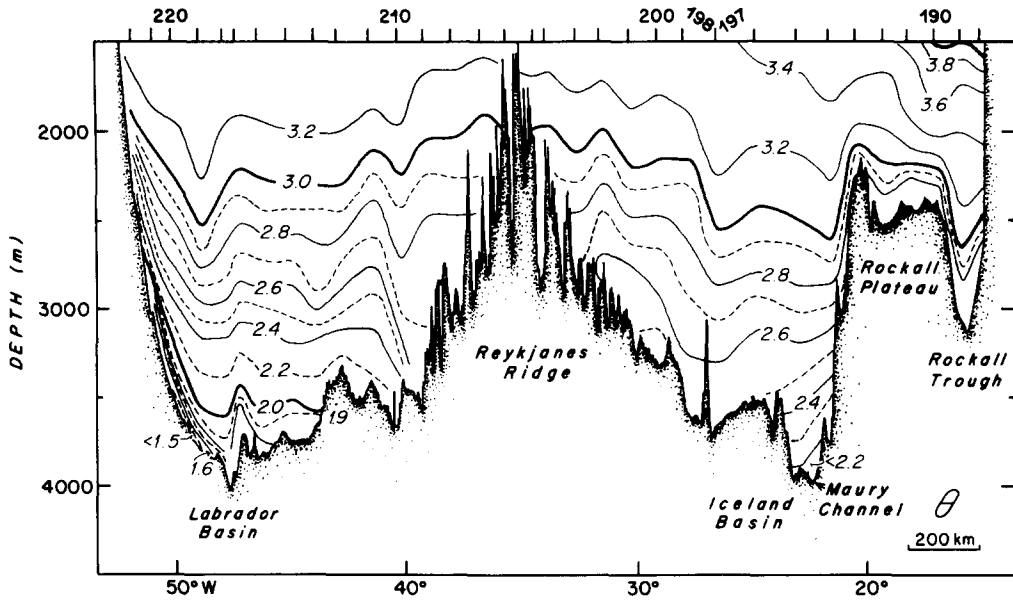


FIG.13a. Zonal section of potential temperature ($^{\circ}\text{C}$) along the *Erika Dan* $53^{\circ}30'N$ transect (see Fig.3) in February 1962 (WORTHINGTON and WRIGHT, 1970).

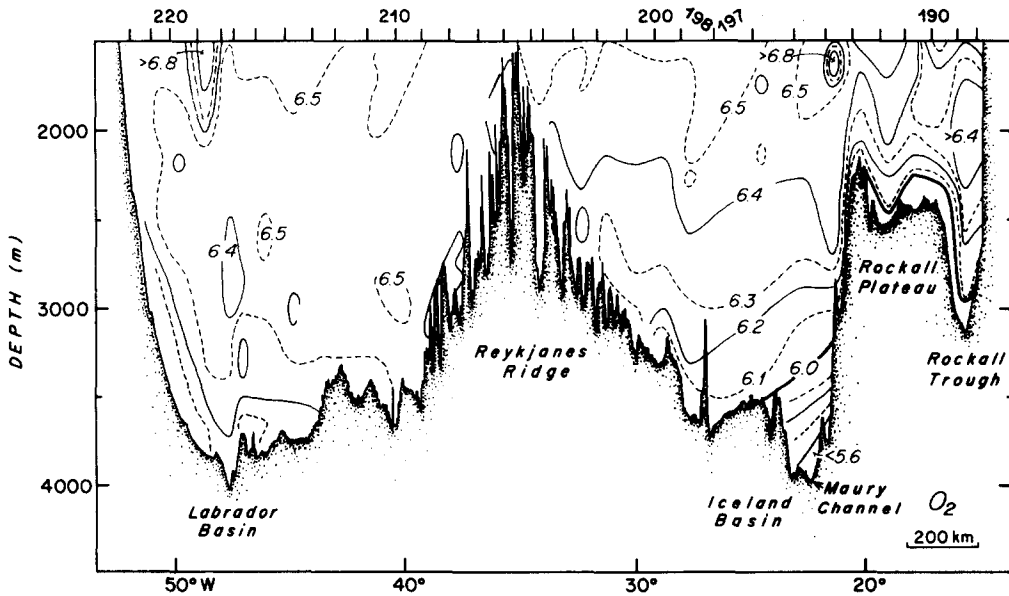


FIG.13b. Zonal section of oxygen (ml l^{-1}) at $53^{\circ}30'N$, as Fig.13a.

showing the strongest northward influence occurring as a western intensified flow along the eastern flank of the mid-Atlantic. The flow is traced back to the eastward flow through the Mid-Atlantic Ridge at the Vema Fracture Zone at 11°N, which supplies AABW as cold as 1.6°C to the eastern basin (Stations 76 to 80, Fig. 10). The section in Fig. 10 crosses this DWBC twice as the Mid-Atlantic Ridge curves west of the section to the north of the Vema Fracture Zone, then curves back to the east of the section farther north. The western intensified flow passes northwestward through stations 66 to 74, with waters as cold as 1.75°C, silicate as high as 53 μmol l⁻¹ and oxygen exceeding 5.8 ml l⁻¹. The western intensified flow returns northeastward through stations 51 to 61, with dilution having warmed the coldest waters to about 1.88°C, and diluted the highest silicates to just less than 50 μmol l⁻¹, while oxygen remains still greater than 5.8 ml l⁻¹. The transport here was estimated by McCARTNEY, BENNETT and WOODGATE-JONES (1991) to be 1.1 x 10⁶ m³ s⁻¹ of water colder than 2.0°C, based on a level-of-no-motion in the middle of the LDW deduced from oxygen and silicate. This section, and others included by McCARTNEY, BENNETT and WOODGATE-JONES (1991) using this level-of-no-motion, indicate some transport of warmer LDW, 0.7 to 1.0 x 10⁶ m³ s⁻¹ between 2.0°C and 2.5°C for a level-of-no-motion at 2.3°C to 2.5°C. At these warmer temperatures, silicate and oxygen levels are typically 45 μmol l⁻¹ and 5.7 ml l⁻¹, respectively. The transport of LDW below 2.5°C thus is estimated at 1.8 to 2.1 x 10⁶ m³ s⁻¹.

The western intensified northward flow is diverted by the shape of the Mid-Atlantic Ridge to become an eastward flow south of the Azores and carries water as cold as 1.95°C (silicates near 47 μmol l⁻¹) over the Madeira Abyssal Plain (Fig. 12). At 37°N the East Azores Fracture Zone forms a substantial abyssal barrier to its continued northward flow in the eastern basin, with only two gaps exceeding 4500m according to SAUNDERS's (1987) review of the regional bathymetry. Following the flow coldest temperatures in the LDW increase from about 1.9°C south of the Azores to warmer than 2.0°C at this Fracture Zone. SAUNDERS (1987) closely examined the flow field at the eastern of the two gaps through the Fracture Zone, the Discovery Gap, and estimated there a northward transport of the coldest LDW, colder than 2.05°C, of 0.21 x 10⁶ m³ s⁻¹ from direct current measurements, and 0.35 x 10⁶ m³ s⁻¹ from geostrophic shear combined with a 3500db level-of-no-motion (a choice guided by the current measurements). Transports at warmer levels, unconfined by the Gap, are not determined in that paper. The geometry of the northward flow in the Madeira Abyssal Plain is unanticipated: he shows a number of sections across the eastern boundary between 32°N and 38°N which show isotherms rising towards the eastern boundary in a narrow region adjacent to the eastern boundary. The sections in the Gap have this rise over the scale width of the channel, order 10km. The surprise is that three sections south of the Gap also show the rise, with a width order 100km, which he describes as a deep eastern boundary current. Thus the eastward flow along the Mid-Atlantic Ridge south of the Azores apparently continues eastward across the Madeira Abyssal Plain, then turns northward with eastern intensification along the Madeira Rise.

A section at 36°N (Fig. 14) used both by SAUNDERS (1987) and McCARTNEY, BENNETT and WOODGATE-JONES (1991) can be used further to quantify the northward transport of LDW. SAUNDERS's (1987) program of direct current determinations in the Gap indicated a level-of-no-motion near 3500db, which when applied to the section gave an estimated transport of 0.5 x 10⁶ m³ s⁻¹ of LDW colder than 2.05°C. McCARTNEY, BENNETT and WOODGATE-JONES (1991) noted this reference level as being roughly equivalent to a temperature of 2.3°C, and used this isotherm as a reference level to the 36°N section in obtaining nearly the same transport. These estimates are both somewhat larger than the SAUNDERS (1987) estimates at the Discovery Gap, which could result from additional transport through the western gap (near 19°W) in the East Azores Fracture Zone that was not included in Saunders's measurement program. The net

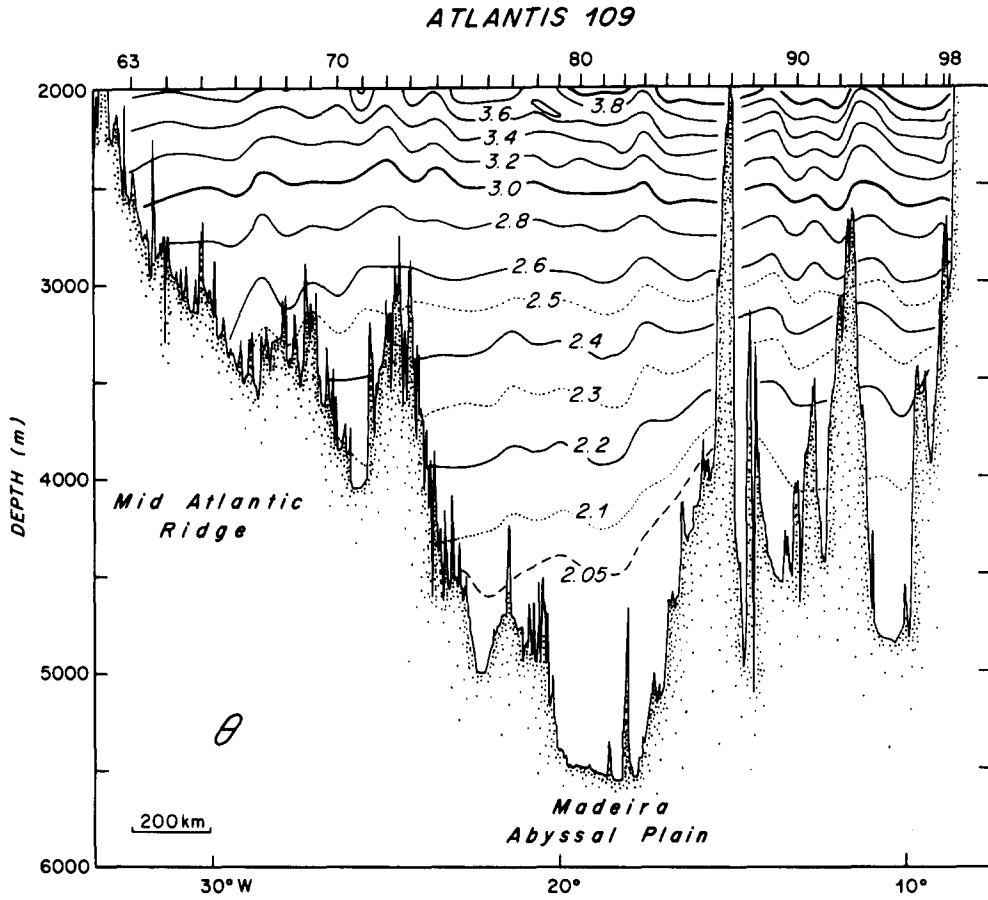
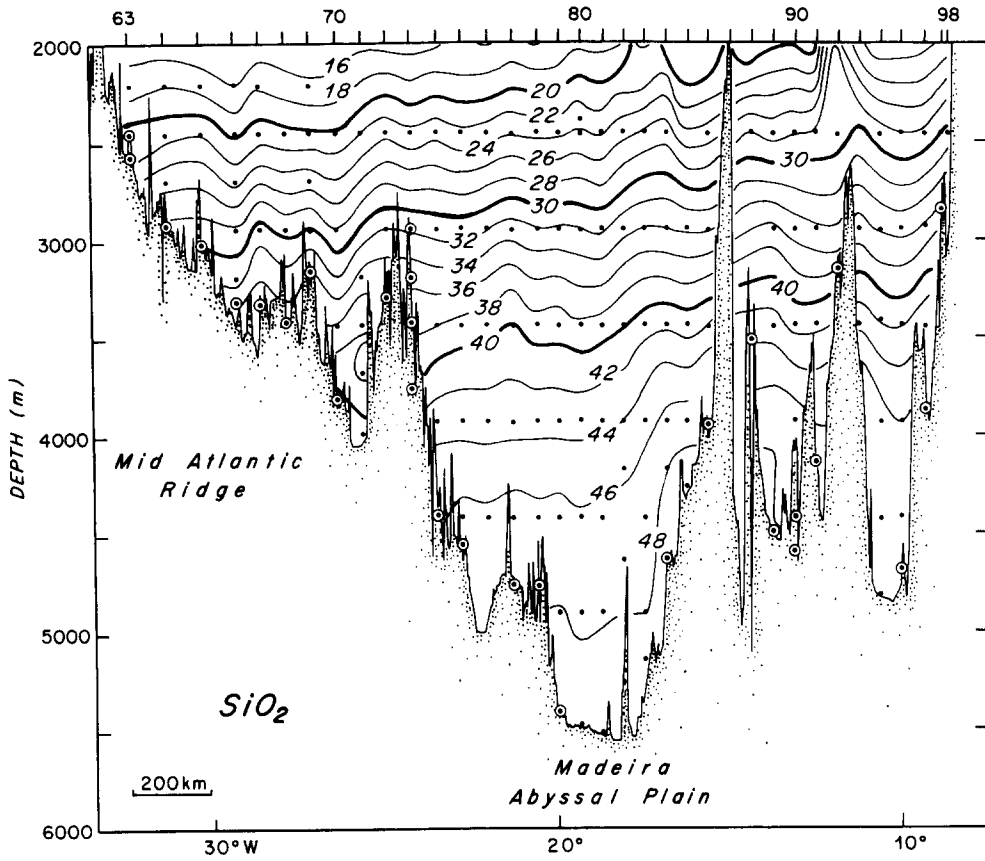


FIG.14a. Zonal section of potential temperature (°C) along the *Atlantis II* 36°15'N transect (see Fig.3) in June, 1981 (ROEMMICH and WUNSCH, 1985; McCARTNEY, BENNETT and WOODGATE-JONES, 1991).

FIG.14b. Zonal section of silicate ($\mu\text{mol l}^{-1}$) at $36^{\circ}15'N$, as Fig.14a.

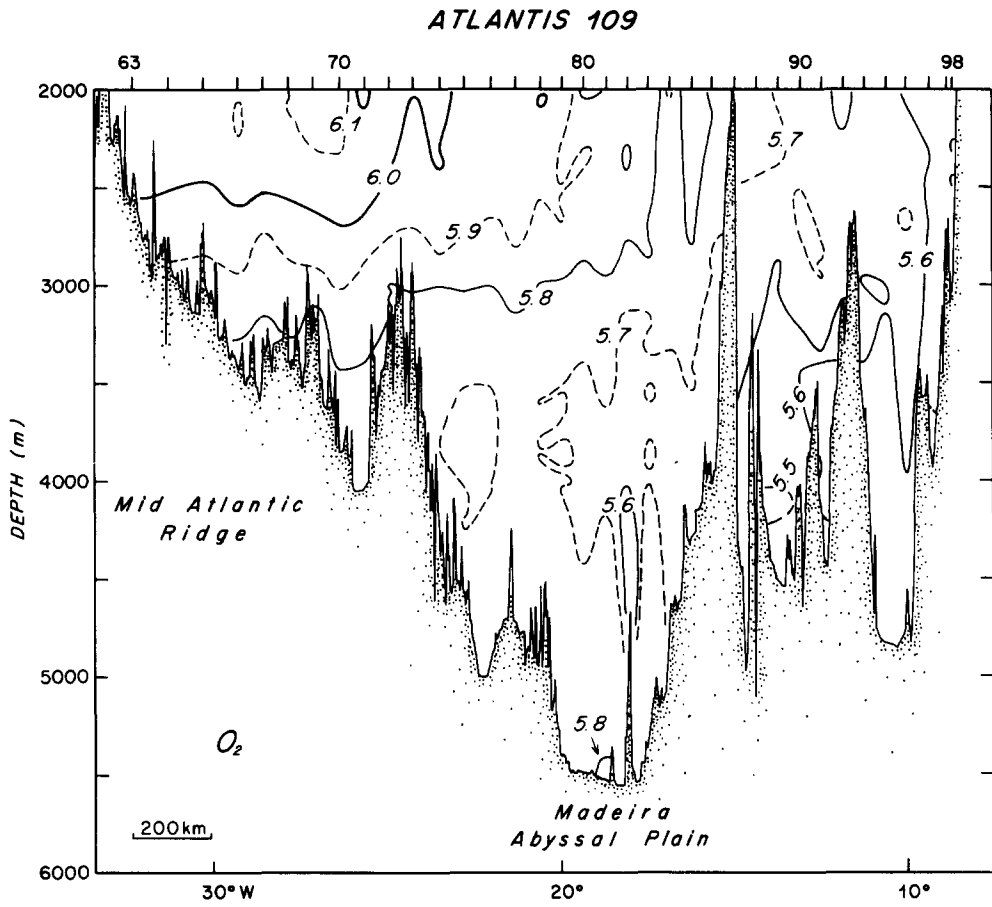


FIG.14c. Zonal section of oxygen ($ml\ l^{-1}$) at $36^{\circ}15'N$, as Fig.14a.

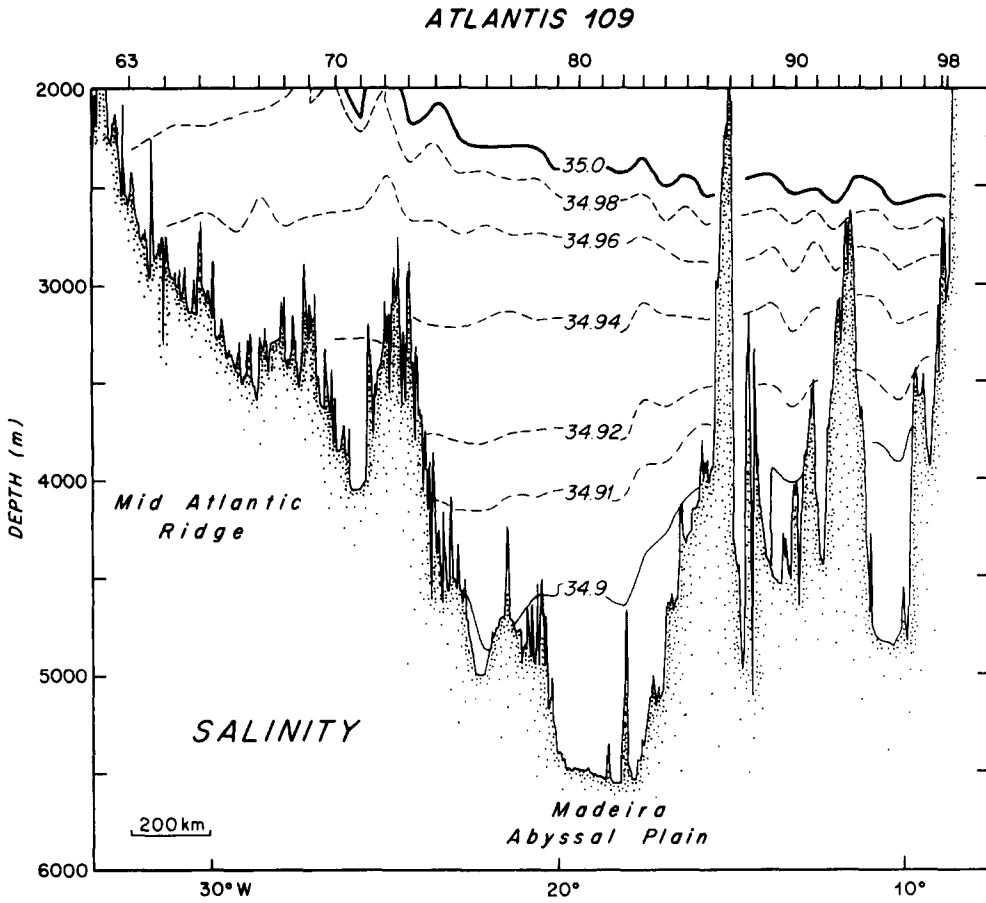


FIG.14d. Zonal section of salinity at 36°15'N, as Fig. 14a.

geostrophic flow at 36°N is the difference between a northward transport of $0.8 \times 10^6 \text{m}^3 \text{s}^{-1}$ east of station 81, and a southward transport of $0.4 \times 10^6 \text{m}^3 \text{s}^{-1}$ to the west of it, indicating a gyral aspect to the deep flow. Both the deep gaps in the East Azores Fracture Zone lie to the north of the northward flowing limb of this system. The silicate and oxygen sections (Figs 14b,c) show the stronger mid-latitude LDW character in the east limb of this flow system, extending well above 2.05°C. The transport calculation can be extended to the LDW between 2.05°C and 2.3°C, yielding an additional net transport at 36°N of $0.9 \times 10^6 \text{m}^3 \text{s}^{-1}$ of this warmer LDW, or a total of $1.3 \times 10^6 \text{m}^3 \text{s}^{-1}$ northward transport of LDW colder than 2.3°C. For comparison at the Vema Fracture Zone, McCARTNEY, BENNETT and WOODGATE-JONES (1991) estimated a net flow below 2.3°C of 2.1–2.5 $\times 10^6 \text{m}^3 \text{s}^{-1}$.

SAUNDERS (1987) notes that the 3500db level-of-no-motion is not a sharply defined choice. The shear signatures at 36°N (Fig. 14) and in his sections near 32°N reach shallower than 3500m to depths of 3000m or less, and a temperature perhaps as warm as 2.5°C. It is tempting to raise the choice of level-of-no-motion to the 2.5°C isotherm, fully above the shear signature, which converts this deep shear to unidirectional flow. Support for this choice comes from the oxygen distribution, which shows that the $<5.7 \text{ml l}^{-1}$ zone at 36°N reaches this isotherm, while in the 20°W section (Fig. 12) the source of such low oxygen water is to the south (not north) of the 36°N section, suggesting northward flow below 2.5°C. Using the 2.5°C isotherm as a level-of-no-motion gives virtually the same net transport of cold LDW as the 2.3°C level does, $0.43 \times 10^6 \text{m}^3 \text{s}^{-1}$ of water colder than 2.05°C, but increases the gyral effect by yielding northward flow of $1.0 \times 10^6 \text{m}^3 \text{s}^{-1}$ in the east and a southward flow of $0.6 \times 10^6 \text{m}^3 \text{s}^{-1}$ in the west. The total flow beneath this alternate level-of-no-motion at 2.5°C is $1.6 \times 10^6 \text{m}^3 \text{s}^{-1}$. It is encouraging that these totals are similar to those given in the preceding paragraphs for the western intensified flow in the Canary Basin southwest of the Azores (1.8 to $2.1 \times 10^6 \text{m}^3 \text{s}^{-1}$) and the ultimate Vema Fracture Zone source (2.1 – $2.5 \times 10^6 \text{m}^3 \text{s}^{-1}$) so providing continuity of both water mass characteristics and transport (with the mild northward decline in transport indicative of the expected upwelling).

3.1.3. Deep flow in the Iberian and West European Basins. These considerations suggest that on the order of $2 \times 10^6 \text{m}^3 \text{s}^{-1}$ of LDW with relatively high silica and low oxygen flow northward into the Iberian Abyssal Plain below about 2.5°C. This is still considerably south of the Rockall Plateau, and the flow must traverse the Iberian and West European Basins. The eastern concentration of the northward flow described by SAUNDERS (1987) for the Madeira Abyssal Plain extends across these two basins. Here only a single graphic is given to illustrate the flow. In the 36°N section (Fig. 14) the shear signature of the northward flow is the eastward rise of LDW isotherms. Figure 15 compares this rise at 36°N, as exemplified by the 2.3°C isotherm, to the topography of the same isotherm in several of the IGY sections (FUGLISTER, 1960) crossing the eastern boundary in the Madeira, Iberian and West European Basins. Two more recent sections are included: firstly, to contrast the westward flow regime at Rockall “47°N”, Ross Hendry’s reoccupation (HENDRY, 1989) of the IGY section near 48°N (Fig. 16), and secondly the meridional section at 20°W (Fig. 12, see also TSUCHIYA, TALLEY and McCARTNEY, 1992). All show a similar pattern of eastward rise near the eastern boundary (northern boundary at 20°W). Although sampling resolution is irregular, a typical scale for the rise in the northern two basins is 200 to 300km, about the same as the feature in the 36°N section across the Madeira Basin (Fig. 14), the included IGY 32°N section (which is terminated at the Madeira Rise for this purpose, rather than the section continuation across the Seine Abyssal Plain, a cul-de-sac) and in SAUNDERS’s (1987) observations at 32°30’N and 33°N at the Madeira Rise.

The full property distributions for the 47°N section are shown in Fig. 16 to illustrate the LDW characteristics accompanying the northward flow. Along this section isopleths of oxygen and

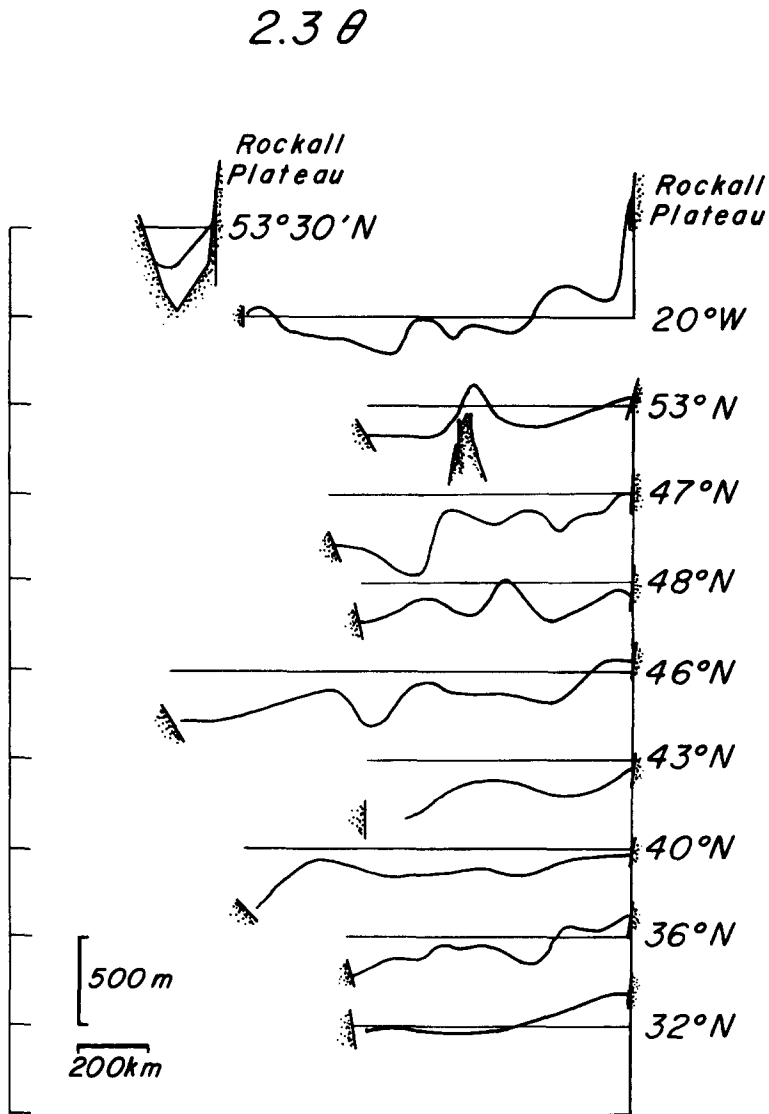


FIG.15. Depth of the 2.3°C isotherm along eastern basin sections at the indicated nominal intersections with the eastern boundary. At 32°N, 40°N, 43°N, 46°N, 48°N and 53°N, data in METCALF (1958), WORTHINGTON (1958, 1959) and FUGLISTER (1960). From Fig.13a at 53°30'N, Fig.14 at 36°N, Fig.16 at 47°N, Fig.12 at 20°W. Isotherms are displaced upwards 500m sequentially in the order of the section's intersection with the eastern boundary, and the horizontal reference line is 3500m. See text.

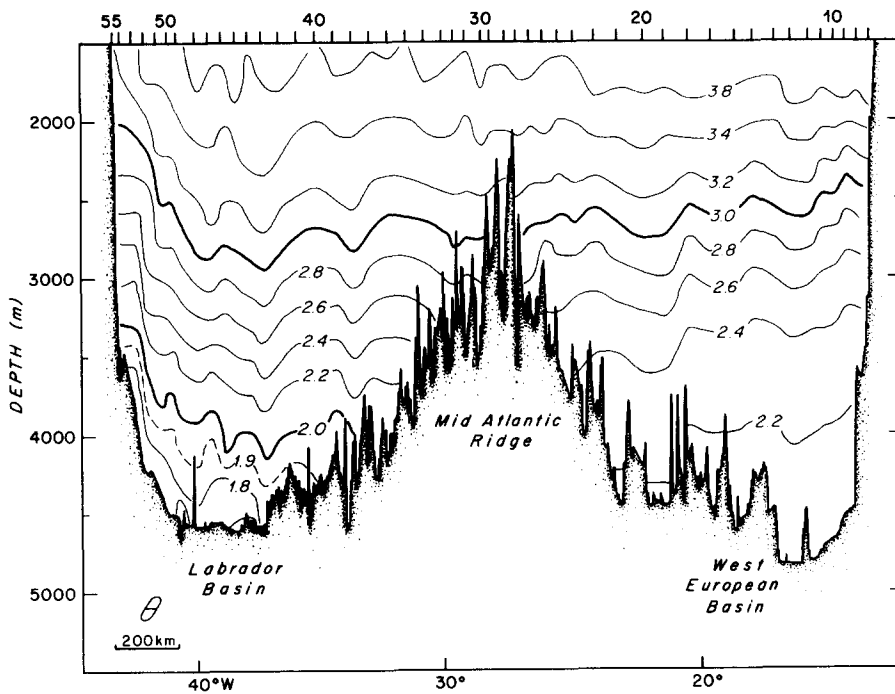


FIG.16a. Zonal section of potential temperature ($^{\circ}\text{C}$) along the Hudson 47°N transect (nominal latitude, see Fig.3 and 18) in June 1982 (HENDRY, 1989).

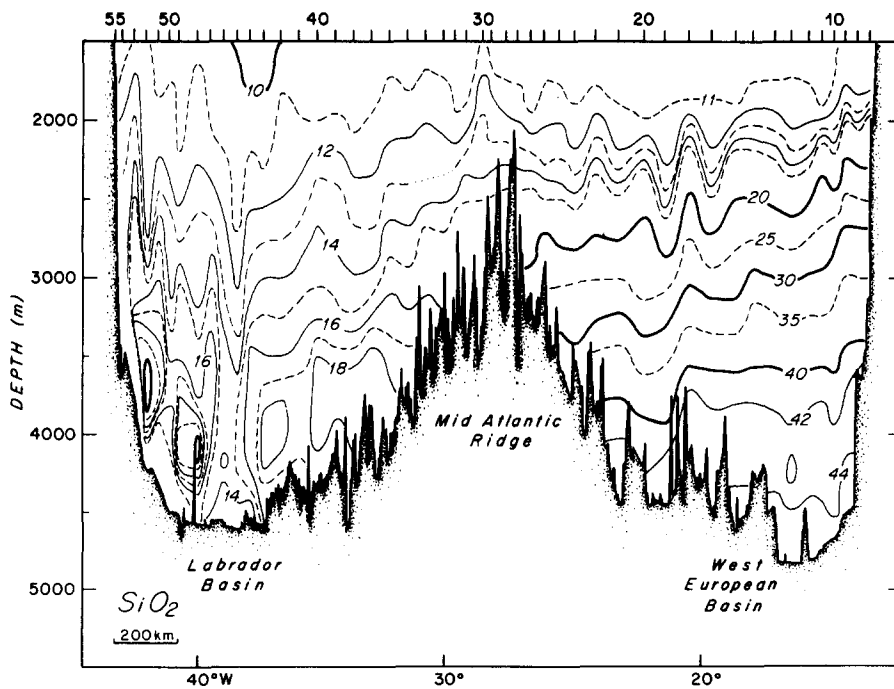
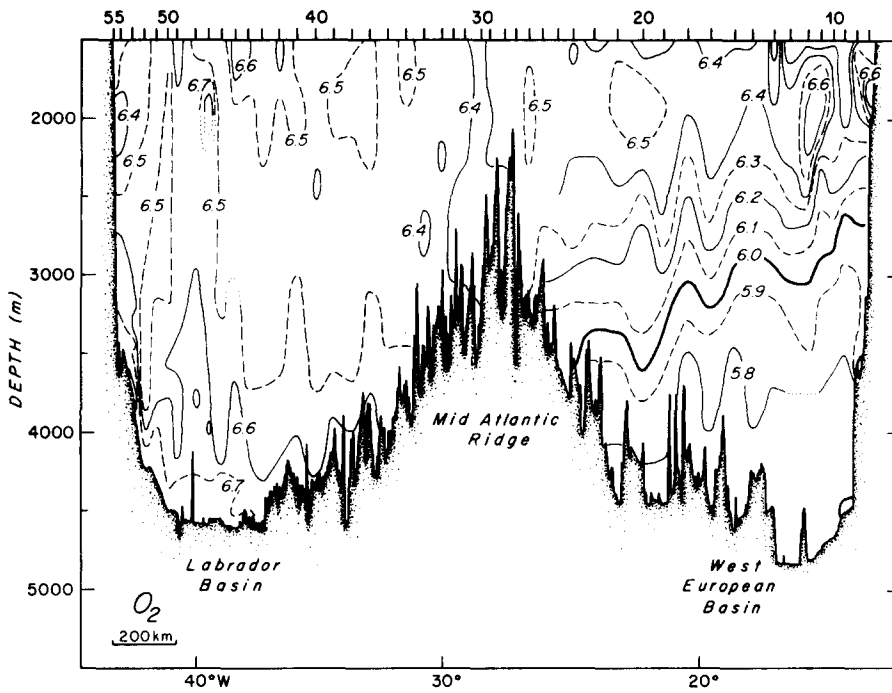
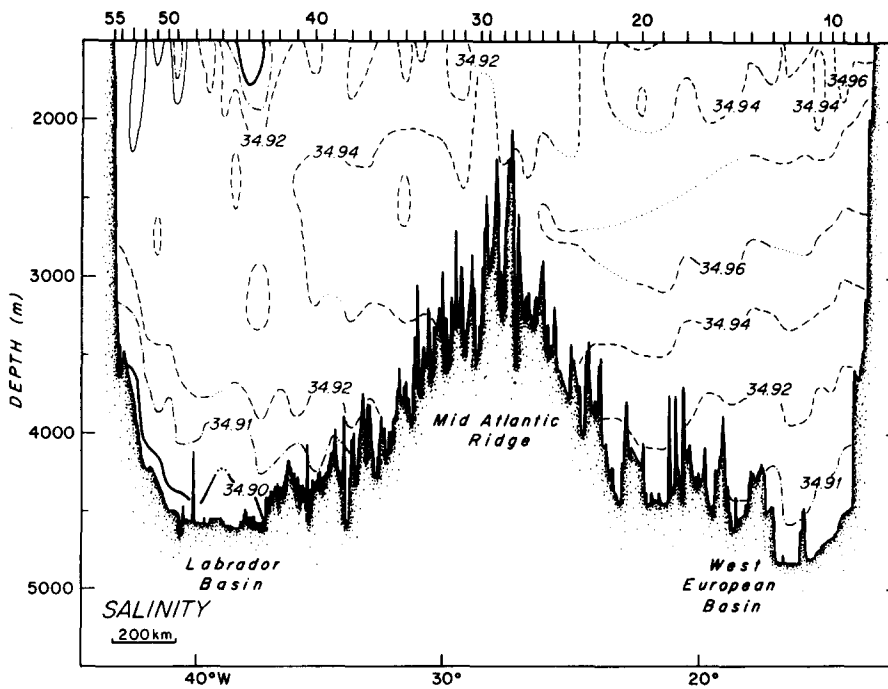


FIG.16b. Zonal section of silicate ($\mu\text{mol l}^{-1}$) at 47°N , as Fig. 16a.

FIG.16c. Zonal section of oxygen (ml l^{-1}) at 47°N , as Fig.16a.FIG.16d. Zonal section of salinity at 47°N , as Fig.16a.

silicate rise more than temperature, indicating that for a given LDW temperature, oxygen is lower and silicate higher in the eastern boundary side of the eastern basin than the Mid-Atlantic Ridge side. Thus the southern source influence is stronger in the east. Similar oxygen patterns for the IGY sections are found in the oxygen sections included in the cruise data reports (METCALF, 1958; WORTHINGTON, 1958, 1959). In the northern *Discovery II* IGY Cruise 3 sections (43°N, 46°N and 53°N, WORTHINGTON, 1959), some of the first North Atlantic silicate data are reported and show the general high-silicate character of the LDW and hint at the eastern intensification of higher silicate water better revealed by improved recent measurements like those shown in Figs 14 and 16.

The sections of Figs 15 and 16 suggest that the eastern intensification of the northward flow described by SAUNDERS (1987) between 32°N and 37°N persists northward through the Iberian and West European Basins and transitions to the DNBC flow noted earlier (Figs 12 and 13) to the south of the Rockall Trough and Plateau. The eastern concentration of the northward flow provides the circulation pathway to bring LDW water to the subpolar basin supporting the MANN, COOTE and GARNER (1973) observation of high-silicate, low-oxygen LDW west of Rockall and their inference that it derived from the northward movement of AABW in the eastern basin.

The distribution of moorings in the West European Basin is extensive in the DICKSON, GOULD, MÜLLER and MAILLARD (1985) compilation (Fig.17). These direct current measurements indicate that there is northwest flow along the continental slope near the location where both the 47°N and 53°N sections (Fig.15) intersected the slope (near 49°N, 11°W), confirming the interpretation of the shear as indicative of poleward flow. The authors note that a poleward flow along the deep continental slope, earlier postulated by SWALLOW, GOULD and SAUNDERS (1977) and ELLETT, DOOLEY and HILL (1979), is finding confirmation as the number of deep records increases. Other evidence for poleward flow along the deep eastern boundary has been described for several locations. DICKSON and McCAVE (1982) discuss the southeast entry to the Rockall Channel, the Porcupine Bank. The next regime to the south, the Bay of Biscay, is described from a sedimentary perspective by AUFFRET and SICHLER (1982). The Iberian region of the boundary is discussed by MEINCKE, SIEDLER and ZENK (1975) and GARDNER and KIDD (1987), while LONSDALE (1982) discussed the complex region of the Madeira, Morocco and Sahara Rises. The latter author suggests that the northward flow begins well to the south and loops around the Seine Abyssal Plain and then turns north again west of the Madeira Rise – the area included in the SAUNDERS (1987) paper. There may indeed be a flow at the eastern boundary this far south, but the McCARTNEY, BENNETT and WOODGATE-JONES (1991) study shows the principal flow axis for the AABW to be in the western part of the eastern basin, as discussed above.

The eastern intensification of the northward flow of LDW through the Madeira, Iberian and West European Basins is an interesting dynamical puzzle. SAUNDERS (1987) describes it as a deep eastern boundary current and gives a rationalization of his Madeira Basin observations (including the section of Fig. 14) as an “upstream boundary current” to the flow through the Discovery Gap. McCARTNEY, BENNETT and WOODGATE-JONES (1991) point out that in the STOMMEL and ARONS (1960) abyssal circulation model, interior flow with low-latitude source characteristics is confined to the eastern part of the interior northward to the critical latitude where the sense of the DWBC flow reverses from north to south through the action of deep recirculation in the northwestern part of the basin. In this interpretation the eastward intensification is not of a boundary current nature, rather it is the southern water mass character that is eastern intensified (north of the critical latitude). SPEER and McCARTNEY (1992) have developed a two abyssal layer extension of the STOMMEL and ARONS (1960) model to further explore this eastward concentration with application to the western basin AABW distribution, which can be extended to the

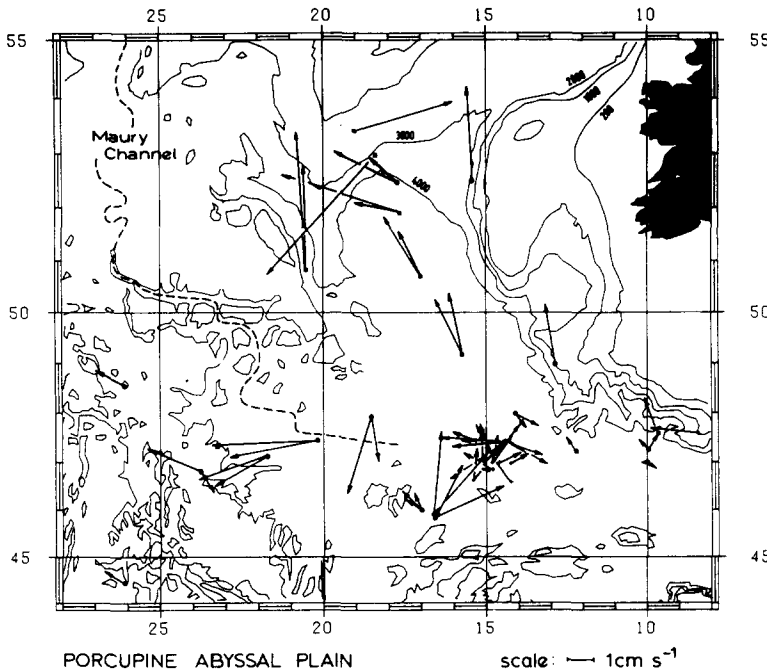


FIG.17. From DICKSON, GOULD, MÜLLER and MAILLARD (1985): mean deep (>2000m) velocity vectors in the West European Basin. The dashed curve is thus inference of a pathway from the central West European Basin to the Maury Channel east of Rockall Plateau. See Figs 18b and c for another interpretation of this pathway. Current meter records range from 8 months to 2 years.

eastern basin situation. The deformable interface between the LDW and the lighter deep water tilts in response to upwelling LDW, and the interface “grounds” along a curve emanating from the western boundary and curving off to the northeast. The LDW is restricted to the area east of this grounding curve, which is progressively restricted to the eastern part of the basin. This limits the shear signature of northward flow to that same region. West of the curve the interior flow is also northeast, but consists of lighter deep water that has come from the southward flowing DWBC which is comprised of recirculating water with northern influence included – thus the west to east water mass contrast in Figs 14 and 16. The original STOMMEL and ARONS (1960) model predicts the eastern concentration of the water mass; the layered extension adds to this an eastern concentration of the shear. The decoupling of the interior and boundary current flows from the dynamics of the deep water sources in these models lends credence to LONSDALE’s (1982, quoted in introduction) idea that the general cyclonic flow along the eastern and northern basin boundaries is not driven by the overflows.

3.1.4. Quantification of the Deep Northern Boundary Current at the Rockall Plateau. The current vectors of Fig.17 suggest a bathymetry following current along the eastern and northern boundary (the Rockall area) of the West European Basin, in agreement with the interpretation of the shear signatures in Figs 11 and 12 as indicative of a DNBC flowing west. The coldest LDW remains in the deepest parts of the West European Basin, passing through the 20°W section (Fig.12) to appear west of the Rockall Plateau in the *Erika Dan* section (Fig.13 and the upper left graph of Fig.15). At somewhat warmer temperatures the northward flow along the eastern boundary penetrates partway into the Rockall Trough. At stations 188 to 189 (Fig.13) the eastward rise of isotherms is not fully resolved because of the shallowness of station 186, but the coldest

bottom temperature, less than 2.6°C at station 188, lies in the northward flow in the eastern Trough. Oxygen concentrations here are low, and the nearest station with silicate data, station 189, shows the high silicate, $26\mu\text{mol l}^{-1}$, of mid-latitude LDW. The flow of LDW into the Trough loops counterclockwise and returns south (stations 189 to 193), then passes west with the colder LDW through the 20°W section (Fig. 12), and turns north into the Iceland Basin (stations 193 to 195, Fig. 13). The clockwise looping of the flow around the southernmost part of the Rockall Plateau is further confirmed by the 2.3°C isotherm along the *Discovery II* 53°N section (Fig. 15), which descends down both eastern and western flanks from a station atop a southward projection of the Plateau near 20°W (shown by the segment of bathymetry on the 53°N curve of Fig. 15). This suggests that the section just caught the southern turning point of the looping DNBC (compare to Fig. 13 intersecting 20°W 200km farther north, and see the topographic charts in Fig. 18).

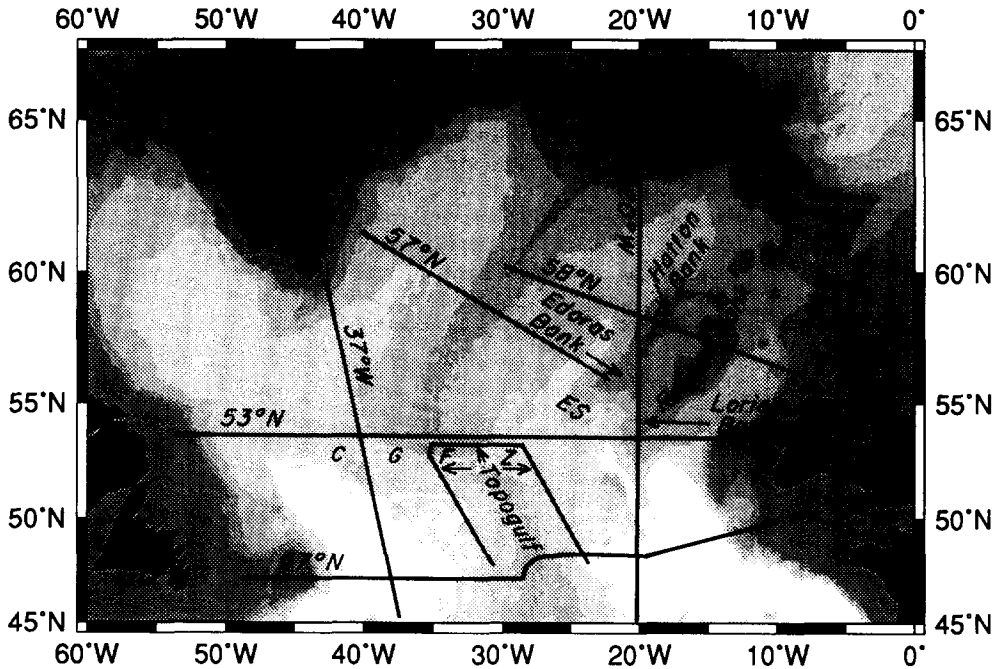


FIG. 18a. Subpolar basin bathymetry contours (from "Etopo 5" data base obtained from the National Geophysical Data Center in 1989, with shading breaks indicating 4000m and 3000m, 2000m and 1000m) and geographic place names referred to in the text. Eriador Seamount, southwest of Edoras Bank, is denoted by ES. Schematic section lines are superimposed on the topography, the individual station locations are given in Figs 18b and c. Property sections along the section lines are: 37°W in Fig. 11, 20°W in Fig. 12, 53°N in Fig. 13, 47°N in Fig. 16, 57°N in Fig. 20, 58°N in Fig. 21 and TOPOGULF in Fig. 22.

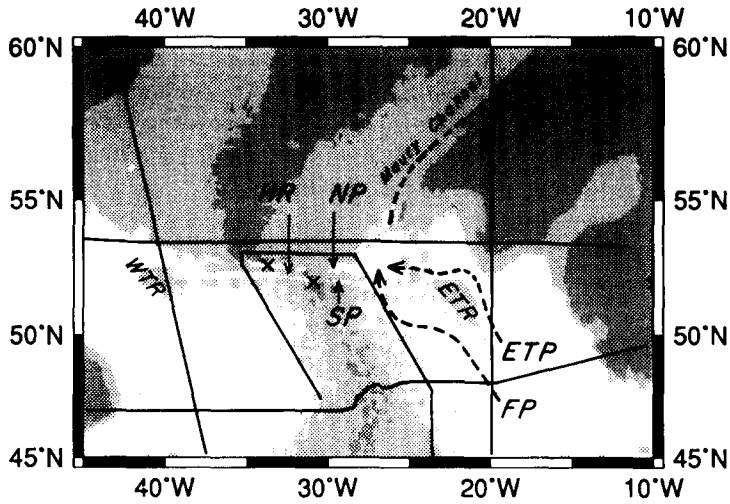


FIG.18b. Bathymetry contours (from "Etopo 5" data base obtained from the National Geophysical Data Center in 1989, with shading breaks indicating 2500m and 3500m) in the West European Basin, the area of the Maury Channel, and the Charlie-Gibbs Fracture Zone. Dots give the station locations for the section lines shown schematically in Fig.18a, x's are two TTO/NAS stations (SCRIPPS INSTITUTION OF OCEANOGRAPHY, 1986), discussed in the text. Letters denote the following features. NP and SP are the northern and south passages of the CGFZ, separated by the HR Hecate Ridge. The sill for the northern passage lies about 75km west of TTO/NAS station 123. The sill for the southern passage lies just east of TTO/NAS station 122. WTR and ETR are the West and East Thulean Rises. ETP and FP are the East Thulean and Faraday Pathways: deep pathways from the central West European Basin to the area at the eastern end of the CGFZ and the Maury Channel in the southern Iceland Basin.

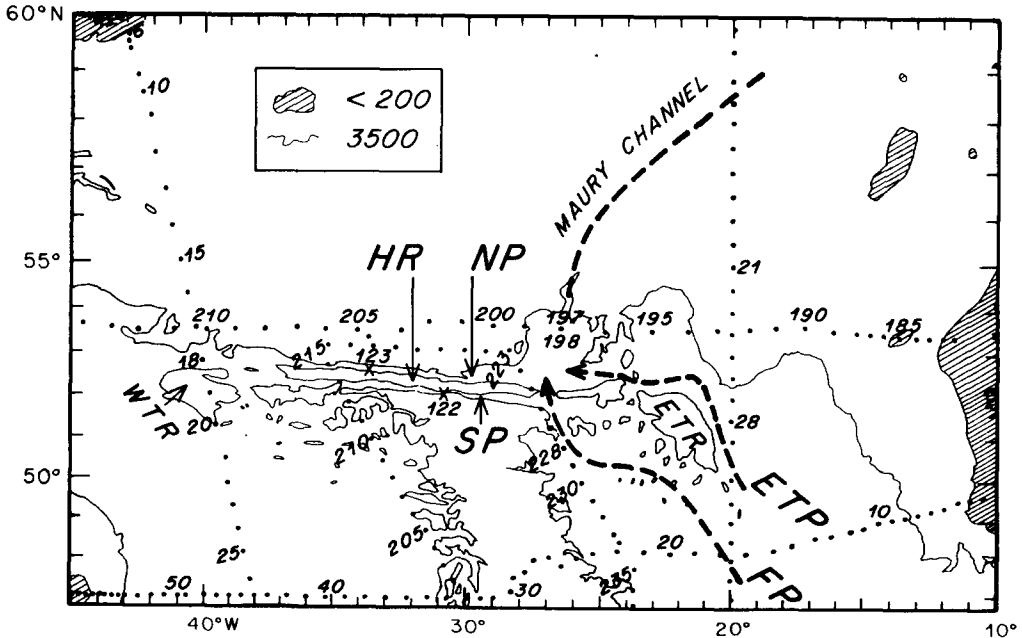


FIG.18c. As Fig.18b, except using 3500m and 200m contours from LAUGHTON and MONAHAN (1984).

At first sight the northernmost vector in Fig. 17 appears to go the wrong way for this DNBC scenario, but it provides a key observation for the present study, allowing the selection of a level-of-no-motion and quantification of the DNBC transport. DICKSON, GOULD, MÜLLER and MAILLARD (1985) noted that a flow reversal with depth occurs over the southern Rockall Plateau. Six full water column moorings over the Plateau flank yielded records consistent with poleward (north and west) flow below 2500m, and reversed flow above about 2000m. They specifically comment that this vector (at 2450m) should be considered part of the reversed flow group. Thus a level-of-no-motion is suggested between 2000m and 2500m, or referring to Fig. 12a, between 2.7°C and 3.3°C. This range falls below the core of the LSW. This level-of-no-motion gives the north and east flow over the Plateau and through the Trough as implied by the LSW distribution, Fig. 7, when applied to the sections of Figs 12 and 13. Below this level-of-no-motion, the DNBC flows westward looping in and out of the Rockall Trough, west across the south flank of the Rockall Plateau, and north into the Iceland Basin.

Along 20°W (Fig. 12) the westward transport, although intensified on the immediate south flank of the Rockall Plateau, accumulates southward over the broader scale of the foot of the Plateau to a deep channel at 46°-47°N as LDW isotherms unevenly descend to their maximum depth near station 38. Part of this westward transport recirculates eastward farther to the south in the West European Basin; south of the deep channel isotherms slope upwards to the south indicating east flow relative to a shallower level-of-no-motion. Geometrically, most of the broader descent of isotherms over the foot of the Rockall Plateau south of the sharp descent at the 3000m isobath is recovered in this broad rise towards the Azores Biscay Rise, so that, in a sense, the net westward transport occurs in the narrow region to the north, and a basin scale gyre occurs to the south of this DNBC. This is the structure adopted for the schematic of Fig. 8. This deep cyclonic gyre appears in the 3000db/4000db dynamic height chart of STOMMEL, NIELER and ANATI (1978). The presence of a recirculating gyre is reminiscent of the STOMMEL and ARONS (1960) model flow pattern discussed above. The distribution of salinity supports this gyre image. The westward flow across 20°W has slightly lower near bottom salinity (≤ 34.91 psu, Fig. 12d) than the eastward flow. The 47°N section shows the northward flowing LDW in the east being the origin of this lower salinity, Fig. 16d.

Figure 19 illustrates for the 20°W section of Fig. 12 the dependence on level-of-no-motion of the estimates of transports of several varieties of LDW, defined by temperature ranges. Three separate station groups are utilized for the calculation: first the narrow DNBC indicated by the sharp rise of isotherms to the north at the southern flank of the Rockall Plateau along 20°W (stations 23 to 27), second the broader region of irregular continued descent to its south (stations 27 to 38) that defines the westward flowing limb of the deep gyre, and third, stations 38 to 44, which define the eastward flowing limb of the gyre. For the coldest layer ($\leq 2.3^\circ\text{C}$), the net westward flow (Fig. 19d) through the West European Basin is 0.8 to 1.4 $\times 10^6 \text{m}^3 \text{s}^{-1}$ based on the DICKSON, GOULD, MÜLLER and MAILLARD (1985) level-of-no-motion range of 2500 to 2000m (2.8° to 3.5°C), resulting principally from the difference between the westward and eastward flowing limbs of the deep gyre. However, for this coldest water, the rough bathymetry of the 20°W section places a great uncertainty on the transport calculations, with the net transport being

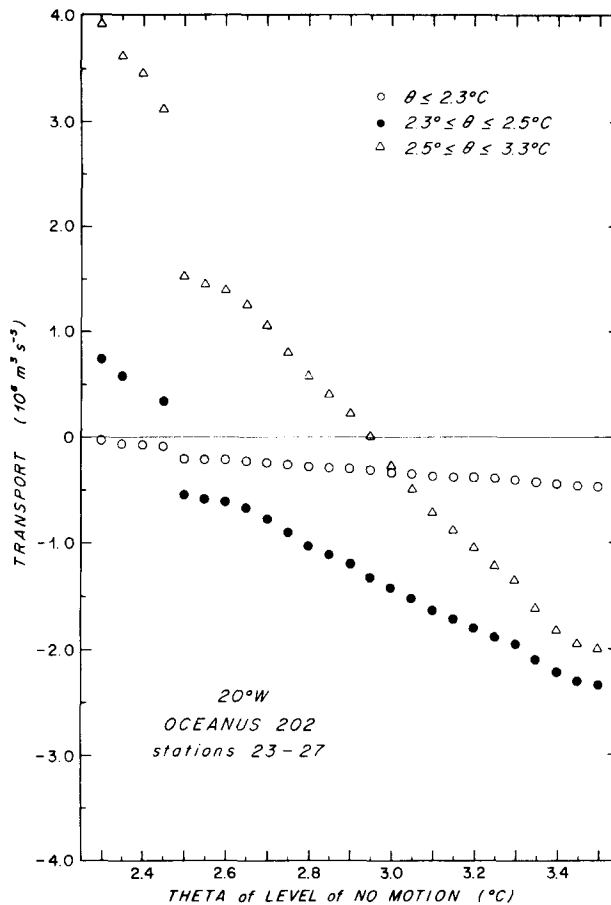


FIG.19a. Volume transports in $10^6\text{m}^3\text{s}^{-1}$ for the indicated temperature classes, as a function of level-of-no-motion, for the narrow DNBC at 20°W .

obtained by subtracting eastward transports in the south (Fig. 19c) of 1.2 to $3.0 \times 10^6\text{m}^3\text{s}^{-1}$, from westward transports in the north (sum of Figs 19a and b) of 1.9 to $4.4 \times 10^6\text{m}^3\text{s}^{-1}$. The greatest uncertainty occurs in the DNBC itself. Stations 26 and 27 document a 600m rise of the 2.3°C isotherm, but the isotherm lies almost completely in the bottom triangle where shear has to be extrapolated downwards. Thus the westward transport of the coldest water in the DNBC 0.3 to $0.5 \times 10^6\text{m}^3\text{s}^{-1}$ (Fig. 19a) is potentially poorly estimated. The presence of 2.2°C water at the base of the shear signature of the DNBC along the *Erika Dan* section, Fig. 13, may indicate that some of the colder water may be transported north towards the Iceland Basin, but sampling along that section is too inadequate to be certain, again because of the bottom triangle problem (here about 1500m).

Between 2.3°C and 2.5°C along 20°W , there is much less involvement of the bathymetry south of the DNBC, and the transports are better defined there, although the bottom triangle problem still influences the DNBC estimate. The narrow westward flow of the DNBC at 20°W (Fig. 12) ranges between 1.0 and $2.3 \times 10^6\text{m}^3\text{s}^{-1}$ (Fig. 19a), while the westward flowing limb of the deep gyre to its south adds 0.4 to $1.2 \times 10^6\text{m}^3\text{s}^{-1}$ (Fig. 19b), giving a total westward transport in the north of 1.4 to $3.5 \times 10^6\text{m}^3\text{s}^{-1}$. But the eastward flowing limb of the deep gyre (Fig. 19c) partly balances

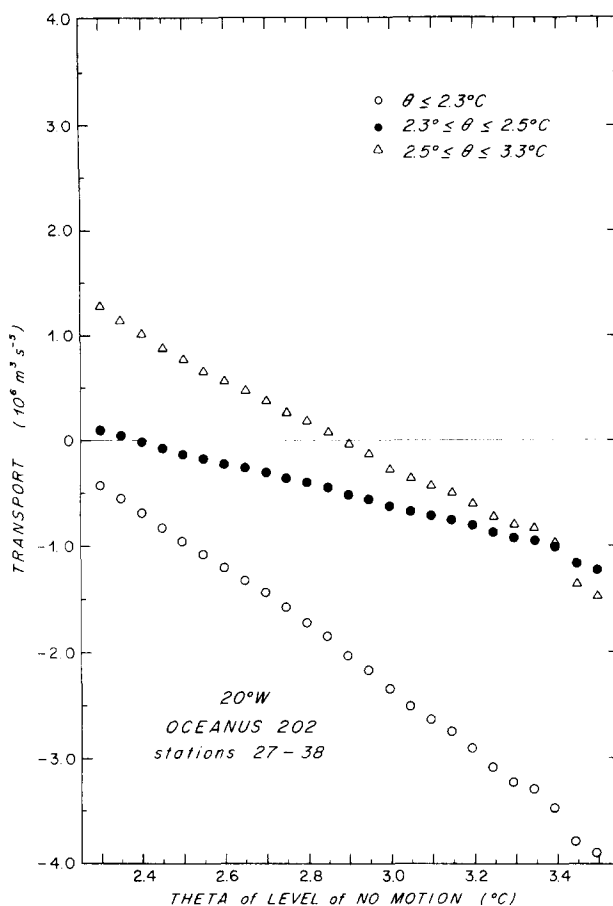


FIG. 19b. As Fig. 19a, but for the westward flowing limb of the deep gyre in the West European Basin.

the westward flowing limb, leaving a residual net westward transport through the West European Basin of 1.0 to $2.2 \times 10^6 \text{ m}^3 \text{ s}^{-1}$ in this temperature class (Fig. 19d).

These ranges, reflecting reference levels between 2.8° and 3.5°C are rather broad. A candidate for best reference level choice is 3.3°C , to achieve eastward flow of all of the LSW core layer and with an average depth in the middle of the DICKSON, GOULD, MÜLLER and MAILLARD (1985) range. With this choice the narrow DNBC transport for the 2.3° to 2.5°C layer (Fig. 19a) is $2.0 \times 10^6 \text{ m}^3 \text{ s}^{-1}$, the westward limb of the deep gyre (Fig. 19b) adds $0.9 \times 10^6 \text{ m}^3 \text{ s}^{-1}$, while the eastward limb of the deep gyre (Fig. 19c) subtracts $1.1 \times 10^6 \text{ m}^3 \text{ s}^{-1}$ to give a net westward flow through the West European Basin of $1.8 \times 10^6 \text{ m}^3 \text{ s}^{-1}$ between 2.3° and 2.5°C . Adding the less well defined (preceding paragraph) net transport below 2.3° for a 3.3°C reference level gives a net westward transport below 2.5°C of $2.9 \times 10^6 \text{ m}^3 \text{ s}^{-1}$ and a cyclonic gyre recirculation of $3.9 \times 10^6 \text{ m}^3 \text{ s}^{-1}$. This agrees well with the estimate of $1.89 \times 10^6 \text{ m}^3 \text{ s}^{-1}$ colder than 2.5°C for the 36°N section well to the south in the Madeira Basin previously discussed, although here the average temperature of the flow below 2.5°C has warmed. Geometrically the best way to visualize this is as sketched in Fig. 8: the northern part of the west flow continues on as a DNBC component, while the southern part is a limb of a recirculating gyre. The dense overflows in the eastern basin part of Fig. 2 amount

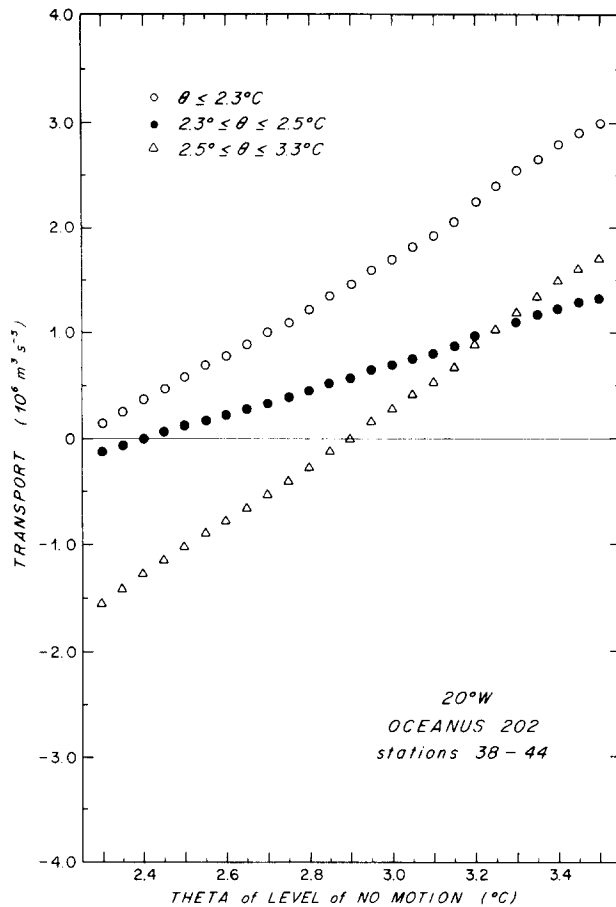


FIG. 19c. As Fig. 19a, but for the eastward flowing limb of the deep gyre in the West European Basin.

to $2.7 \times 10^6 \text{ m}^3 \text{ s}^{-1}$ so indicating rough equality between the northern source and southern source contributions to the DNBC in the eastern basin.

The next warmer class of LDW, 2.5°C to 3.3°C , spans a salinity maximum layer in the LDW beneath the LSW. The salinity section (Fig. 12d) shows that this layer is restricted to the West European Basin, north of the Azores Biscay Rise, with a sharp transition to the lowest parts of the Mediterranean outflow salt tongue south of the Rise. The salinity maximum layer laterally coincides with the deep gyre and DNBC in the West European Basin, whose shear signatures extend up through this layer to the LSW. The direction of flow reverses for the range of reference levels described above, since they fall within the temperature range defining the layer. The net flow in this layer shifts from a westward $1.8 \times 10^6 \text{ m}^3 \text{ s}^{-1}$ for a 3.5°C reference level to an eastward $0.5 \times 10^6 \text{ m}^3 \text{ s}^{-1}$ for a 2.8°C reference level. A small net westward transport of $1.0 \times 10^6 \text{ m}^3 \text{ s}^{-1}$ occurs for the favored reference level of 3.3°C , with the DNBC transporting $1.4 \times 10^6 \text{ m}^3 \text{ s}^{-1}$ westward (Fig. 19a), the northern gyre limb $0.8 \times 10^6 \text{ m}^3 \text{ s}^{-1}$ westward (Fig. 19b), and the southern gyre limb $1.2 \times 10^6 \text{ m}^3 \text{ s}^{-1}$ eastward (Fig. 19c). This gyre aspect seems responsible for the lateral homogeneity of the salinity maximum layer in the West European Basin, which is in marked contrast to the strong meridional gradients of salinity in the same depth range in the Iberian Basin (Fig. 12d). With

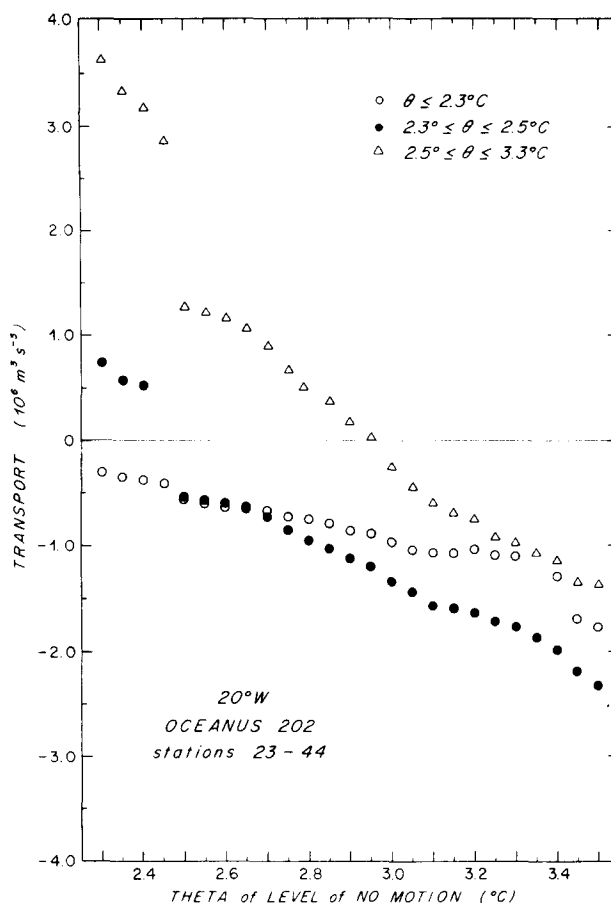


FIG.19d. As Fig.19a, but for the net flow in the West European Basin.

this 3.3°C reference level there is a net eastward flow of LSW (3.3°C to 4°C) amounting to $1.1 \times 10^6 \text{m}^3 \text{s}^{-1}$ with only a slight gyre structure and an eastward net transport of $13.4 \times 10^6 \text{m}^3 \text{s}^{-1}$ of water warmer than 4.0°C is indicated between stations 23 and 44. This warm water transport is similar to the estimated total of the warm to cold water conversion in the northern North Atlantic, e.g. $13.0 \times 10^6 \text{m}^3 \text{s}^{-1}$ by WORTHINGTON (1970) (see Fig.4); $15.6 \times 10^6 \text{m}^3 \text{s}^{-1}$ by HALL and BRYDEN (1982); and $14.1 \times 10^6 \text{m}^3 \text{s}^{-1}$ by McCARTNEY and TALLEY (1984) (see Fig.6).

3.1.5. Deepflow in the Iceland Basin. To complete the documentation of the flow of southern origin waters in the eastern basin, we shift attention northwards to the Iceland Basin. The Iceland Basin is confined between the Rockall Plateau and the Reykjanes Ridge (Fig.18), with its maximum depth axis north of 54°N being the Maury Channel along the base of the west flank of the Plateau (west of Eriador Seamount, Edoras Bank and Hatton Bank). According to the topography of LAUGHTON and MONAHAN (1984) (Fig.18c), there are two distinct pathways connecting the Maury Channel at 54°N west of the Plateau to the 20°W section south of the Plateau, shown as dashed contours in Fig.18b. One pathway begins at 50°30'N and passes between the East Thulean Rise and the Lorient Bank, the southernmost tip of the Rockall Plateau, and is

silled between 3600 and 3700m. In addition to this being a pathway to the Iceland Basin, it also passes along the eastern end of the northern passage of the CGFZ at 52°30'N. For convenience, I call this the "East Thulean Pathway". The other pathway passes through very rough topography along the flank of the Mid-Atlantic Ridge and through a sill of similar depth at 27°W, 53°N. The rough topography is part of the Faraday Fracture Zone, so for convenience I call this the "Faraday Pathway". Its sill is a fissure through the median transform ridge that separates the northern and southern passages of the CGFZ. Parts of this dividing wall are called the Hecate Bank, so for convenience I call this elongated wall the Hecate Ridge. The current vectors in Fig. 17 include two near 20°W at the eastern end of each of these two pathways; both indicate strong flows into them. DICKSON, GOULD, MÜLLER and MAILLARD (1985) describe the southern of the two vectors as a confirmation of C.G.H. Rooth's personal communication to them suggesting the Faraday Pathway (which they called "Maury Channel", Fig. 17) as a conduit carrying cold water from the West European Basin to the Iceland Basin. The East Thulean Pathway would seem to be an equally viable candidate, as it is similarly silled; both pathways lead to the eastern end of the northern passage of the CGFZ which in turn connects to the Maury Channel west of Rockall Plateau.

The *Erika Dan* section (Fig. 13) is at a latitude of 53°30'N, and shows water as cold as 2.19°C in the East Thulean Pathway at the base of the flank of the Lorient Bank. The section passes south of Eriador Seamount at 25°W (Fig. 18), close enough to record part of the isotherm slope reversal associated with the DNBC following the Rockall Plateau. Stations 196 to 198 are just to the south of the Maury Channel, in the eastern part of the northern passage of the CGFZ, into which both deep Pathways from 20°W lead. These stations defined a northward flow (rising isotherms to the east) with a coldest observed temperature of 2.51°C (160m above local maximum depth). Later stations in this area (SCRIPPS INSTITUTION OF OCEANOGRAPHY, 1986; HARVEY and ARHAN, 1988) showed coldest temperatures at the bottom in this area, near 2.35°C, and high-silicate values, confirming the southern origin of the waters. These temperatures are consistent not only with the 3600 to 3700m sill acting on the East Thulean Pathway temperature profile west of Lorient Bank in the *Erika Dan* section (Fig. 13), but also with the similar sill depth at the fissure of the Hecate Ridge acting on the Faraday Pathway temperature profile.

This spot in the eastern CGFZ will be discussed further below, but first the flow of the DNBC in the Iceland Basin will be considered. Figure 20 shows a section crossing the west side of the Rockall Plateau, the Iceland Basin, the Reykjanes Ridge, and the Irminger Basin (Fig. 3 and 18a). This section was the basis of the MANN, COOTE and GARNER (1973) inference of northward flow of AABW from the mid-latitude eastern basin to the Iceland Basin. The eastern intersection of this section with the Rockall Plateau north of Edoras Bank is 250km farther north (Fig. 18a) than the *Erika Dan* section shown in Fig. 13, and the Iceland Basin between the Plateau and the Reykjanes Ridge has shoaled from 4000m to 3200m, with the deepest part being the Maury Channel. Coldest temperatures are correspondingly higher at 2.5°C. The shear signature of northward flow is indicated through the rise of isotherms towards the Plateau (stations 68 to 70), here better resolved than in the *Erika Dan* section. Both sections show the northward flow of the DNBC as being very narrow with a sharp eastward rise of isotherms, in contrast to the broad southward flow seen along the east flank of the Reykjanes Ridge. The high-silicate LDW influence is apparent, extending westwards beyond the northward flow of the DNBC into the southward flow along the Reykjanes Ridge. In the southward flow along the Reykjanes Ridge, one station (67) shows silicate increasing to a maximum of 27µmol l⁻¹ at the bottom, at a temperature of 2.51°C. Farther up the Ridge, the highest silicate water is undercut by lower silicate water, so the southern source water appears as a silicate maximum typically 200m above the bottom. The LDW influenced water (higher silicate and lower oxygen) flowing north thus loops

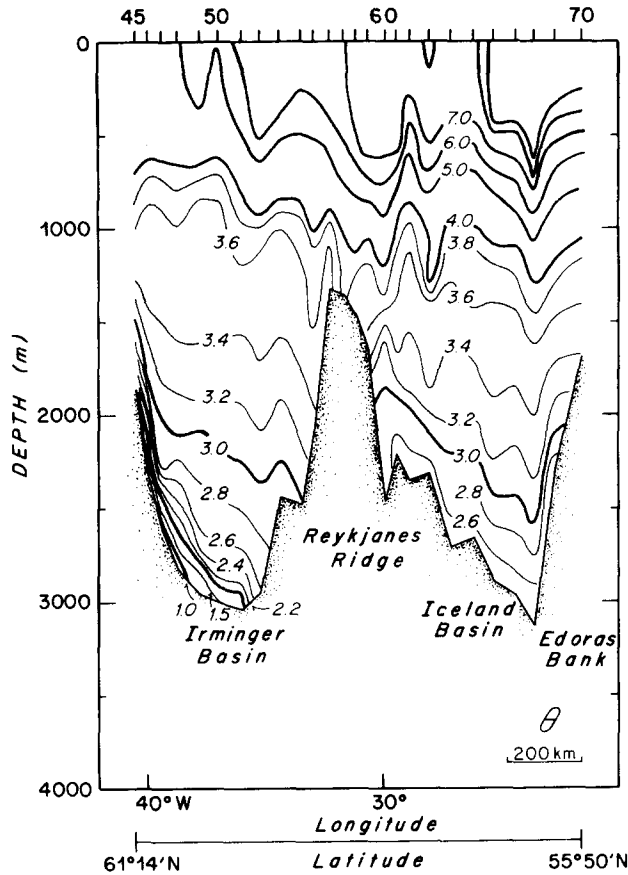


FIG.20a. Quasi-zonal section of potential temperature ($^{\circ}\text{C}$) along the Hudson 57°N transect (nominal latitude, see Figs 3 and 18) in February-March 1967 (GRANT, 1968).

and returns with the waters from the Faroe Bank Channel and Iceland-Faroe Ridge Overflows that flow southwest along the east flank of the Reykjanes Ridge. This is the entrainment of LDW influenced water into the dense overflow fed DNBC that is included in the schematic of Fig.8. In parallel with this silicate image, the oxygen distributions of the *Erika Dan* section (Fig.13b) and the *Discovery* 53°N section (WORTHINGTON, 1959) show low oxygen near the bottom over the east flank of the Reykjanes Ridge, where the southwest flow of the DNBC occurs. Silicates were determined at *Erika Dan* stations 198, 200, 201, 203 to 206 (Fig.18b for locations). The first two stations, over the deeper levels of the Reykjanes Ridge, show near bottom silicates of $20\text{--}24\mu\text{mol l}^{-1}$, the other stations, higher up the Ridge flank, have lower bottom silicates of $13\text{--}16\mu\text{mol l}^{-1}$.

The flow from south of Rockall northwards into the Iceland Basin shapes the sediments of the Hatton Drift along its northward path and along the Gardar Drift on the eastern flank of the Reykjanes Ridge as it loops back to the south, as described by McCAYE, LONSDALE, HOLLISTER and GARDNER (1980). They also note that the deep water is of lower salinity and higher silicate indicative of its being "contaminated with" AABW.

An idea of how far this loop of southern originating DNBC water extends to the northeast into

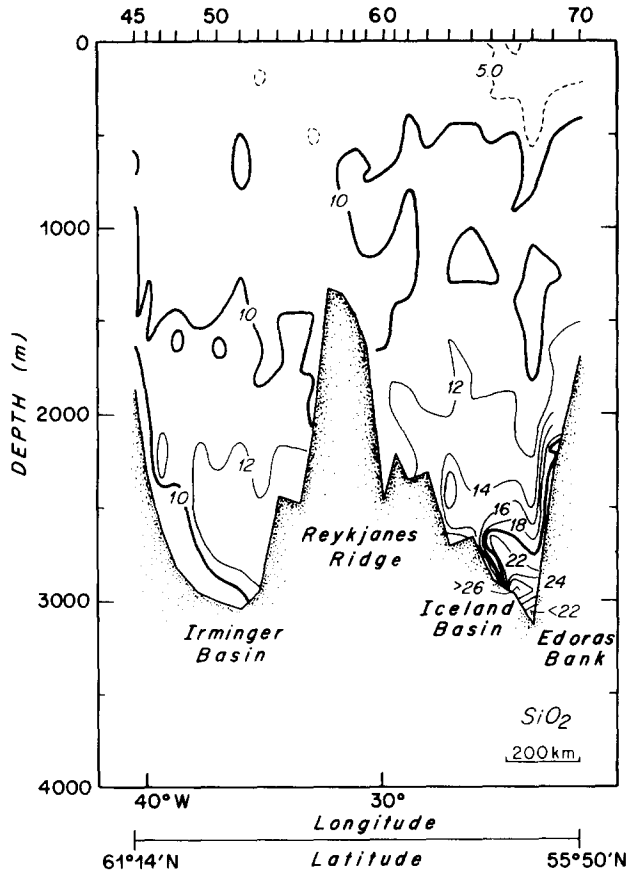


FIG.20b. Quasi-zonal section of silicate ($\mu\text{mol l}^{-1}$) at 57°N , as Fig.20a.

the Iceland Basin before looping west and back southwest is given by the 20°W section (Fig.12). The northern Iceland Basin is crossed meridionally, centered at 20°W and 60°N , where maximum depths have shoaled farther to less than 2800m. The Faroe Bank Channel and Iceland-Faroe Ridge Overflows have already descended through the depth range of the LSW, and have been warmed well above 2°C . The more northern stations show the typical elevated salinity and oxygen levels of the overflow, and silicate levels less than $10\mu\text{mol l}^{-1}$. At the deepest part of the section, there is less overflow influence, with highest oxygen ($\geq 6.4\text{ml l}^{-1}$), and lowest silicates ($\leq 12\mu\text{mol l}^{-1}$) at the very bottom, and an oxygen minimum ($\leq 6.3\text{ml l}^{-1}$) and silicate maximum ($\geq 15\mu\text{mol l}^{-1}$) centered about 300m above the bottom at a temperature near 3°C . These characteristics require an admixture of LDW, for neither the overflow waters, nor the entrained warm waters, nor the entrained LSW have the necessary low-oxygen and high silicate. TTO station 142 in the Faroe Bank Channel (SCRIPPS INSTITUTION OF OCEANOGRAPHY, 1986) shows that neither the very cold and dense overflow water nor the local SPMW that overlies it, have silicate levels greater than $10\mu\text{mol l}^{-1}$ or oxygen values less than 6.4ml l^{-1} . The silicate levels for the LSW at 20°W (Fig.11c) and in the older section shown in Fig.18 are 10 or $11\mu\text{mol l}^{-1}$, and oxygen values about 6.4-

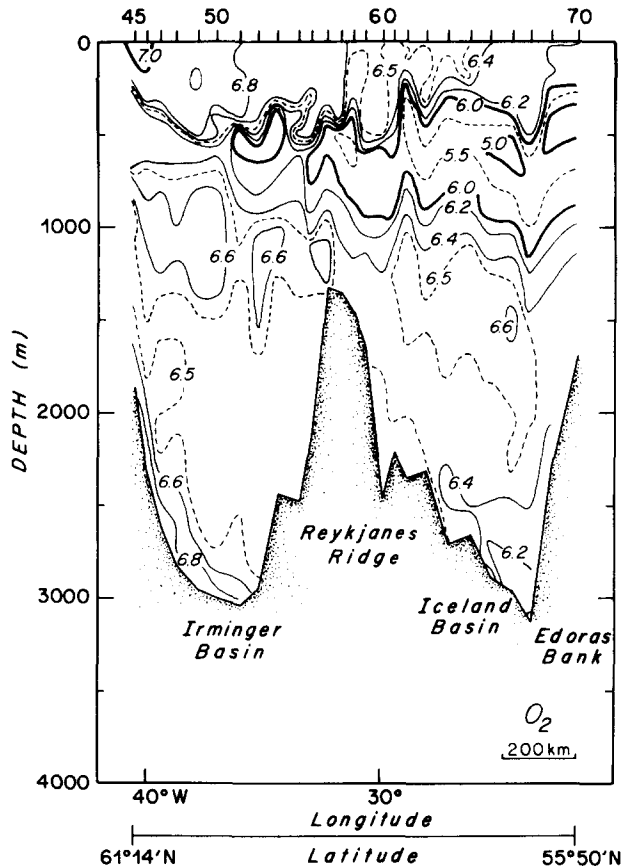


FIG.20c. Quasi-zonal section of oxygen (ml l^{-1}) at 57°N , as Fig.20a.

6.6 ml l^{-1} . None of these can supply the higher silicate and lower oxygen water observed.

The simplest explanation of the high-silicate “nose” in the northeast Iceland Basin is that it represents the northeast protrusion of the LDW influenced loop of the DNBC described above. The northeast limit of the loop may be close to the 20°W section, since the nose is practically at the sea floor, and the shear normal to the section is westward throughout the Iceland Basin with only the slightest indication of isotherm slope reversal at the Hatton Bank of the Rockall Plateau. A nearly orthogonal section (Fig.21) which intersects the 20°W section at this Hatton Bank location (20°W station 14, Fig.12) still shows the isotherm bowl that is the geostrophic signature of the loop, with steeply rising isotherms at the intersection with 20°W , and an oxygen minimum spanning the bowl, as well as elevated silicates⁴. This suggests a nearly northward flow along

⁴The IGY sections from the third *Discovery* IGY cruise (at 43°N , 46°N , 53°N and 58°N , Fig.14) includes silicate determinations (WORTHINGTON, 1959); only the distribution at 58°N is shown here, Fig.21. Overall these silicate data are noisy and appear to have magnitudes about 20% higher than modern data; probably a standardization problem.

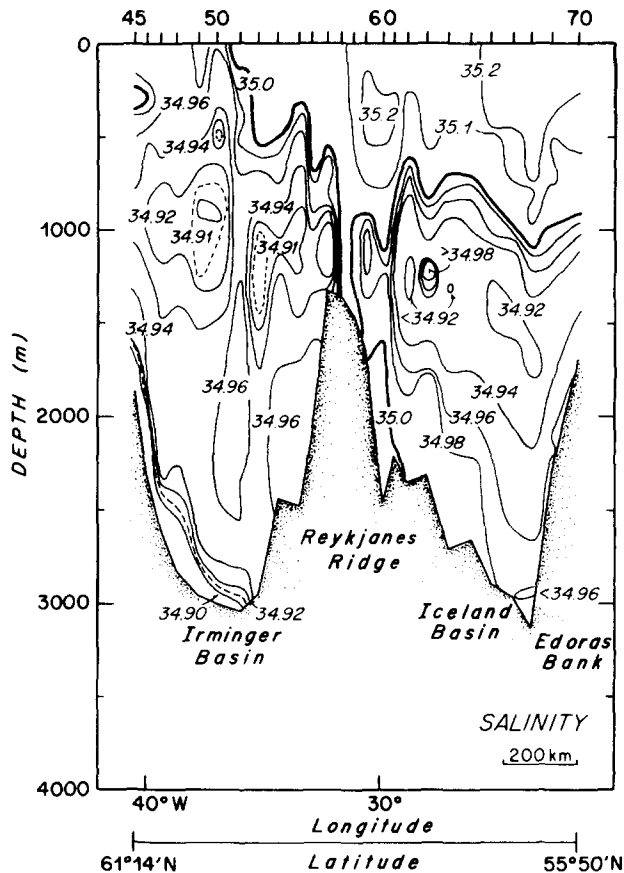


FIG.20d. Quasi-zonal section of salinity at 57°N, as Fig.20a.

20°W. It thus appears that as the basin shoals northward, the northward flow of the DNBC along the west flank of the Rockall Plateau leaves the flank and turns west and southwest in its interaction with the west and southwest flow of the combined Faroe Bank Channel and Iceland-Faroe Ridge Overflows, and that this is a source of lower oxygen and higher silicate waters compared to other waters which become entrained into the Overflows.

Over the eastern flank of the Reykjanes Ridge, the broad region of eastward descending isotherms (Figs 12, 19 and 20) is the signature of the southwest flow of the DNBC towards the CGFZ. This is usually identified as the flow of the Iceland-Scotland Overflow Water, but the discussion above suggests this to be a bit of a misnomer, not only because of the large amounts of entrainment of both warmer waters and LSW that must occur to elevate the temperature above 2.4°C, but also because a significant flux of LDW from the south is involved. It appears that the farther downslope along the Ridge flank one samples, the stronger is the influence of the LDW. The classic image (e.g. Figs 4 and 2) has this southwest flow, dominated by the Overflows, turn west through the CGFZ. There is a possibility of a fairly direct flow of LDW from the East Thulean and Faraday Pathways to the sill region of the CGFZ, which is included on the LDW schematic

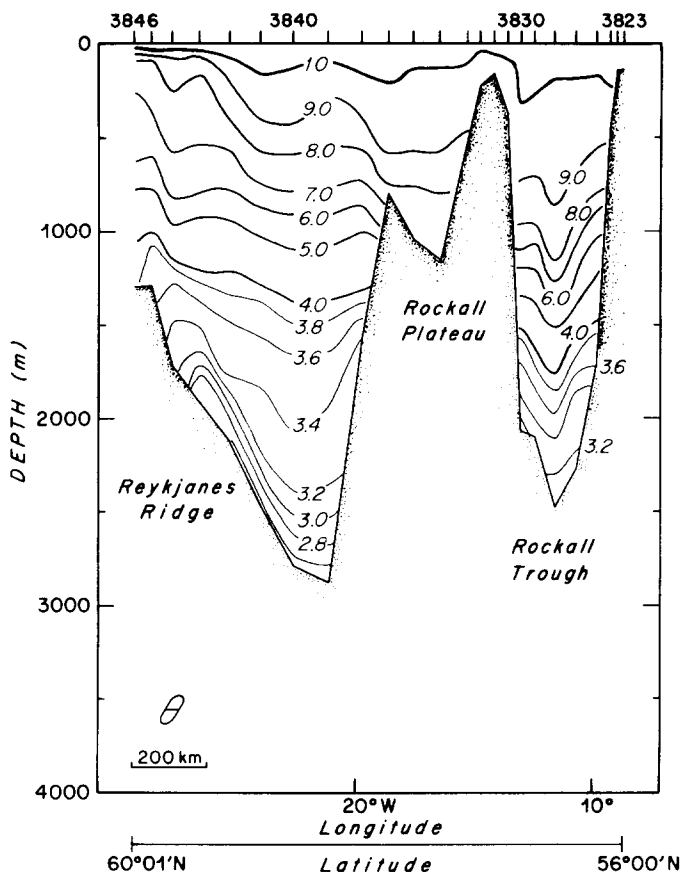


FIG.21a. Quasi-zonal section of potential temperature ($^{\circ}\text{C}$) along the *Discovery II* 58°N transect (nominal latitude, see Figs 3 and 18) in August 1958. (FUGLISTER, 1960; WORTHINGTON, 1959).

of Fig.8 as emanating from the western limit of the West European Gyre flow.

Corroboration of this overall scenario of the northward flowing LDW at the eastern boundary feeding a DNBC that flows west to the south of Rockall and then north into the Iceland Basin is found in the tritium data reported by ÖSTLUND and GRALL (1987). Sampling in this general area has been far too sparse to resolve the narrow flow components described here, but the data are suggestive nonetheless. A section from the Faroe Bank Channel down the central axis of the Iceland Basin to near 53°N (their page 23), shows the water in the Channel having tritium greater than 1.56 TU81N through the entire water column (lowest in the very cold water at the bottom and greater than 2.9 TU81N for temperatures above 0°C). South along the section a low-tritium layer, ≤ 1.5 TU81N, "intrudes" from the south beneath the higher tritium water. A quasi-zonal section (their page 29, also Fig.8b in ÖSTLUND and ROOTH, 1990) was made from the central Labrador Sea to the Bay of Biscay which crosses over the southern part of the Iceland Basin and passes south of the Rockall Plateau. East of the Reykjanes Ridge tritium is ≤ 1.5 TU81N below 2000m almost everywhere, and is ≤ 1.0 TU81N in the northern part of the West European Basin south of the Rockall Plateau. This is consistent with the predominance of LDW in the West

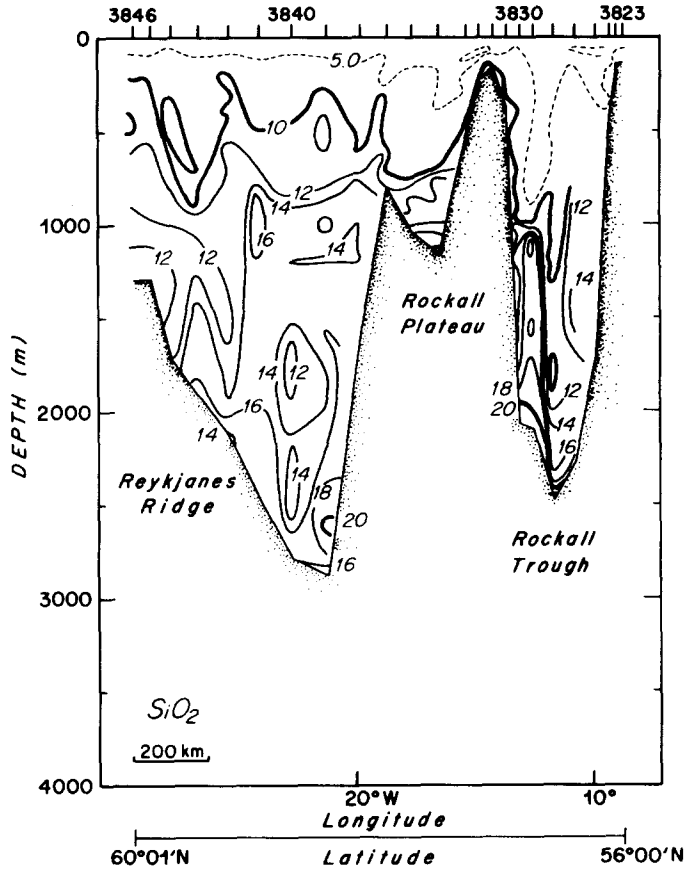


FIG.21b. Quasi-zonal section of silicate ($\mu\text{mol l}^{-1}$) at 58°N, as Fig.21a.

European Basin and its intrusion northward into the Iceland Basin and westward towards the CGFZ. Their quasi-zonal section farther north (their page 27, also Fig.8a in ÖSTLUND and ROOTH, 1990) passes from southeastern Greenland in the west across the Rockall Trough in the east. It shows low tritium LDW ($\leq 1.0 \text{ TU8IN}$) intruding into the Rockall Trough from the south, and a low tritium layer ($\leq 1.5 \text{ TU8IN}$) "draped" over the Rockall Plateau in a fashion similar to the low oxygen layer in the *Erika Dan* section, Fig.12b. These low-tritium levels confirm the southern origin of the LDW penetrating well northward into sub-polar latitudes of the eastern basin.

3.1.6. Deepflow at the Charlie-Gibbs Fracture Zone. The southwest return flow of the DNBC along the east flank of the Reykjanes Ridge crosses the Ridge to the western basin where the Ridge deepens southward, principally near the CGFZ (53°N, Fig.18). WORTHINGTON (1970, 1976) reviews most of the early work on this region that leads to the picture (Figs 3 to 5) of the DNBC looping southwest along the eastern flank of the Reykjanes Ridge, turning westward through the CGFZ, and turning north into the Irminger Basin. WORTHINGTON and VOLKMANN (1965) estimated the westward transport at the CGFC to be $4.6 \times 10^6 \text{ m}^3 \text{ s}^{-1}$ below the level-of-no-motion in the lower LSW. The westward turn is not actually restricted to the CGFZ except at the coldest

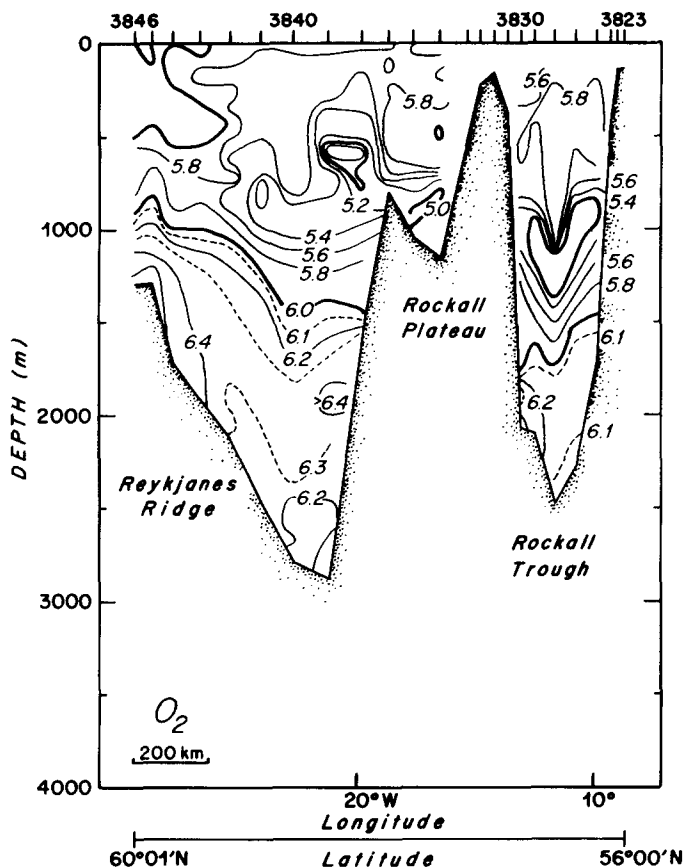


FIG.21c. Quasi-zonal section of oxygen (ml l^{-1}) at 58°N , as Fig.21a.

levels. For example, in the section of Fig.20, elements of the DNBC system reach as shallow as the LSW near 1500m, and these shallow components can turn west near 59°N well north of the CGFZ. The strongest overflow influence at this section appears at station 60 between 1600 and 2300m. A passage through the Reykjanes Ridge near 55°N provides the first opportunity for westward flow as deep as 2500m, still well north of the CGFZ. The first bolus of higher silicate LDW along this section occurs at station 64 near 2500m, but the strong LDW layer seems mostly deeper than that, so the silled passages of the CGFZ are the only route for westward flow of this denser water. Other studies (GARNER, 1972; SCHMITZ and HOGG, 1978; DICKSON, GURBUTT and MEDLER, 1980; SHOR, LONSDALE, HOLLISTER and SPENCER, 1980) have discussed current meter measurements in the two deep passages of the CGFZ, which have sill depths between 3600 and 3700m. An estimate of westward transport of $2.4 \times 10^6 \text{m}^3 \text{s}^{-1}$ below 2000m (about 3.1°C) in the northern deep passage of the CGFZ is reported by SHOR, LONSDALE, HOLLISTER and SPENCER (1980), although the array utilized did not sample the full passage width, being restricted to the north side of the passage. DICKSON, GURBUTT and MEDLER (1980) found the southern passage to have mean westward flow in the north, but mean eastward flow in the south, with the opposing

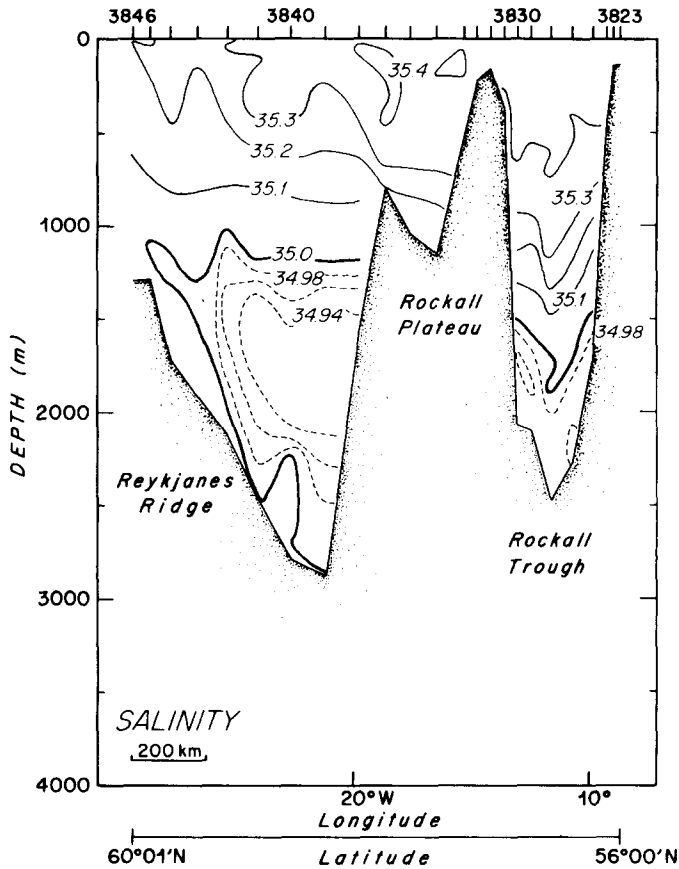


FIG.21d. Quasi-zonal section of salinity at 58°N, as Fig.21a.

flows nearly cancelling. The total flow field apparently not being resolved, they did not estimate total transport, and questioned the SHOR, LONSDALE, HOLLISTER and SPENCER (1980) northern passage estimate on the basis of the restriction of its measurement to the north side of the passage.

SAUNDERS (1992) reports on transport estimates from 13-month-long records at eight moorings spanning both passages of the CGFZ. His preliminary estimate of $2 \pm 0.5 \times 10^6 \text{ m}^3 \text{ s}^{-1}$ has been upgraded to $2.4 \pm 0.5 \times 10^6 \text{ m}^3 \text{ s}^{-1}$ (personal communication), and represents the westward transport of water more saline than 34.94 at 35°W between 51°45'N and 52°50'N. His continuing analysis may yield information on the relations of this measurement to the transport of the less saline component at this location, and to possible additional westward flow north and south of the array. Perhaps it will ultimately yield a transport estimate for $\sigma_\theta > 27.8$ to be added to Fig. 2.

HARVEY (1980) summarized available hydrographic data for the area, and noted that bottom water temperatures colder than 2.2°C are found in the Labrador Basin, but that the coldest water east of the CGFZ sills appears to be warmer than 2.4°C at depths below 3000m. With temperatures this cold and depths this deep, there is (Figs 20 and 12) a possibility that fairly strong LDW could be present at the sill area of the CGFZ. On the other hand, SHOR, LONSDALE, HOLLISTER and

SPENCER (1980) reported two short sections just west of the sill of the northern passage near 35°W, with bottom temperatures colder than 2.30°C, silicate values less than 15.2 μmol l⁻¹, and oxygen as high as 6.55 ml l⁻¹, which is clearly western basin water. They interpreted this as representing western basin water flowing westward in the northern passage, which they explained by eastward flow in the southern passage (to the west of its sill at 30°W), turning north through a fissure in the Hecate Ridge between the two passages, and then turning west to flow over the northern passage sill to the point of their observation. While this is possible, SCHMITZ and HOGG (1978) have noted that the strong low-frequency variability in their own current meter records could support eastward flow for long enough to pull water from the Labrador Basin to the sill, in opposition to a long-term mean westward motion.

Included in the circulation schematic of Fig. 8 is a contour which shows a fairly direct flow from the neighborhood of the southern Rockall Plateau to the CGFZ with minimal looping into the Iceland Basin and thus with minimum interaction with the dense overflow water. One way to think about it is that the northern loop represents a southern influence on the northern source waters, while conversely the direct path is more a southern source flow influenced by northern source waters. This direct path appears to be part of a westward extension of the deep gyre and DNBC south of the Rockall Plateau to the neighborhood of the sills of the two deep passages of the Zone. MANTYLA and REID (1983) show high-silicate LDW at the bottom penetrating west to almost 30°W. Evidence is shown in Fig. 22 for the circulation that brings this high-silicate LDW so far west. This hydrographic section has three legs, the central one oriented almost zonally near 53°N, just to the north of the northern passage of the CGFZ, and the other two almost northwest-southeast at mean longitudes of 26°W and 33°W, bracketing the Mid-Atlantic Ridge and crossing the CGFZ on both sides of the Ridge (Fig. 18). These TOPOGULF sections have been discussed in detail by HARVEY and ARHAN (1988).

On the broadest scale the central and eastern legs of the section show isotherms descending irregularly eastward (stations 215 to 223) from the crest of the Reykjanes Ridge just northwest of the sill of the northern passage (at 34°57'W, 52°42'N, depth 3675m according to SHOR, LONSDALE, HOLLISTER and SPENCER, 1980) and southeastward across the CGFZ (stations 223 to 228). Isotherms then sharply reverse slope to rise southeastward (stations 228 to 231) and become more or less level in a region with significant mesoscale wiggles (stations 231 to 241). Station 228, where isotherms reach maximum depth, was situated at the maximum depth location in the Faraday Pathway at this longitude. Thus the TOPOGULF section shows an isopycnal bowl centered on the Faraday Pathway. At 20°W (Fig. 12) station 38 at the maximum depth of the eastern entrance to this Pathway also has maximum isotherm depth, and defined the southern limit of the westward flow of the deep gyre discussed above. This similarity of isopycnal geometry and the continued association of the isopycnal bowl with the Faraday Pathway suggest the extension of the deep gyre across the intervening 450km. The mean velocities of DICKSON, GOULD, MÜLLER and MAILLARD (1985) show strong flow into the Pathway (Fig. 17). At the TOPOGULF section the overall shear signature for the westward flow parallel to the CGFZ (stations 223 to 228) is stronger (steeper slope and greater total isopycnal descent) than the shear signature for the southwestward flow along the Reykjanes Ridge towards the north wall of the northern passage of the CGFZ (stations 215 to 223), which is the traditional DNBC flow path to the CGFZ.

The second evidence for the westward extension of the deep gyre to the TOPOGULF section is the presence of high-silicate and low-oxygen LDW (hereafter "more extreme" LDW) in the lower samples of stations 221 to 224 and 226 to 241 (Fig. 22). Bottle sampling is too coarse (mostly 500m) to allow determination of the thickness of this more extreme LDW, which usually appears only in the deepest bottle, typically sampling 100m above the bottom. Given the sections across

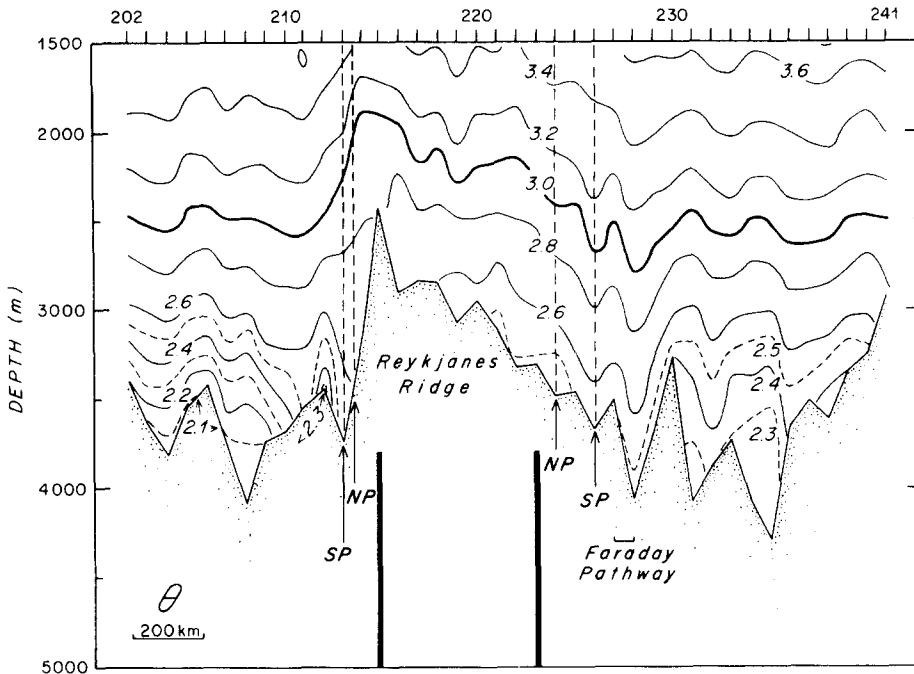


FIG. 22a. Section of potential temperature ($^{\circ}\text{C}$) along the TOPOGULF section. The central panel is zonally oriented from the crest of the Reykjanes Ridge eastward, just north of the CGFZ. The left panel is quasi-meridional passing south from the left (west) end of the central panel just west of the sill of the northern passage of the CGFZ and 300km west of the sill of the southern passage. The right panel is also quasi-meridional passing south from the right (east) end of the central panel 500km east of the northern sill and 200km east of the southern sill. Detailed topography is not available for this cruise. NP and SP denote the northern and southern passages of the CGFZ and HR the Hecate Ridge dividing the two passages, according to LAUGHTON and MONAHAN (1984) bathymetry, Fig. 18c. The vertical lines denote the location of the northwest and northeast corners of the section. See Figs 3 and 18. HARVEY and ARHAN, 1988, data in TOPOGULF GROUP (1986).

the Iceland Basin (Figs 12, 20 and 21), the more extreme the LDW observed at the CGFZ, the less of a loop into the Iceland Basin the LDW can have taken. For example, at TOPOGULF station 221, well up the flank of the Reykjanes Ridge in 3150m of water and well above the CGFZ sill depth, the bottom silicate of $28.0\mu\text{mol l}^{-1}$ and oxygen of 5.95ml l^{-1} are the most extreme of any sample along the *Hudson* section of Fig. 20, but on the other hand are indistinguishable from the water at the same temperature south of Rockall along 20°W (Fig. 12) in the area of the westward flow of the DNBC and the northern limb of the deep gyre. Unfortunately, neither the deepest water sample at TOPOGULF station 220 nor the two deepest water samples at station 219 were obtained, so the degree of penetration of this LDW up the slope of the Reykjanes Ridge cannot be ascertained from these data. The salinity data (HARVEY and ARHAN, 1988, their Fig. 14), shows the associated low-salinity layer defined by the 34.96psu contour reaching west to station 219 but not to 218, suggesting a westward limit of about 32°W for this area just north of the CGFZ. A TTO/NAS station (123, SCRIPPS INSTITUTION OF OCEANOGRAPHY, 1986) in the middle of the northern passage of the CGFZ (Fig. 18b) about 50km south of TOPOGULF station 217 shows silicate as

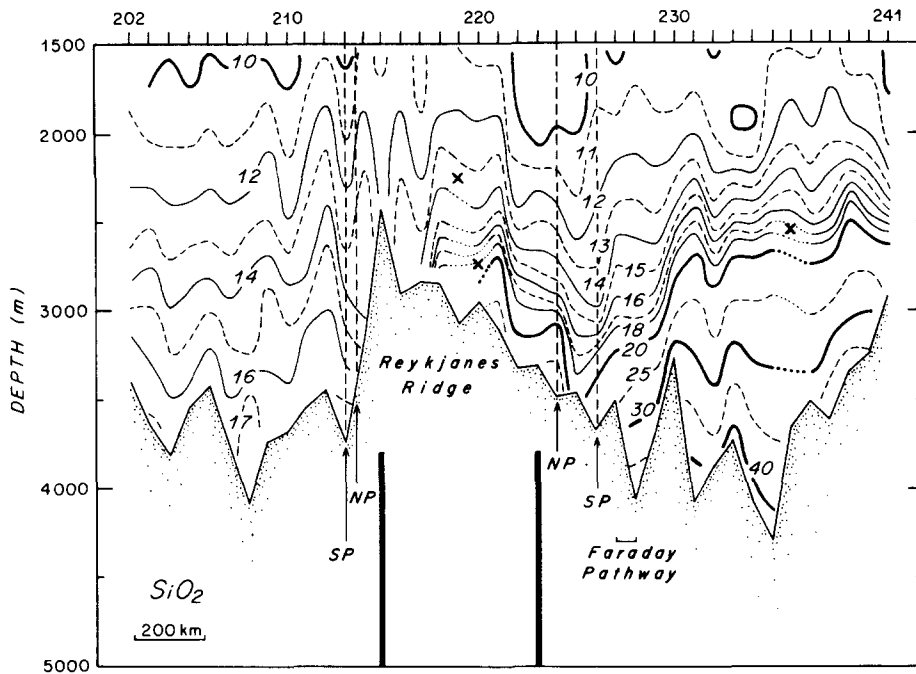


FIG.22b. Section of silicate ($\mu\text{mol l}^{-1}$) as Fig.22a. Note that in general the deepest water sample is about 100m above the deepest temperature measurement (by CTD). The x's indicate the deepest sample at stations 219 and 220.

high as $20.3\mu\text{mol l}^{-1}$. So the elevated silicate has penetrated farther west within the northern passage of the CGFZ than in the TOPOGULF section just to the north of the passage.

In the eastern quasi-meridional oriented part of the TOPOGULF section (Fig.22, stations 223 to 241) the continued descent of isopycnals to the southeast indicates westward flow towards the CGFZ sills. The stations nearest the two passages of the CGFZ are stations 226 sited in the middle of the southern passage, and stations 224 and 225 which bracket the northern passage but are away from its maximum depth of 3800m. The isopycnal slope reversal at the southern wall of the southern passage, defined by stations 226 and 227, indicates eastward flow and at first glance could be taken as a confirmation for the shear of the current meter observations 200km to the west by DICKSON, GURBUTT and MEDLER (1980) of mean eastward flow at the southern wall and mean westward flow at the northern wall of this same southern passage. But the LAUGHTON and MONAHAN (1984) topography (see Fig.18c) shows that just 25km east of this section is the fissure in the Hecate Ridge that connects the Faraday Pathway via the southern passage of the CGFZ to the northern passage, joining the East Thulean Pathway, and thus connecting both Pathways to the CGFZ and to the Maury Channel to the north. The shear reversal is thus equally likely a local signature of flow at this fissure.

The LDW in the TOPOGULF stations (223 to 228, Fig.22) which span the CGFZ, is rather variable in its character (as sampled primarily by the deepest bottle at these stations). Typical characteristics are silicates between 22 and $29\mu\text{mol l}^{-1}$, oxygen values between 5.9 and 6.1ml l^{-1} , with the most extreme characteristics at station 228 of silicate $39\mu\text{mol l}^{-1}$ and oxygen 5.8ml l^{-1} ,

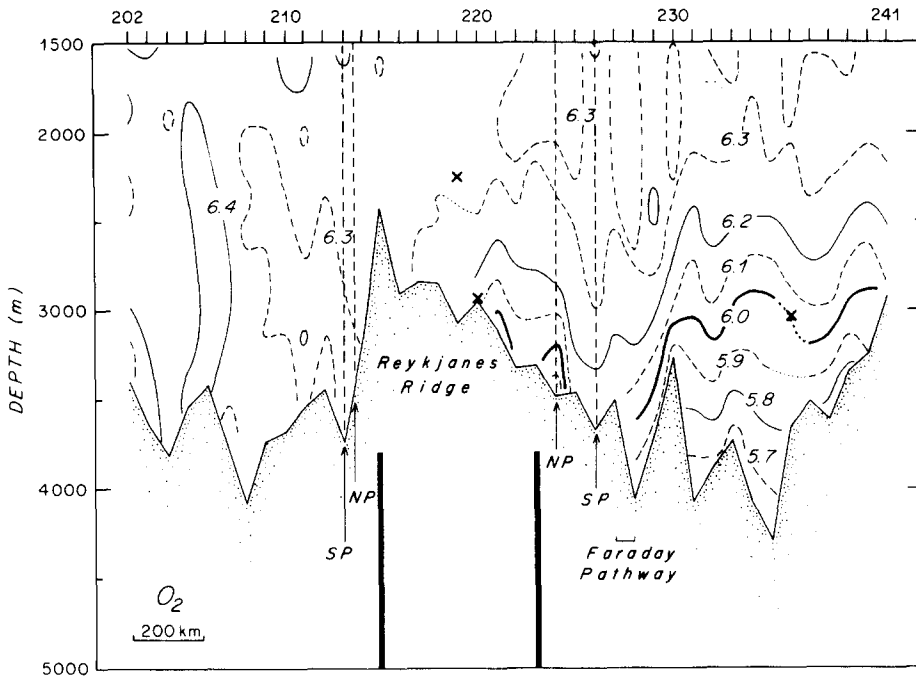


FIG.22c. Section of oxygen (ml l^{-1}), as Fig.22a.

and the least extreme at station 225 of silicate $18.8 \mu\text{mol l}^{-1}$ and oxygen 6.2ml l^{-1} . Some data are available farther west along the CGFZ near the sills which can be examined for evidence of influence of this eastern basin LDW on the waters flowing to the western basin. The TTO/NAS program (SCRIPPS INSTITUTION OF OCEANOGRAPHY, 1986) placed isolated stations (Fig.18b) in the southern passage of the CGFZ (station 122) and the northern passage (station 123). The southern passage station falls a short distance west of the southern sill, close to where DICKSON, GURBUTT and MEDLER (1980) measured mean velocities showing the eastward-westward counterflow. The station reached a depth of 4300m, and recorded water as cold as 2.44°C , with silicate $18.6 \mu\text{mol l}^{-1}$ and oxygen 6.3ml l^{-1} . Silicate drops below $15 \mu\text{mol l}^{-1}$ only above about 2700m or a temperature above 2.85°C . The northern passage station falls in a deep (4236m) area of the passage about 75km east of its 3675m sill. Here the bottom temperature is also 2.44°C , with silicate $19.4 \mu\text{mol l}^{-1}$ and oxygen 6.3ml l^{-1} , but silicate rises to a maximum of about $20.4 \mu\text{mol l}^{-1}$ at 3940m, with a temperature there of 2.53°C and oxygen 6.2ml l^{-1} . Silicate drops below $15 \mu\text{mol l}^{-1}$ only above about 2200m or a temperature above 2.8°C . Reference to the central and eastern TOPOGULF sections suggests that these two stations in the CGFZ contain LDW from well down the flank of the Reykjanes Ridge with its stronger southern influence, rather than the less extreme waters higher up the flank which have more northward source influence. The section in Fig.20, about 500km north-northeast of the northern passage of the CGFZ, shows the northern source waters, well up the Ridge flank, with silicates less than $11 \mu\text{mol l}^{-1}$ and oxygen values greater than 6.4ml l^{-1} . The elevated salinity of this water is the traditional tracer of this water mass in the western basin. Salinity values of the overflow in this section are noticeably higher than in the TOPOGULF data (Fig.22). This reflects real changes in the Iceland-Scotland Overflow Water described by SWIFT (1984a,b). Down the flank, the salinity is not so elevated, reflecting LDW influence and

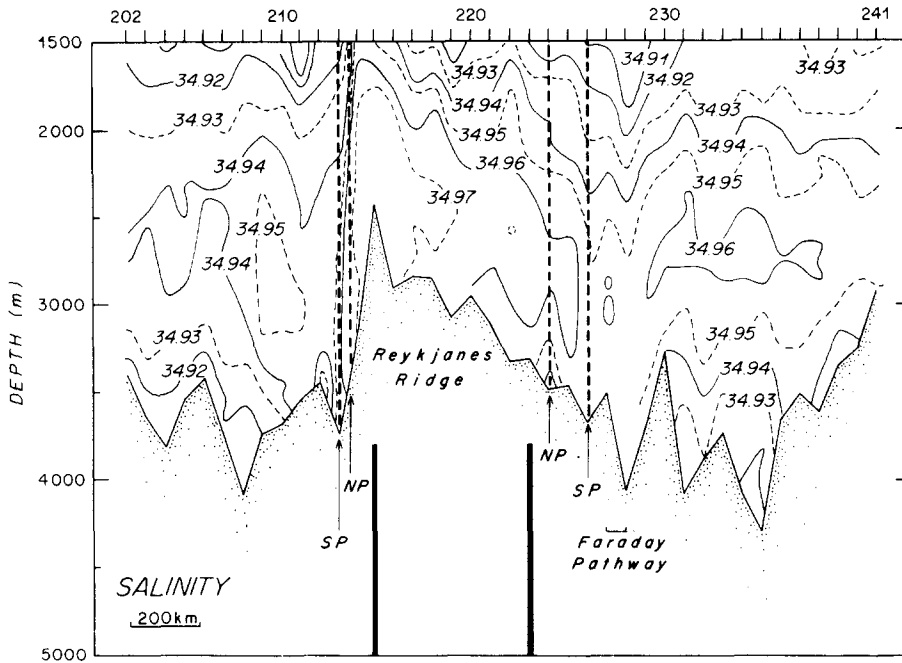


FIG.22d. Section of salinity, as Fig.22a.

the admixture of southern originating LDW has also introduced higher silicate but lower oxygen, creating the water mass seen in the two passages of the CGFZ.

The western TOPOGULF section (Fig.22) shows isotherms shallower than 3000m steeply descending southward across the CGFZ from stations 214 to 215 north of the northern passage sill. Unfortunately, the stations are poorly sited for examination of the water mass flowing west implied by the isotherm slope. Station 214 falls on the northern wall of the northern passage, and samples only to a temperature of 2.74°C at 3150m, neither deep enough nor cold enough to sample the water with the greater LDW influence. It recorded a near-bottom silicate of 14.2 $\mu\text{mol l}^{-1}$ and oxygen of 6.51ml l $^{-1}$, which corresponds to waters well up the eastern flank of the Reykjanes Ridge, as to be expected at a sample depth 500m above the CGFZ sill depth. The next station 213 is south of the Hecate Ridge in the southern passage (and well west of its sill). Thus the depths of the northern passage are not sampled at all in this section. The station in the southern passage falls near the maximum depth, 3820m, of that passage, sampled water as cold as 2.50°C, with silicate reaching 17.7 $\mu\text{mol l}^{-1}$ and oxygen 6.2ml l $^{-1}$. This appears to be a slightly diluted version of the waters found in the two TTO/NAS stations discussed above from farther east, suggesting that the westward flow in the passages of the CGFZ carries LDW with a recognizable southern originating component to the western basin.

The westward flow at the CGFZ carries dense waters of both northern and southern origin to the western basin. Shifting focus to the western basin, before considering the subsequent flow and evolution of the waters from the eastern basin, it is necessary to consider the possibility of northward flow of AABW and LDW from the mid-latitude western basin to its subpolar basin.

3.2 Western basin Antarctic Bottom Water and Lower Deep Water

In the western basin the AABW characteristics progressively fade northwards and tend to be stronger in the eastern half of the basin at mid-latitudes (WÜST, 1933, 1935; MANTYLA and REID, 1983). The abyssal distributions of Fig.9 show that the AABW and LDW abruptly (short meridional scale) weaken in strength upon encountering the deep anticyclonic recirculation gyre of the Gulf Stream. This fading reflects primarily a lateral closure of the AABW and LDW circulations, by westward flow past Bermuda and confluence with the DWBC south of the Gulf Stream, with part of the mid-latitude character in the temperature range 1.8 to 2.0°C being diluted by admixture of North Atlantic Deep Water recirculating in the gyre (McCARTNEY, 1991). Within the deep Gulf Stream recirculation gyre the situation is more difficult. There the residual AABW is warmer than 1.7°C with highest silicate values rarely exceeding 40µmol l⁻¹, indicating dilution by northern waters since the AABW to the south has silicate values considerably higher at these same temperatures. North of about 34°N the dominant shear signature is the recirculating gyre itself, rather than the net shear indicative of net meridional flow. An idea of the deep gyre signature strength can be gained by examining the deep isotherm bowl in Fig.9, stations 273 to 290.

For the present study the issue is the continuation of AABW influence to higher latitudes. Although quantification of any net flow of AABW towards the subpolar basins is desirable, it may be unattainable because of the predominance of the deep gyre circulation; the net flow being a small residue from opposing flows whose transports are larger by an order of magnitude or more. In the Gulf Stream recirculation gyre the AABW influence, albeit dilute, is easily distinguishable from the deepest waters east of Newfoundland, where the very low-silica Denmark Strait Overflow Water (DSOW) dominates. This contrast is one of WORTHINGTON's (1976) principal arguments for a deep circulation system east of Newfoundland separate from that of the deep Gulf Stream.

3.2.1. Silicate distribution in the Newfoundland, Labrador and Irminger Basins. WORTHINGTON (1976) showed that south of the Grand Banks in the deep circulation of the Gulf Stream system silicate increases towards the bottom to values well above 35µmol l⁻¹ near the bottom. East of Newfoundland (in the western basin) the low-silicate DSOW is found at the bottom overlain by water with silica as high as 25µmol l⁻¹ (near 1.9°C), with silicate decreasing monotonically above this maximum. The structural demarcation falls at the Southeast Newfoundland Rise. He used temperature-silicate and temperature-salinity correlations to illustrate this contrast; here we show deep property sections along the same stations (Fig.23). The section is oriented southwest-northeast ("Trough" section in Fig.3) and conveniently bridges the two sections of Figs 9 and 11. The crest of the Southeast Newfoundland Rise lies near station 333. Unfortunately, silicates were not obtained at the deepest bottle at both stations 332 and 334, and at the two deepest bottles at station 333, so the degree of DSOW influence is incompletely resolved. The overall impression is that the low-silicate influence of the DSOW is strongest at the northeast edge of the Rise, and this is also true in other regional data (MANN, GRANT and FOOTE, 1965; MANN, COOTE and GARNER, 1973; CLARKE, HILL, REINIGER and WARREN, 1980).

The interpretation of this diagonal section by WORTHINGTON (1976) has proved controversial (CLARKE, HILL, REINIGER and WARREN, 1980). Upper water shear indicates the Gulf Stream flowing southeast through the section between stations 327 and 331, and there is a northwest flow between stations 331 and 336. Deep isotherms (Fig.22a) also indicate a similar shear reversal, with an associated transition in deep silicate and salinity from strong AABW influence to DSOW influence (Figs 22b,c). The controversy is: to what degree, if any, are the opposing shallow flows connected by counterclockwise turning streamlines somewhere to the southeast of the section, and

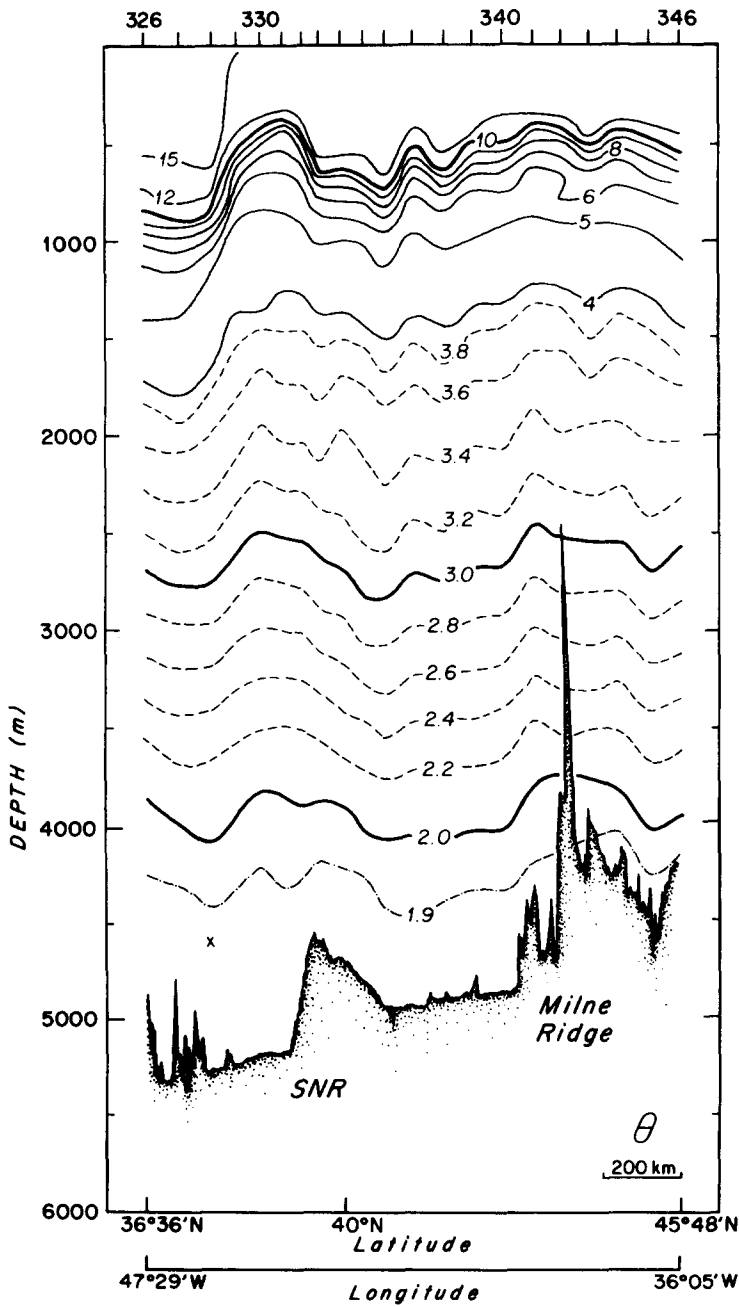


FIG.23a. Section of potential temperature ($^{\circ}\text{C}$) across the Southeast Newfoundland Rise (SNR), *Atlantis II* cruise 9, March 1964 (WORTHINGTON, 1976). "Trough" section on Fig.3; south is on left. Station 328 sampled only to 4606m – the x in the section.

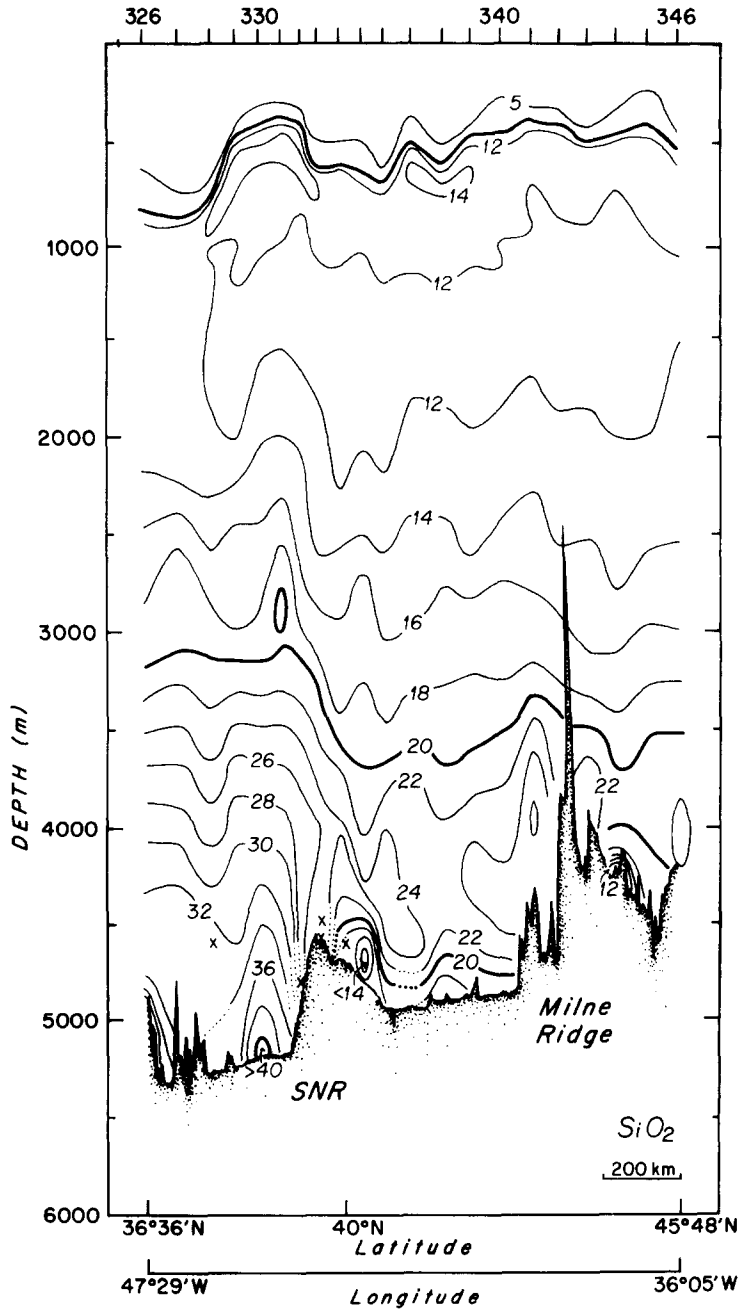


FIG.23b. Section of silicate ($\mu\text{mol l}^{-1}$) across the Southeast Newfoundland Rise, as Fig.23a. Note missing samples near bottom over the Southeast Newfoundland Rise. (x's at stations 332-334 and 328 denote bottles without silicate data.)

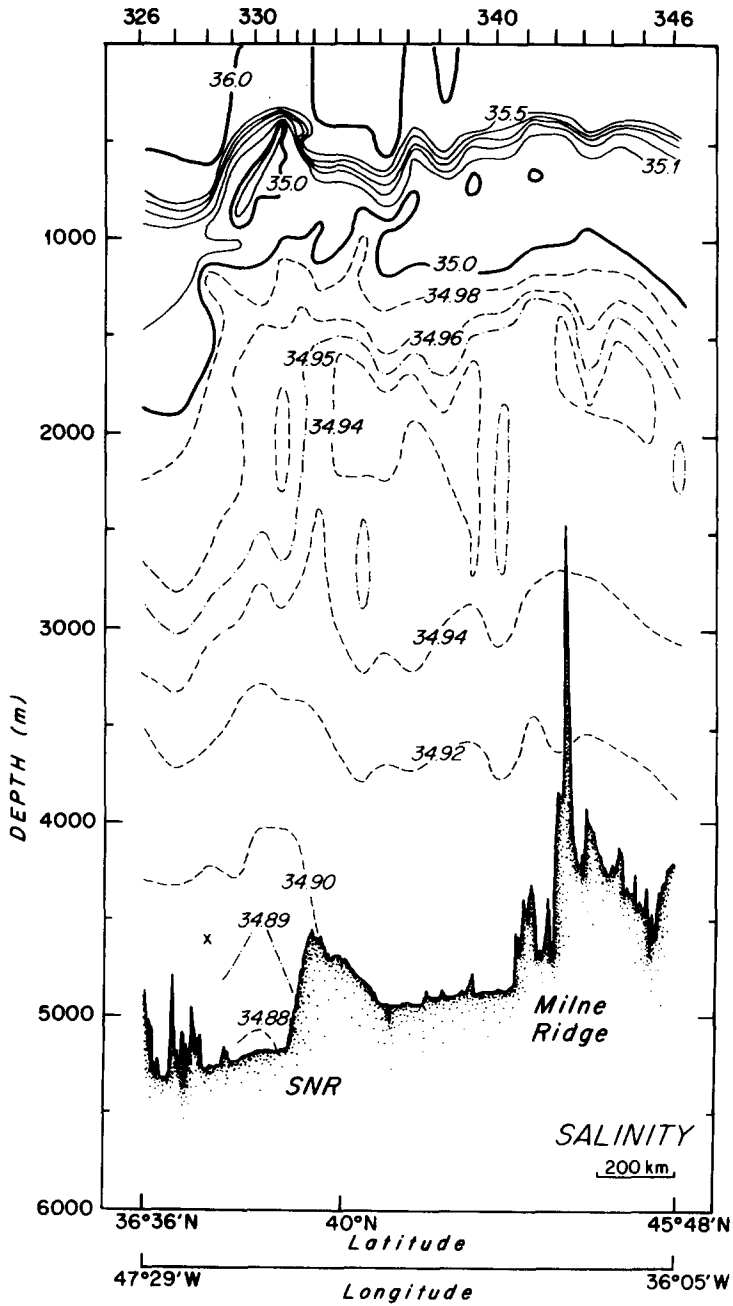


FIG.23c. Section of salinity, as Fig.23a.

to what depth do parallel flows exist.

For the near bottom water, the sharp transition near station 331 from higher silicate, lower salinity water, with a maximum value at or very near the bottom beneath the Gulf Stream, to lower silicate and higher salinity water to the north, with the latter extremes separated from the bottom by northern originating dense water, is part of the basis of WORTHINGTON's (1976) contention that the deep water circulations are separate. Along this section the transition falls near 39°N and 45°W, and the water to its southwest resembles closely that beneath the deep recirculating gyre along the 53°W section (Fig.9). Along the section of Fig.11, which lies farther east in the eastern Newfoundland Basin, a similar structural change in silicate occurs near stations 30 to 33: from stations with higher silicates increasing to a maximum near the bottom in the south, to stations with maximum silicates above $18\mu\text{mol l}^{-1}$ separated from the bottom by colder water with silicates sometimes lower than $16\mu\text{mol l}^{-1}$. This transition occurs slightly farther north than along the section of Fig.23, and although similar in structure, involves silicate levels lower by roughly 20%. There is an associated very slight salinity transition from more saline water (at a given temperature) where silicate is high, to fresher water where silicate is low. This transition occurs across an unnamed fracture zone extending west from the Mid-Atlantic Ridge near 43°N that includes the Altair and Milne Seamounts, and that has substantial area less than 4000m (Figs 1 and 24a). A relatively narrow deep passage between this feature and the Flemish Cap is the only western basin pathway for cold deep water flow between the Subtropical Basin and the Subpolar Basin. A small gap exists between the Milne Seamounts and the rest of the "Milne Ridge", as I will call this feature for the subsequent discussion, but the main passage is west of the Seamounts, and is only about 200km wide at the 4000m level, I will call this the "Flemish-Milne Narrows".

It appears that there are two transitions in the deep water system between the subtropical and subpolar gyres. These can be recognized in the horizontal distribution of deep silicate. Figure 24a shows the distribution of stations in the mid- and high-latitude western basin used for charting silicate. The data were collected in seven different years (1964, 1966, 1967, 1972, 1981, 1982 and 1983) over a period of two decades. The region around the Southeast Newfoundland Rise includes synoptic surveys from the years 1964 (June), 1966, and 1972. These three surveys, which are geographically intermingled, can be contoured without violation of a single station. This is remarkable, for current meter measurements by FOFONOFF and HENDRY (1985) show the region to be dominated by low-frequency variability, and there is evidence of decadal scale evolution in the deep waters of the subpolar basin (BREWER, BROECKER, JENKINS, RHINES, ROOTH, SWIFT, TAKAHASHI and WILLIAMS, 1983) and the subtropical basin (ROEMMICH and WUNSCH, 1984). The only data set specifically excluded because of its incompatibility is the *Atlantis II* data of early 1964 (Fig.23). This section shows the high-silicate layer penetrating north of the Rise as defined by the $24\mu\text{mol l}^{-1}$ contour above bottom silicates of $16\text{--}18\mu\text{mol l}^{-1}$. The three other data sets, including one sampled only a few months after the *Atlantis II* section, show the high-silicate layer defined by values well above $30\mu\text{mol l}^{-1}$ above bottom silicates of $20\text{--}25\mu\text{mol l}^{-1}$. While this could reflect a decadal variation, it could also result from a standardization problem in the *Atlantis II* data, which appears to be lower by about 20% than the three other data sets. The pattern of silicate distribution is the same in all four data sets.

In the DWBC and in part of the Newfoundland Basin north of the Southeast Newfoundland Rise, a deep silicate maximum is found some distance above the bottom. Figure 24b focuses on this feature by contouring the field formed from the sample defining this maximum at each station. On the chart the area where this maximum is observed is north and/or west of the dotted curve (from Fig.24a). South and/or east of this curve silicate increases monotonically with depth so that the maximum is at the bottom, and that is what is contoured. In the Newfoundland Basin, where

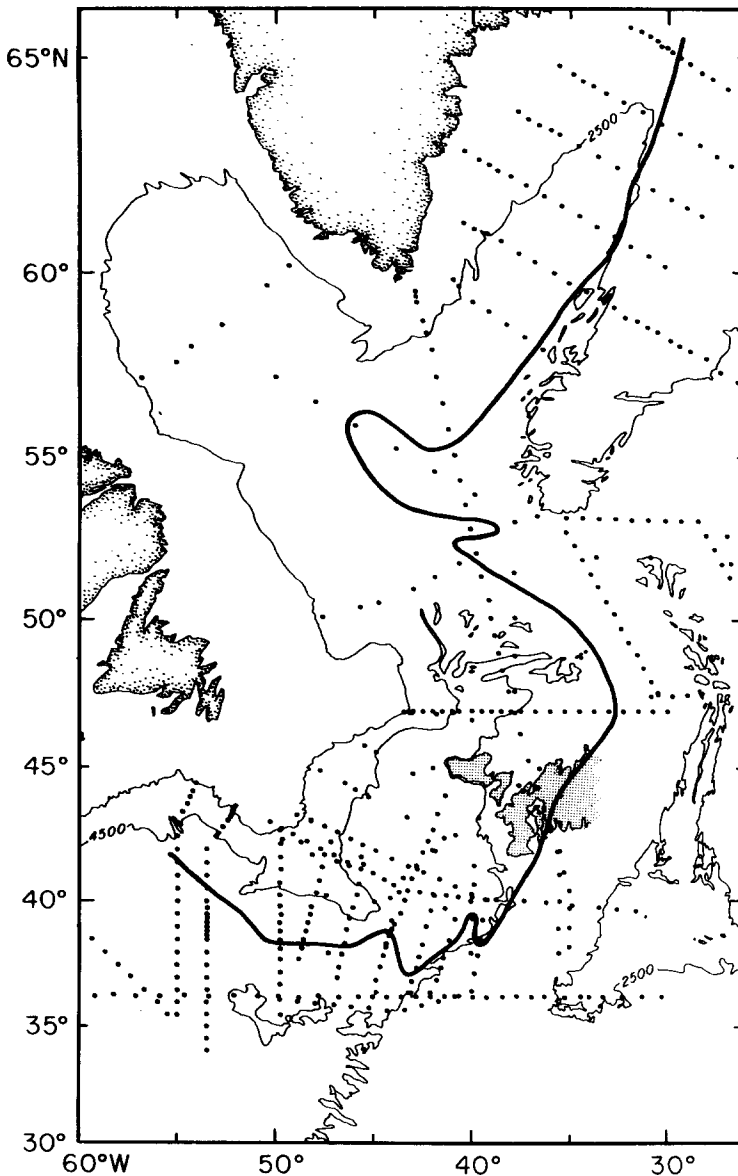


FIG.24a. Data base of the silicate charts (Figs 24b and c). Data sources: CLARKE, HILL, REINIGER and WARREN (1980); HOGG, PICKART, HENDRY and SMETHIE (1986); KNAPP and STOMMEL (1985); ROEMMICH and WUNSCH (1985); HENDRY (1989); SCRIPPS INSTITUTION OF OCEANOGRAPHY (1986); GRANT (1968); MANN, GRANT and FOOTE (1965); THE TOPOGULF GROUP (1986) and the transect of Fig.11. The hatched area denotes the area less than 4000m to the east of the Flemish-Milne Narrows, this and the 2500m and 4500m contours are from SEARLE, MONAHAN and JOHNSON (1982) and LAUGHTON and MONAHAN (1984). The heavy curve is the boundary between the domain with maximum silicate above the bottom (to the left of the curve) and the domain with maximum silicate at the bottom (to the right of the curve). This curve is repeated as a dotted curve on Figs 24b,c and d. The salinity chart, Fig.24d, used data only north of 47°N.

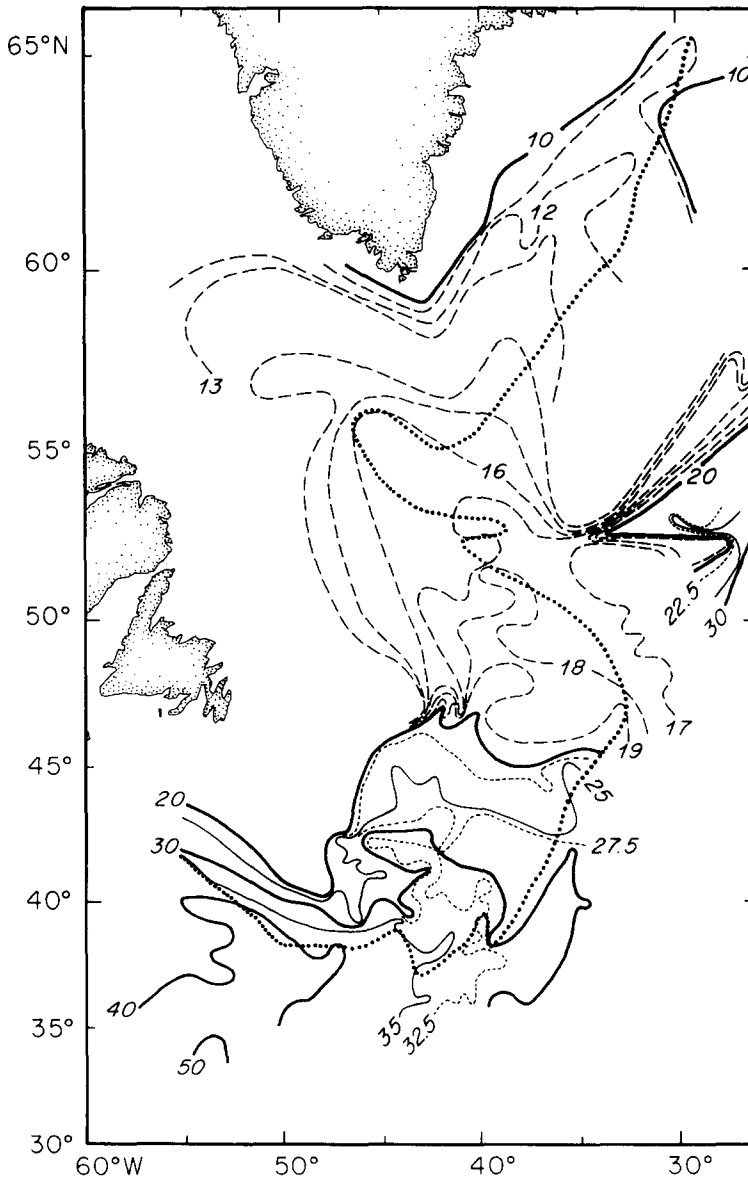


FIG.24b. Silicate ($\mu\text{mol l}^{-1}$) at the deep silicate maximum. This occurs above the bottom to the left of the dotted curve, and at the bottom to the right of the curve. Curve as Fig.24a.

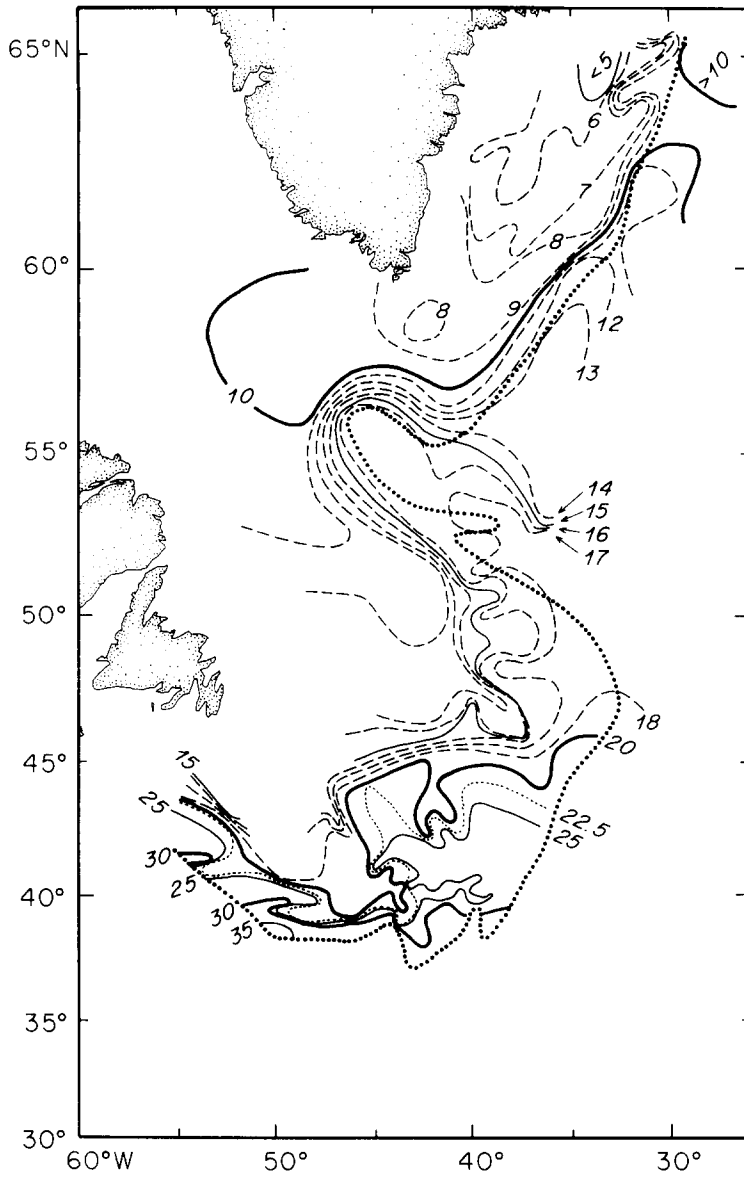


FIG.24c. Silicate ($\mu\text{mol l}^{-1}$) at the near bottom silicate minimum, beneath the silicate maximum.
Curve as Fig.24a.

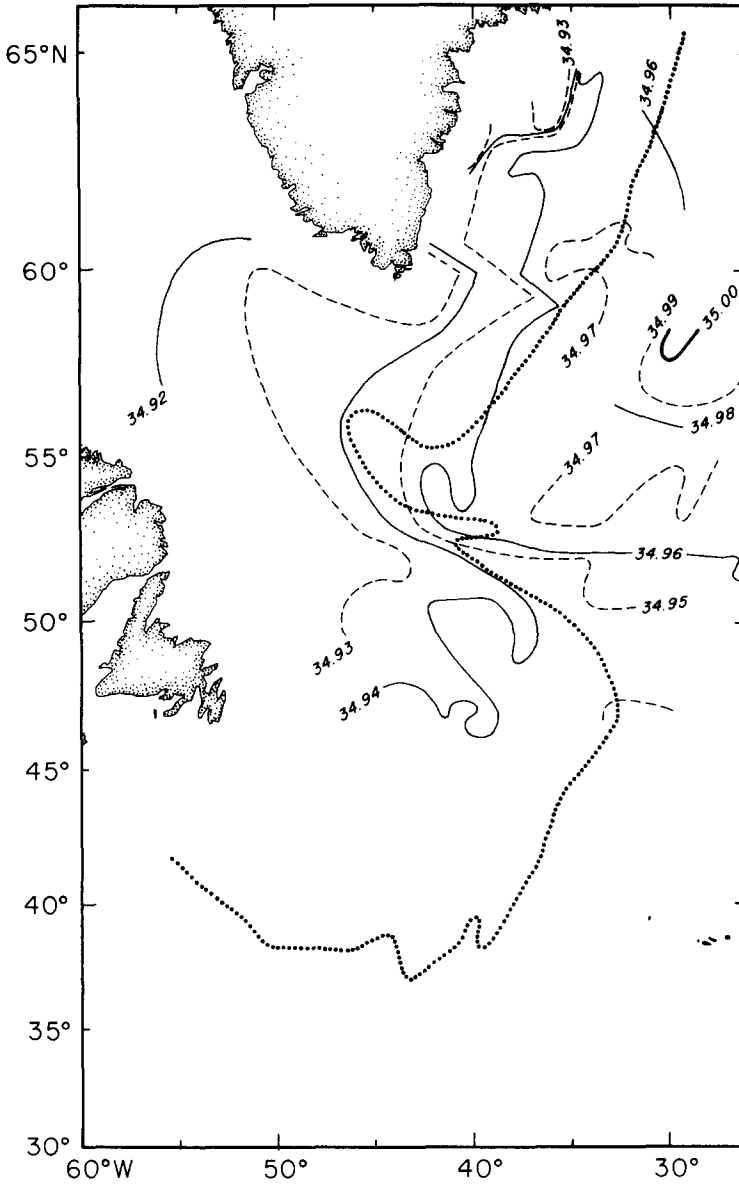


FIG.24d. Salinity at the deep salinity maximum. Curve as Fig.24a.

the silicate maximum has highest values, its associated temperature lies between 1.9°C and 2.1°C. In the Labrador Basin the maximum is associated with slightly warmer temperatures, between 2.0°C and 2.3°C, and even warmer in the Irminger Sea, typically between 2.2°C and 2.5°C. South of the Southeast Newfoundland Rise and/or the DWBC, where silicate rises monotonically to the bottom, the data generally have the coldest associated temperatures at the station, below about 1.9°C. For the area west of the CGFZ and over the western flanks of the Reykjanes and Mid-Atlantic Ridges the maximum silicate is also at the bottom, with the associated temperatures between 2.1°C and 2.4°C, and with the warmest values tending to occur over the shallower levels of the Ridges.

The first transition region is the area of the Southeast Newfoundland Rise. From the pool of high-silicate AABW in the southwest, a tongue of somewhat lower silicate water turns counterclockwise 180° on a broad arc following the deepest pathway ($\geq 4500\text{m}$) to the Newfoundland Basin. Maximum silicates at the beginning of this turn are just under $40\mu\text{mol l}^{-1}$, but decline rapidly following the turn, dropping below $30\mu\text{mol l}^{-1}$ at the end of the turn where the Rise joins the north-south oriented east flank of the Grand Banks of Newfoundland. The tongue turns northward through the Newfoundland Basin and undergoes a second transition at the Flemish-Milne Narrows, where a decrease in silicate from greater than $25\mu\text{mol l}^{-1}$ to less than $20\mu\text{mol l}^{-1}$ occurs. From there northwards the high silicate tongue follows the west flanks of the Mid-Atlantic and Reykjanes Ridges in the Labrador Basin, and then turns into the Irminger Basin along its deepest axis, with a steady decline in silicate that is somewhat intensified at 57°N. The tongue axis lies west of the dotted curve that delineates the western edge of the region where the silicate maximum is at the bottom, except northwest of the CGFZ. Thus over much of its length the feature exists as a three-dimensional tongue, with lower silicate above and below as well as to both sides. The exception is the region northwest of the CGFZ, where the highest silicates defining the tongue are at the bottom, with lower values above and to either side. This region will be named the West Thulean Tongue, as a convenient name for the subsequent discussion. It projects north of west from the sill area of the CGFZ, and passes through the maximum depth passage between the West Thulean Rise and the flank of the Reykjanes Ridge (Fig.18).

The low-silicate influence on the silicate maximum chart (Fig.24b) begins in the northern Irminger Sea at the Denmark Strait, and is intensified at the northern and western boundaries. The distribution of the silicate maximum in the DNBC along the coast of Greenland and the DWBC along Labrador and Newfoundland suggests the progressive confluence into this southward trending flow of waters from the high-silicate tongue that lies offshore. Just south of the Denmark Strait, the silicate maximum is about $8\mu\text{mol l}^{-1}$. In the stations in the DNBC at the south tip of Greenland, the silicate maximum ranges from $9.5\mu\text{mol l}^{-1}$ to $13\mu\text{mol l}^{-1}$. Little further evolution occurs until the Flemish-Milne Narrows, where the maximum silicate values in the DWBC rise to $13\text{--}18\mu\text{mol l}^{-1}$. Little additional increase occurs as the DWBC makes the turn around the Southeast Newfoundland Rise to the Slope Water, and the main visual impression of this area is the bulge of low-silicate water over the Southeast Newfoundland Rise as the DWBC is first deflected southeast by the Rise before turning west. This bulge forms the pivot around which the northward flowing tongue of high-silicate water makes its 180° counterclockwise turn to enter the Newfoundland Basin.

The second silicate chart (Fig.24c) focuses on the lower silicate water beneath the silicate maximum. Lowest silicate values in Fig.24c are found just to the south of the narrows of the Denmark Strait and are caused by the descending plume of cold dense DSOW from the narrows. Sections from north of the narrows sill (GRANT, 1968) show the dense source waters between -0.5° and 1°C , with silicates between 5 and $8\mu\text{mol l}^{-1}$. Through entrainment of warm water and

LSW, the temperature of the DSOW entering the northern edge of the chart has been elevated considerably above its source values, with only a very few near bottom samples colder than 1.0°C occurring along the western side of the Irminger Basin. Silicate values, though, show little change for both entraining water masses are nearly equally low in silicate, between about 6 and 10 $\mu\text{mol l}^{-1}$. The concentration of the lowest silicate increases southwards along the western boundary of Irminger Basin. This low silicate layer in the Irminger Basin is bounded in the east by a sharp gradient to the area over the Reykjanes Ridge flank where there is no minimum and silicate increases monotonically to the bottom – and is higher in value (Fig.24b).

The low-silicate layer is moving south, based on the shear distributions inferred from the temperature sections for these data (GRANT, 1968; MANN, 1969) and the current meter results of DICKSON, GMITROWICZ and WATSON (1990), and it undercuts the axis of the silicate maximum tongue (Fig.24b). Thus it appears that as it progresses southwards the undercutting low-silicate water gains silicate through exchange with the overlying silicate maximum tongue which is intruding northwards in the central Basin. Together these two fields suggest a deep level-of-no-motion in the central Irminger Basin, between the low-silicate waters near the bottom and the silicate maximum layer. This is consistent with the current meter measurements and velocity sections reported by DICKSON, GMITROWICZ and WATSON (1990) in connection with Fig.2. But this deep level-of-no-motion occurs only in the central basin, both to east and west the flow otherwise appears columnar. In the west the flow is unidirectional and southward, while over the western flank of the Reykjanes Ridge, where the undercutting low-silicate water is absent, the flow is unidirectional and northward through the water column; as first suggested by IVERS (1975), and supported by the SPMW distribution (McCARTNEY and TALLEY, 1982), the LSW distribution (Fig.7; and TALLEY and McCARTNEY, 1982), and the upper parts of the DNBC (the high-salinity water described by SWIFT, 1984a). Basically the flow is a columnar cyclonically turning system, with a degree of “folding under” of the southward flowing low-silicate water beneath the northward flowing high-silicate water in the mid-basin causing a flow reversal with depth.

The sharp gradient of silicate in the central Irminger Basin is also present in the central Labrador Basin. To the west of the dotted curve of Fig.24c, the continental slope broadened DWBC sweeps around the periphery of the Labrador Sea to the Flemish-Milne Narrows, gradually increasing in silicate to about 13 $\mu\text{mol l}^{-1}$. To the east of the dotted curve at latitudes 50° to 57°N is the West Thulean Tongue, with higher silicate values increasing to the bottom (Fig.24b). At about 53°N low-silicate water penetrates from the west into the western extremity of the northern passage of the CGFZ (to station 18 of the *Knorr* section of Fig.10). This extrusion distorts the west side of the Tongue, undercutting it near the northwest limit of the 17 $\mu\text{mol l}^{-1}$ contour on the silicate maximum chart (Fig.24b). The tongue is the immediate source for the higher silicate waters in the Irminger Basin on both silicate charts.

Northward flow from this area of the Labrador Basin is the traditionally identified pathway into the Irminger Basin for the eastern basin waters passing west through the CGFZ. In older treatments it is the elevated salinity of the eastern basin waters that allows the identification of flow path, for example, the salinity distribution charts on the 3.4, 3.2, 3.0, 2.8 and 2.6°C surfaces in the WORTHINGTON and WRIGHT Atlas (1970). This high-salinity influence is shallower in the water column than the silicate charts being discussed here, lying above the silicate maximum at associated temperatures near 3°C. Figure 24d shows the deep salinity maximum for the northern part of the present data set (at and north of the 47°N section data on Fig.24a). Note the similarity of the shape of the high-salinity tongue to the deeper high silicate tongue in the eastern Labrador and Irminger Basins suggestive of parallel northward movement of the salinity maximum and the

deeper higher silicate waters (except for the eastward extrusion of low-silicate water at the bottom into the CGFZ noted above). The higher salinity contours are restricted to stations north of the southern defining wall of the southern passage of the CGFZ, passing north of the West Thulean Rise between the Rise and the flank of the Reykjanes Ridge. The *Knorr* section of Fig. 11d shows this high-salinity aspect of the West Thulean Tongue (stations 16-18, the 34.96 contour).

On the salinity chart a discontinuity is contoured in the southern Irminger Basin (the kinks in the 34.96-34.93 contours). This reflects the data south of there being from the 1980s, while north of there it is from 1967, and as noted by BREWER *et al.* (1983) deep water salinities in the subpolar basin declined in the interim by about .01-.02. SWIFT (1984b) has contrasted deep water characteristics from these two periods along the DNBC and the DWBC. The climatic change in salinity is a major fraction of the horizontal range in salinity. It is interesting that this change is not reflected in the deep silicate fields. If there has been a corresponding climatic change in silicate, it is evidently small relative to the horizontal range of silicate, since there is no evidence of time dependence in the silicate charts.

The tritium data previously noted (ÖSTLUND and GRALL, 1987, their pages 27 and 29, also shown by ÖSTLUND and ROTH, 1990, their Fig. 8) show that the higher salinity of the West Thulean Tongue coincides with the tritium minimum layer, ≤ 1.5 TU81N. This correspondence continues north into the Irminger Basin to just south of the Denmark Strait sill (page 25 of ÖSTLUND and GRALL, 1987). SMETHIE and SWIFT (1989) give full property sections for this section, which show an overlap of the ≤ 1.5 TU81N tritium minimum layer with the salinity maximum (≥ 34.94) and silicate maximum ($\geq 12 \mu\text{mol l}^{-1}$) layers.

While the immediate origin of the higher silicate water in the eastern Irminger Basin is the West Thulean Tongue with silicate near $17 \mu\text{mol l}^{-1}$ west of the CGFZ, it is difficult to ascertain the relative contributions to the Tongue's water mass of westward flow through the CGFZ and northward flow in the eastern Labrador Basin from the Flemish-Milne Narrows. The salinity maximum chart (Fig. 24d) suggests a dominance of the westward flow from the CGFZ on the water mass of the West Thulean Tongue at that depth. The silicate maximum chart (Fig. 24b) shows the Tongue to have silicates between 16 and $18 \mu\text{mol l}^{-1}$ with possible sources both to the east and to the south. The low-tritium character of the Tongue could come from either the westward flow through the CGFZ, or northward flow in the western basin, or a combination of both. TTO station 225 falls in the Flemish-Milne Narrows, Fig. 18b ($46^{\circ}55'N$ and $41^{\circ}49'W$, SCRIPPS INSTITUTION OF OCEANOGRAPHY, 1986; ÖSTLUND and GRALL, 1987), and shows the coincidence of the ≤ 1.5 TU81N tritium minimum layer with the silicate maximum layer ($\geq 16 \mu\text{mol l}^{-1}$).

HARVEY (1980) places the coldest limit on eastern basin waters penetrating westward through the CGFZ as warmer than about $2.4^{\circ}C$, based on a fairly extensive data set principally from the O.W.S. *Charlie* (nominal position $52^{\circ}45'N$, $35^{\circ}30'W$) data contributions. His bottom temperature chart shows a decrease to colder temperatures westward from the sills of the CGFZ, which requires a western basin component to the water mass given the robustness of the $2.4^{\circ}C$ limit through the O.W.S. *Charlie* data. As noted in the preceding section, waters just warmer than $2.4^{\circ}C$ were observed just east of the sills at TTO stations in each of the two passages of the CGFZ, with silicates of $18-20 \mu\text{mol l}^{-1}$. The TOPOGULF western section (station 213, Fig. 22, bottom temperature $2.50^{\circ}C$) establishes continuity of the $17 \mu\text{mol l}^{-1}$ contour westward to the longitude of the northern passage sill. As noted above, the southern part of the northern passage is not sampled in that data set; so the possibility of stronger eastern basin influence cannot be ruled out because of the sparse station coverage of the region immediately west of the TOPOGULF survey. On Fig. 24b, the 19 and $20 \mu\text{mol l}^{-1}$ contours protruding through the northern passage are contoured as closing at the sill near $35^{\circ}W$, since no stations showing silicates higher than $19 \mu\text{mol l}^{-1}$ are found

in the present station coverage until far to the southwest in the *Knorr* section of Fig.11. The continuity of the $18\mu\text{mol l}^{-1}$ contour between the TTO station in the CGFZ to the *Knorr* section is suggested by an isolated station (from SHOR, LONSDALE, HOLLISTER and SPENCER, 1980) showing a silicate maximum of $18.2\mu\text{mol l}^{-1}$ at a temperature of 2.35°C , with silicate above $17\mu\text{mol l}^{-1}$ for temperatures between the bottom temperature of 2.31°C and about 2.5°C . But the continuity of $18\mu\text{mol l}^{-1}$ is only suggested, for it assumes that higher silicates were present but "missed" in mid-passage during the TOPOGULF sampling (Fig.22). This contouring is possibly misleading, for the *Knorr* section stations with silicates above $17\mu\text{mol l}^{-1}$ had temperatures near 2.0° - 2.2°C , colder by more than 0.3°C than the water with high silicate observed in the sill area of the passages of the CGFZ. These higher silicate values with associated colder temperature on Fig.24b appear to be of southern origin, rather than from the high-silicate water emerging from the Flemish-Milne Narrows, both because of the contour shape, and the colder temperatures.

Adding to the confusion of this area is the observation by SHOR, LONSDALE, HOLLISTER and SPENCER (1980) just west of the CGFZ northern passage sill of western basin of waters colder than 2.3°C , with silicates no higher than $15.2\mu\text{mol l}^{-1}$. This demonstrates that at least occasionally western basin deep waters can penetrate east along the northern passage to the neighborhood of its sill at 35°W . This datum is not included on the charts of Fig.24; if included it would be contoured as an isolated "bubble" at the location of the TOPOGULF section's crossing of the northern passage, disconnected from the source for waters of this low a silicate far to the west. The next nearest stations to the west of this spot are stations 16 to 18 in the *Knorr* section (Fig. 11) which are located in the western extension of the northern passage of the CGFZ between the West Thulean Rise (station 19) and the sections nearest (and least deep) approach to the Reykjanes Ridge (station 15). The salinity section (Fig.11d) shows that the elevated salinity signature of eastern basin influence is restricted to these three stations (the 34.96 contour), at a temperature of 2.6 to 3.0°C . Silicate values (Fig. 11b) are higher than $16\mu\text{mol l}^{-1}$ for temperatures below 2.5°C for these three stations except for the very cold (1.767°C) sample at the bottom of station 18 with its silicate of $15.0\mu\text{mol l}^{-1}$ located at 4230m in the passage's deep axis. A further eastward excursion of this low-silicate extrusion (Fig.24c) would be required to distort the west edge of the Tongue enough to bring the DWBC low-silicate water to the sill area of the northern CGFZ passage farther east.

Leaving aside observations like those detailed in the preceding paragraph which point to possible low-frequency variability in the geometry of the deep water masses (or bad data), there remains an ambiguity in the steady state interpretation of the West Thulean Tongue. The uncertainty arises because high silicate values are found at temperatures colder than HARVEY's (1980) 2.4°C cutoff for the coldest eastern basin water at the CGFZ's sills and yet salinities remain slightly elevated. The former points to a southern origin, while the latter points to an eastern origin. There are at least three explanations which are not mutually exclusive.

First, as discussed briefly in the preceding section, the structure of the mean velocity fields in the two passages of the CGFZ seems complex, and is still poorly resolved. If mean flows involve a lateral counter flow system, like DICKSON, GURBUTT and MEDLER (1980) observed in the southern passage of the CGFZ, then the data coverage in Fig.24 is inadequate to resolve any high- and low-silicate components associated with the counterflow. In addition, there is strong low-frequency variability in the passages with implied long zonal "sloshing" scale (SCHMITZ and HOGG, 1978). There are cold waters with low silicate west of the passage sills, and cold waters of high silicate to the east. If the "sloshing" is of sufficiently long coherence scale, then both extremes of water type may reach the sill.

Second, HARVEY and ARHAN (1988) noted that the deepest waters of the westward flow in the

western TOPOGULF section (stations 213 to 215, Fig.22) have very low potential vorticity. This vertical homogeneity is not present in the stations of either the central or the eastern TOPOGULF sections, and seems to represent a vertical stirring of the westward flowing water as it passes through the CGFZ. Such mixing could be drawing on the energy of unidirectional mean flow in the confines of the passages, or of the counterflows if they exist, or on the low-frequency fluctuations. Westward flow from the CGFZ along the Tongue with mixing as water overrides the colder (and denser) waters of the western basin could cause the elevated silicate water to influence colder waters. *Knorr* stations 16, 17 and 18 (Fig.11) have their maximum silicates of 16.7, 17.5 and 17.6 $\mu\text{mol l}^{-1}$, respectively, at temperatures of 2.39, 2.25, 2.15°C, not dramatically colder than the coldest waters believed to penetrate west of the sills. While such vertical mixing is plausible, alone it does not explain the vertical displacement of the silicate maximum in the west to colder temperatures than at and east of the sills.

Third, high-silicate water at these colder temperatures is found in the southeastern Labrador Basin north of the Milne Ridge (Figs 11, 24b and 24c); this is also a region where silicate basically increases monotonically to the bottom. So northward flow of the silicate maximum tongue emerging from the Flemish-Milne Narrows could directly advect high-silicate water from the south into the West Thulean Tongue. This suggests that the maximum silicate axes extending from the Flemish-Milne Narrows is a flow path; the evidence in the geostrophic shear distribution for this flow is discussed in the next section.

3.2.2. Geostrophic shear in the Newfoundland and Labrador Basins. The distribution of silicate in the deepest waters of the Newfoundland, Labrador and Irminger Basins as described above suggests an overall cyclonic flow in these basins: a southward flow of low-silicate DSOW along the western sides of the basins, and a northward flow along the eastern sides. The DNBC and DWBC components of this circulation are familiar. The inferred northward flow in the region offshore of these currents, and the abrupt transitions in silicate that occur following this flow also have signatures in the distribution of deep shear. The general structure of the shear in the Newfoundland and Labrador Basins can be deduced from the sections of Figs 11, 13, 16 and 23. Deep isotherms (below, say, 3.0°C) descend across the boundary current to their maximum depth in mid-basin, then rise towards the opposite side of the basin. If a level-of-no-motion is assumed in the deep water, then below that level cyclonic flow results.

WORTHINGTON (1976) used such a level in the Newfoundland Basin but only for the DWBC; over the rest of the basin he used instead a bottom level-of-no-motion which resulted in anticyclonic deep flow away from the DWBC. He thus inferred a narrow DWBC filament on the continental slope, with most of the deep isotherm bowl shear translated to northward deep flow beneath the North Atlantic Current and southward flow farther offshore. With the broader scale distributions of silicate (Fig.24) now available, his section across the Southeast Newfoundland Rise (Fig.23) can be reinterpreted. Station 337 has the maximum isotherm depth that defines the isotherm bowl in the Newfoundland Basin. Between stations 336 and 331 the upper water flow is northwest, as indicated by WORTHINGTON (1976). To what depth does the northwest flow penetrate, and how shallow does the southeast flow near the bottom implied by the low bottom silicates extend? Below 3000m, station 331 defines the northeast boundary of the higher silicate and lower salinity LDW and AABW in the deep Gulf Stream system. At first glance, the superposition of the deep silicate maximum over the lower bottom silicate suggests a level-of-no-motion between these features – near, but not at, the bottom. However, the existence of shear indicative of a deep gyre in the Newfoundland Basin allows a different scenario, with a level-of-no-motion above the silicate maximum. High silicate water flows northwest through stations 336 to 341 and returns southwest through stations 336 to 331, parallel to the underlying low-silicate

water, not anti-parallel to it. A pair of sections from two years later makes this circulation more apparent.

Figures 25 and 26 show two orthogonal sections, from this area, that are used in the charts in Fig. 24. The first (Fig. 25) is close to a reoccupation of WORTHINGTON's (1976) Fig. 23, and the structure is similar: the Gulf Stream flows southeast through stations 8 to 10, with station 10 defining the northeast limit of the southern pool of high-silicate and low salinity LDW and AABW that lies beneath the Stream. Reversed isotherm slopes between stations 10 and 13 define the northwest flow of the upper waters whose depth penetration is the present issue. Lower silicate and higher salinity are found at the bottom at these stations, and the overlying silicate maximum layer at 4000-4500m is not as strong as at the adjacent stations on either side. Stations 13 to 18 define the upper water anticyclonic closure of WORTHINGTON's (1976) "northern gyre" and at stations 14 to 16 an isolated pocket of stronger silicate maximum water is found associated with lower salinity. On Fig. 24b this region (on this section, and others) defines the tongue of high silicate turning counterclockwise around the Southeast Newfoundland Rise. Figure 26 is an orthogonal section intersecting that of Fig. 25 at the center of the upper water anticyclone at station 13 (station 33 is the reoccupation of station 13). The thermocline topography is not as well behaved as on the other section. In this orthogonal plane the upper water anticyclone center is slightly west at station 37, with stations 37 to 43 defining the North Atlantic Current, and stations 37 to 28 (or all the way to 21) being the recirculation. In the deep water, station 37 defines the westward edge of a pool of water with higher silicate maximum than occurs beneath the North Atlantic Current which is correspondingly lower in salinity. A level-of-no-motion above this pool gives deep flow from this pool of high-silicate water to the north into the Newfoundland Basin.

The deep shear and silicate distributions can be united into a consistent framework by choosing a level-of-no-motion above the silicate maximum layer, giving a counter-rotation to the deep water relative to the shallow water. In other words, beneath WORTHINGTON's (1976) anticyclonic gyre at thermocline levels is a cyclonic gyre within the deeper water. This gyre is not purely a recirculating system, but rather is partially connected with the deep circulation southwest of the Southeast Newfoundland Rise. On the "west" side of the deep gyre low-silicate water with slightly higher salinity flows south at the bottom of the DWBC east of the Grand Banks (Fig. 24c) and turns southeast along the poleward side of the Rise as it rounds the Rise in the clockwise direction so supplying the westward flow of the DWBC of the Slope Water region. Only part of the southward flow affects the turn to provide the continuation of the DWBC flow, the rest recirculates northward on the "east" side of the deep cyclonic gyre, to provide the low-silicate influence at the bottom of the Basin. High silicate water from the pool of AABW and LDW in the south rounds the Rise in the counterclockwise sense and enters the "east" side of the gyre. Some of this escapes northward to the Labrador Basin through the Narrows, the rest recirculates southward on the "west" side of the cyclonic gyre to provide the deep silicate maximum in the DWBC.

The preceding paragraph points out the dual circulation aspects of the system involving elements of recirculation within each geographic basin, but with flow between the basins. Both aspects can be recognized in the geographic distribution of deep shear. The dynamic thickness between 3000db - 4000db was charted by STOMMEL, NILER and ANATI (1978) (Fig. 27a). Part of the DWBC lies above 4000db, so is not included on the chart. With a level-of-no-motion at 3000db or shallower, the overall circulation shown east of Newfoundland is cyclonic. The two silicate transitions at the Rise and at the Narrows (Fig. 24) coincide with two circulation boundaries. The Narrows splits the cyclonic gyre's central dynamic height maximum; this is indicative of some degree of recirculation around these two gyre centers which are superimposed on the overall elongated cyclonic gyre, and the northern silicate transition lies along the saddle

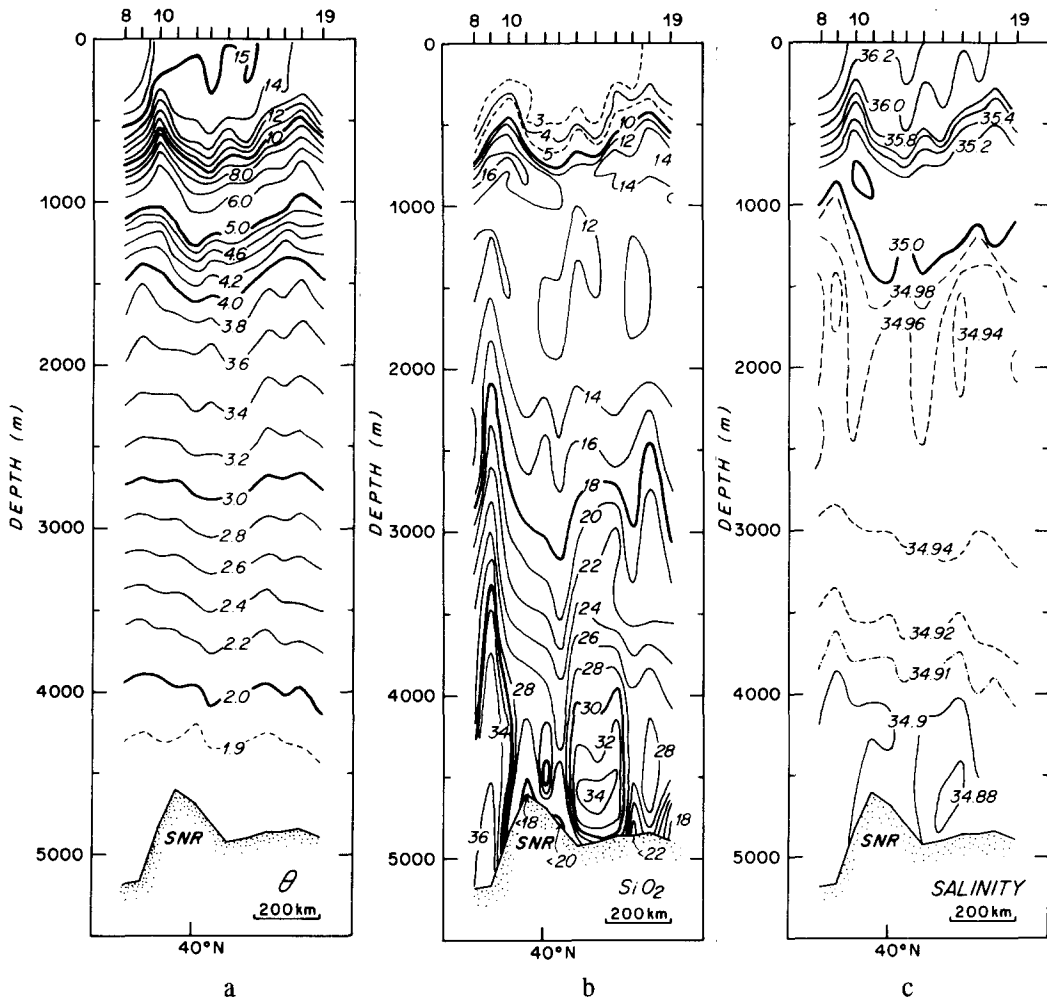


FIG.25a. Section of potential temperature (°C) across the Southeast Newfoundland Rise (SNR), *Baffin* cruise BI-0566, April 1966 (GRANT, 1968). The meridional dotted section in Fig.3; south is on left.

FIG.25b. Section of silicate (μmol l⁻¹) across the Southeast Newfoundland Rise, as Fig.25a.

FIG.25c. Section of salinity, as Fig.25a.

point between the maxima. The second silicate transition, over the Rise, coincides with the disconnection, in their contouring of the data, between the Newfoundland gyre and the region south of the Rise. This isolation is partially a contouring ambiguity: Fig.27b shows an alternative contouring of the same data which was chosen intentionally to emphasize the possibility of connection between the contours across the Rise (station locations are indicated by dots to show the contouring control). Bearing in mind the continuity of DWBC flow across the Rise, it seems sensible to extend the 20 and 30dyn mm contours around the Rise, though data voids and potential sampling problems over steep topography make the lowest dynamic thickness offshore of the

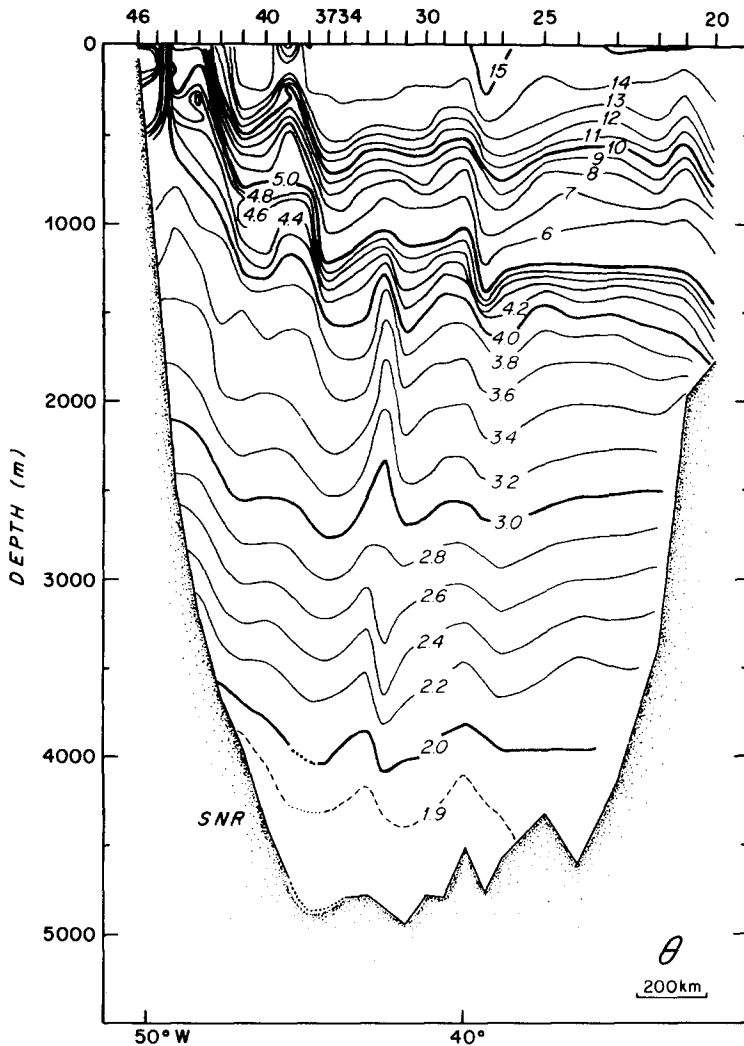


FIG.26a. Section of potential temperature ($^{\circ}\text{C}$) parallel to and north of the axis of the Southeast Newfoundland Rise (SNR), *Baffin* cruise BI-0566, April-May 1966 (GRANT, 1968). Note: no data below 3900m at station 38, and station 33 is a reoccupation of station 13 of Fig.25. This section appears as the zonal dotted line in Fig.3.

4000db contour poorly sampled. It does not violate the data to connect the 40dyn mm contour from the deep Gulf Stream southwest of the Rise to the Newfoundland gyre northeast of the Rise, through a large area without stations.

Figures 27c and d are similar alternative contourings of a different data set, the 1972 data discussed by CLARKE, HILL, REINIGER and WARREN (1980), a substantial subset of the data used in Fig.24 which has better station placement in the region of the ambiguity. They show the maximum dynamic thickness value in the Gulf Stream region as 73dyn mm and a comparable maximum of 77dyn mm in the Newfoundland gyre. In Fig.27c (contoured like 27a) WORTHINGTON's (1976) "trough" of low dynamic thickness protrudes from the western boundary out along the Rise, with the maximum value along its axis being only 37dyn mm. Thus the saddle point in

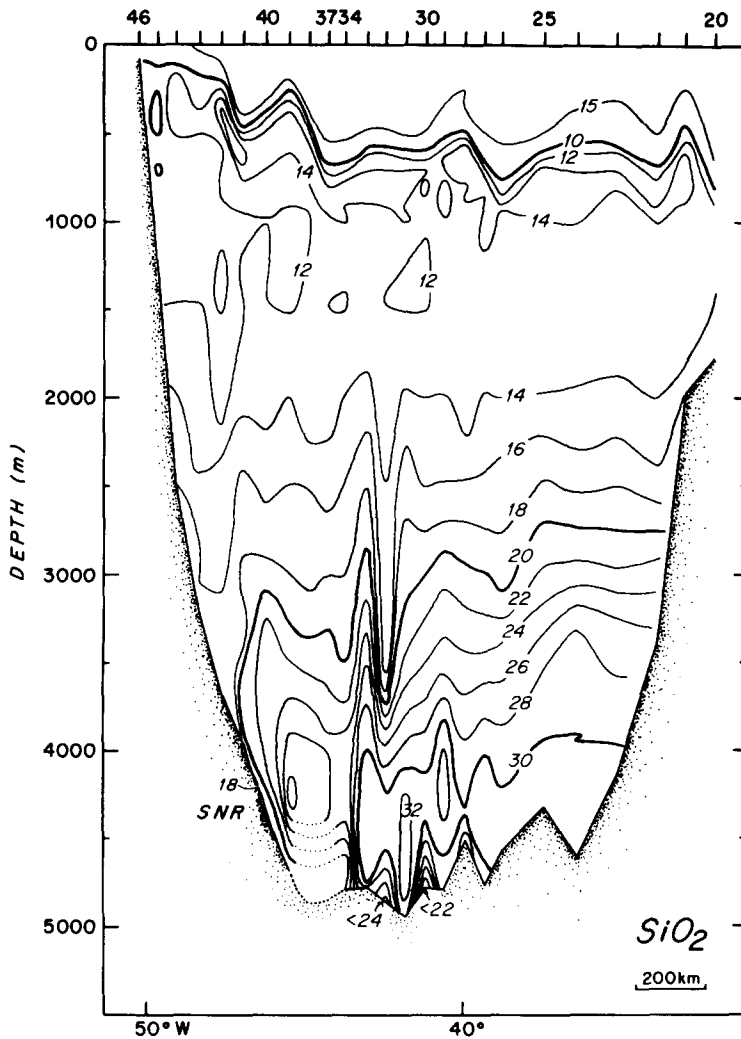


FIG.26b. Section of silicate ($\mu\text{mol l}^{-1}$) across the Southeast Newfoundland Rise as Fig.26a.

the circulation in this contouring is deep enough to break the continuity of the 40 dyn mm, implying almost complete isolation of the gyre circulations southwest and northeast of the Rise. The alternative contouring shown in Fig.27d (contoured like Fig.27b) results in these gyre circulations connecting across the Rise near the 4500m contour, thus providing an increased gyre-gyre flow through the continuity of the 40 dyn mm contour.

The contouring of Fig.27d may look a bit forced relative to that of Fig.27c, but there are three reasons to consider it to be the more realistic rendering. First, the contouring of Fig.27c takes the DWBC on an eastward loop far from the foot of the continental slope into mid-basin and back onto the slope. In Fig.27d the DWBC is shown more as a bathymetry following current. Second, the circulation of Fig.27d is more consistent with the silicate distributions (Figs 24b,c) as not only

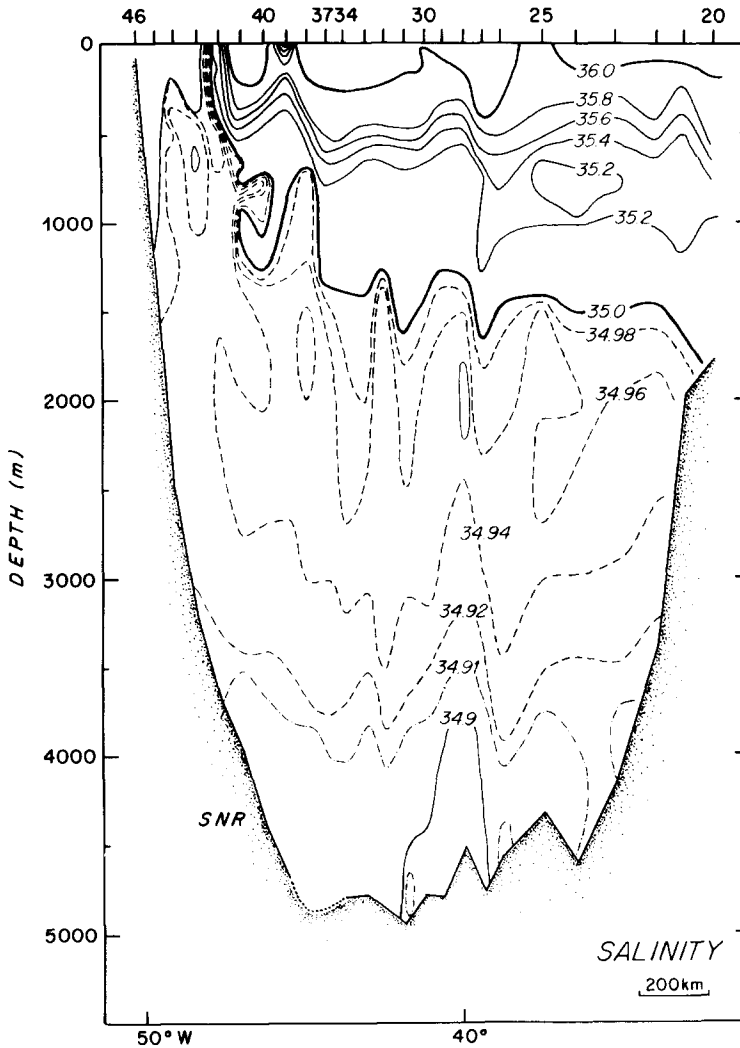


FIG.26c. Section of salinity, as Fig.26a.

does the bathymetry following DWBC coincide with the low-silicate water's restriction to the continental slope but also the northward flow across the Rise east of 45°W coincides with the high-silicate water protruding around the Rise into the Newfoundland Basin. Third, the eastward extent of the low dynamic thickness values imply that an eastward extension of the trough (as Fig.27c) may not be typical for this region. Figure 27e is a contouring of the dynamic thickness for the 1966 data used in the silicate maps of Fig. 24. The sections of temperature and silicate are shown in Figs 25 and 26. The field of dynamic thickness for these data shows a continuity of the 40dyn mm contour that seems unambiguous, because there are four stations aligned across the Rise with values of 43, 44, 45 and 46dyn mm at locations near where stations on Figs 27c and 26d showed 31, 30 and 12dyn mm .

The double maximum of the Newfoundland gyre dynamic thickness seen in Fig.27a is less pronounced in the 1972 data (see Fig.27c) with the saddle point of 50dyn mm being only 9dyn mm

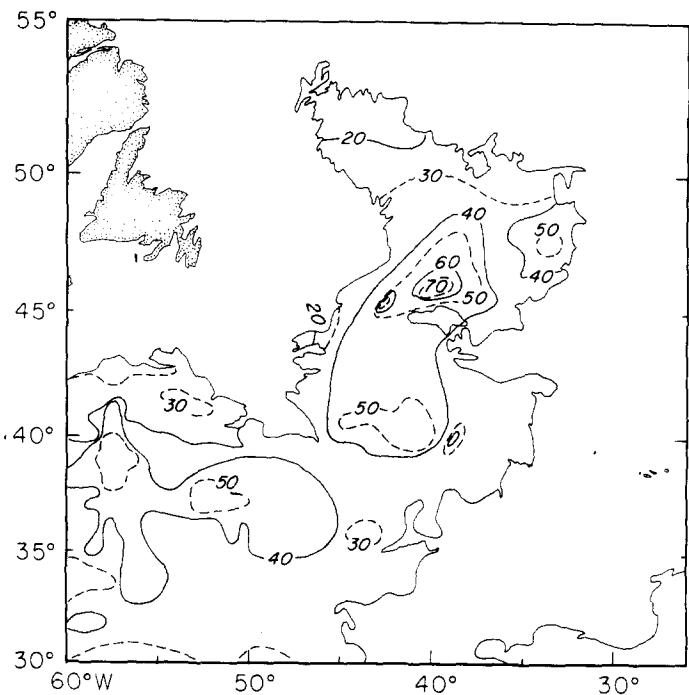


FIG.27a. Dynamic thickness between 3000db and 4000db (in dynamic millimeters, with 400 subtracted from contour labels). From STOMMEL, NIILER and ANATI (1978).

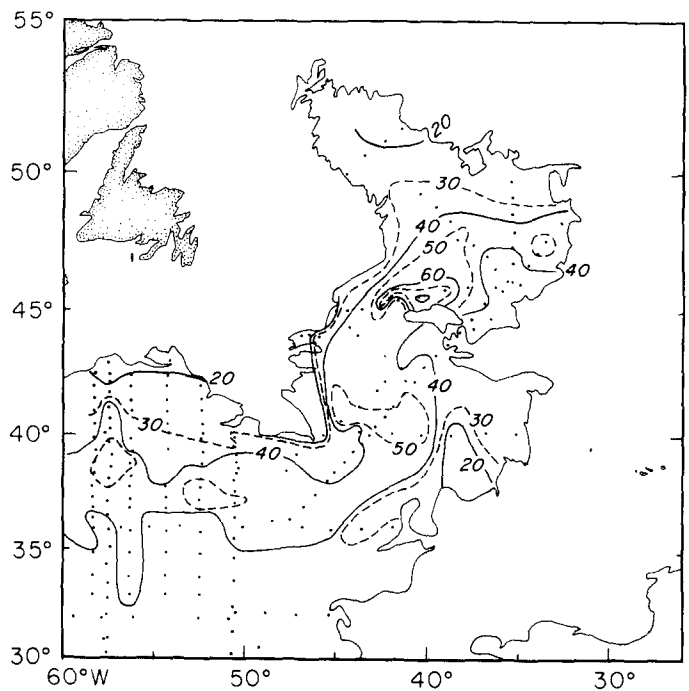


FIG.27b. As Fig.27a, but re-contoured with contours allowed to extend larger distances between station lines (stations indicated by dots).

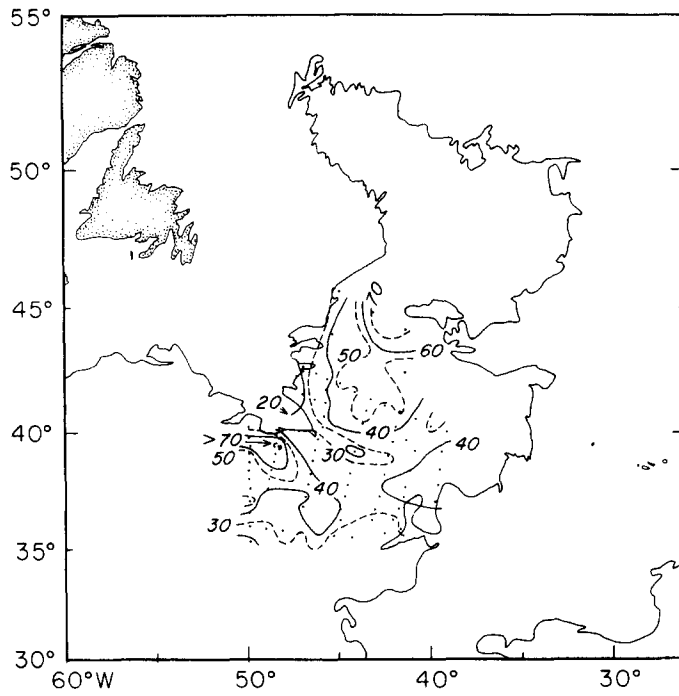


FIG.27c. As Fig.27a, but for the 1972 data of CLARKE, HILL, REINIGER and WARREN (1980).

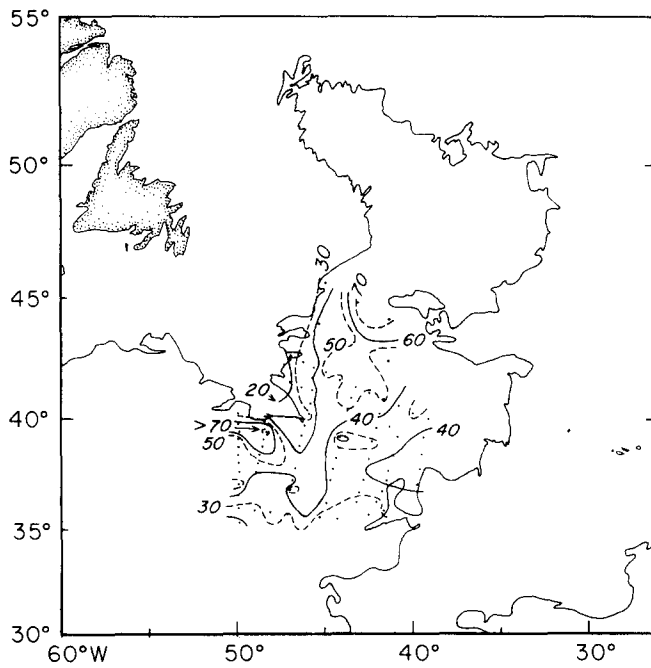


FIG.27d. As Fig.27c, alternate contouring.

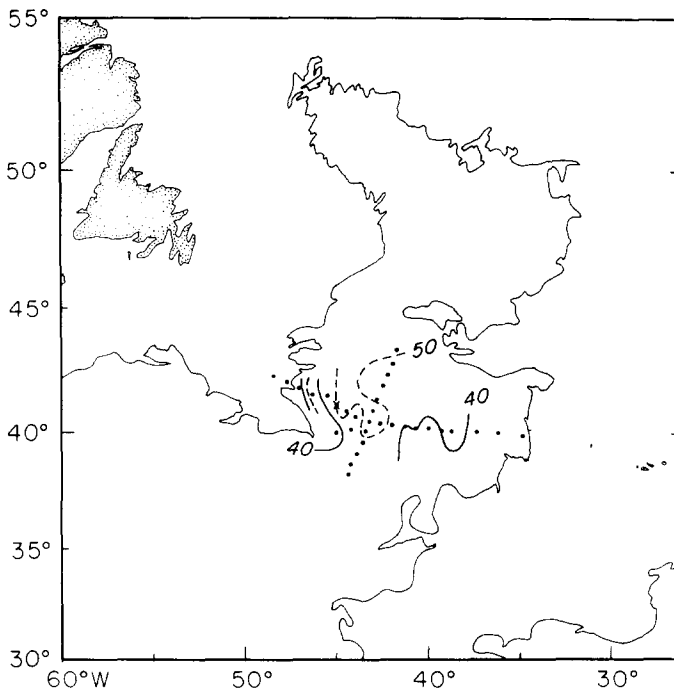


FIG.27e. As Fig.27a, but for the 1966 data of GRANT (1968).

lower than the southern maximum. But the data defining the saddle are widely spaced, so the saddle could be weaker. The data at the Flemish-Milne Narrows shows that the high value contours surrounding the northern maximum protrude southward into the Narrows (Fig.27c) rather than closing north of the Milne Ridge as the contouring (through a data void) of Fig.27a suggested. This improves the consistency of the implied circulation with the silicate distributions of Fig.24, as this southward protrusion of dynamic thickness contours parallels the crowding of silicate contours that marked the second silicate transition (at the Narrows).

After this paper was accepted, the author's attention was drawn to a paper by ARMI and WILLIAMS (1991), which described current meter data from the southern flank of the Southeast Newfoundland Rise (nominally 39°N, at 46°W and 44°W) and related hydrographic data – including the 1972 silicate data from Fig.24. They found periods of persistent westward flow (along isobaths) as well as periods of weak flow. Sometimes these stations showed northern influence – low silicate and high oxygen – and sometimes the higher silicates and lower oxygen of the deep Gulf Stream. Their interpretation drew on the idea of a deep cyclonic recirculation (HOGG, 1983; HOGG, PICKART, HENDRY and SMETHIE, 1986) beneath and north of the Gulf Stream. They suggested that sometimes the moorings sample the westward flow of this deep cyclonic recirculation (which involves LDW in the present terminology), while at other times they sample the DWBC flow carrying DSOW influence. They estimated a westward transport of $19\text{--}50 \times 10^6 \text{m}^3 \text{s}^{-1}$ from these measurements, which therefore is indicative of a boost to the westward flow due to deep recirculation. These measurements and their interpretation support the present idea of a mid-depth level-of-no-motion (they suggest 2000m), since their moorings are placed on the onshore side of the ridge of maximum dynamic thickness (on Fig.27a-d) south of the Rise.

It is necessary to use dynamic thickness fields at shallower levels to examine the circulation in the central and northern Labrador Basin, because of the general shoaling with latitude of the western basin. STOMMEL, NILER and ANATI (1978) also charted the dynamic thickness between 1500db and 3000db, showing a pattern similar to that of Fig.27a to the east of Newfoundland, except that the shallower levels permitted the recognition of the DWBC contours turning across the Rise. Otherwise, their contouring indicates the same separateness of the circulation to the two sides of the Rise (with the same ambiguity of contouring) and the double maximum of dynamic height for the Newfoundland Gyre. In the Labrador Basin southwest of Greenland they showed a strong cyclonic gyre separated from the Newfoundland gyre by a saddle point. Here, though, their contouring is incorrect: they showed only a single 40dyn mm contour crossing the saddle between two 60dyn mm contours, instead of the required two, and a data entry error made the depth of the saddle stronger than it actually is. Figure 28a shows a corrected contouring of this region, based on their data. The station with the data entry error is shown by the x (actual value 85dyn mm recorded as 49dyn mm). The contouring ambiguity at the Southeast Newfoundland Rise is indicated by dotted contours. Figure 28b shows the Labrador field for a more dense data set.

In both contour renderings the Labrador gyre dominates the northwest quadrant, but a bridge connects across the saddle to the Newfoundland gyre (80dyn mm contour on Fig.28a, and 60dyn mm contour on Fig.28b). This bridge is well to the west in the Labrador Basin, lying at the offshore edge of the DWBC at the foot of the continental slope. In the north, the Labrador gyre protrudes east to the southern Irminger Basin, but remains isolated from the aforementioned bridge by an area of lower dynamic height in mid-basin. This area sheds some light on the West Thulean Tongue, for the lower dynamic thickness contours and the Tongue's silicate and salinity contour are congruent (compare Figs 24b,c and d to 28a and b). The Tongue coincides with a set of dynamic thickness contours that emerge westward from the CGFZ, and correspond to flow looping northwest through the Tongue before extending northeast into the Irminger Basin. While the congruence is striking, the pseudo-streamline character of dynamic thickness cannot be carried so far as to assert that all the water in the Tongue emerges from the CGFZ, for two reasons. A spatially non-uniform level-of-no-motion or a variable reference level velocity would cause the flow not to parallel the dynamic thickness contours, and the dynamic thickness for constant pressures samples different water types in the different regions of the chart, since the depth of a given deep isopycnal ranges over hundreds of meters through the combined effects of geostrophy and variable water depth. But it is encouraging that the sharp transition of near bottom silicate (Fig.24c) conforms well to the shape of the dynamic thickness contours, and that the overall sense of flow inferred from the silicate distributions is reflected in the relative baroclinic flow.

The high dynamic thickness bridge in Figs 28a and b isolates the circulation of the higher silicate waters of the Tongue from the DWBC in the west. To the degree that the dynamic thickness contours represent the advection pathways, the high-silicate water loops through the southern Irminger Basin to join the DNBC to the southeast of the southern cape of Greenland. This presumably provides the final transport boost to raise the DNBC transport from the $10.7 \times 10^6 \text{m}^3 \text{s}^{-1}$ south of the Denmark Strait to the $13.3 \times 10^6 \text{m}^3 \text{s}^{-1}$ at the Cape Farewell (Fig.2). Downstream from there the Labrador Gyre, and the high dynamic height bridge to the Newfoundland Gyre provide a circulation barrier to further advective exchange with the high-silicate waters. This dynamic isolation and the homogenization action of the recirculation component of the Labrador gyre seems responsible for the comparative homogeneity of the DWBC silicate distributions in the DNBC and DWBC from southeast of Greenland to the Flemish-Milne Narrows. The evolution that does occur may reflect vertical exchange between the parallel flowing and superimposed silicate maximum and silicate minimum waters (Figs 24b,c).

4. CONCLUSIONS

Returning to my original theme, the DNBC transport distribution of Fig.2, a few transport sums seem appropriate given the additional circulation components shown in Fig.8 and discussed in sections 2 and 3. The eastern basin overflows shown on Fig.2 ($\sigma_\theta \leq 27.8$) total $2.7 \times 10^6 \text{ m}^3 \text{ s}^{-1}$. From

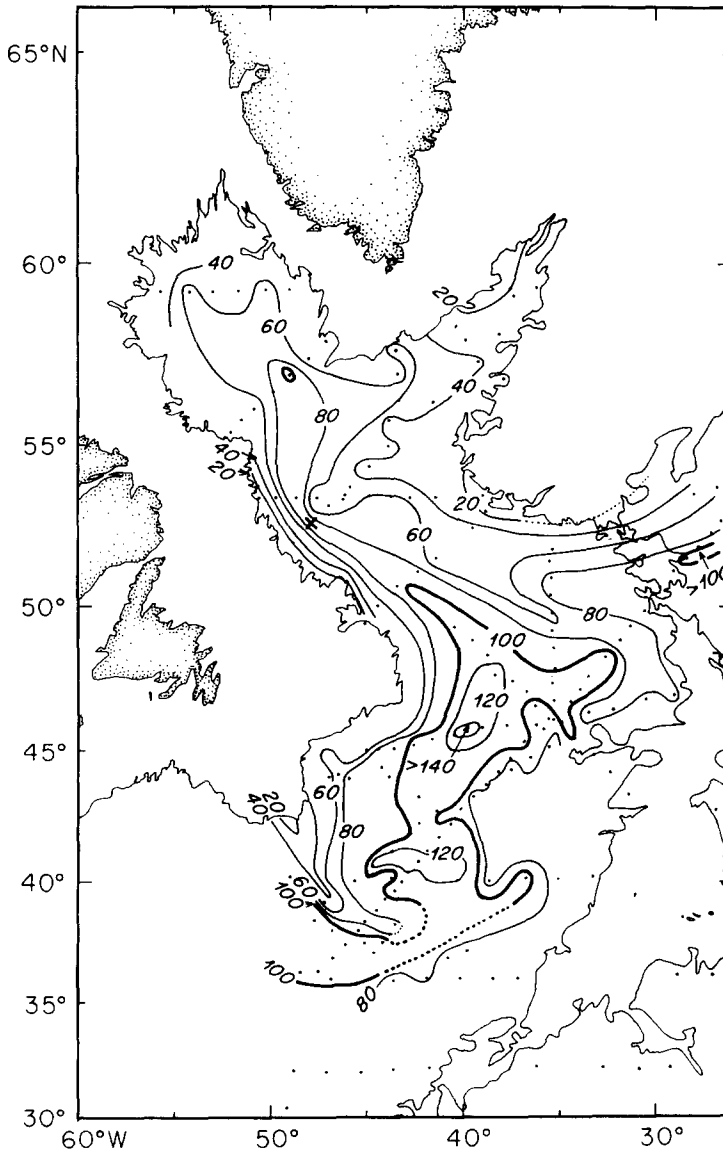


FIG.28a. Dynamic thickness between 1500db and 4000db (in dynamic millimeters, with 600 subtracted from contour labels). From STOMMEL, NIILER and ANATI (1978), but modified for a contouring error and an erroneous datum entry (the station indicated by x).

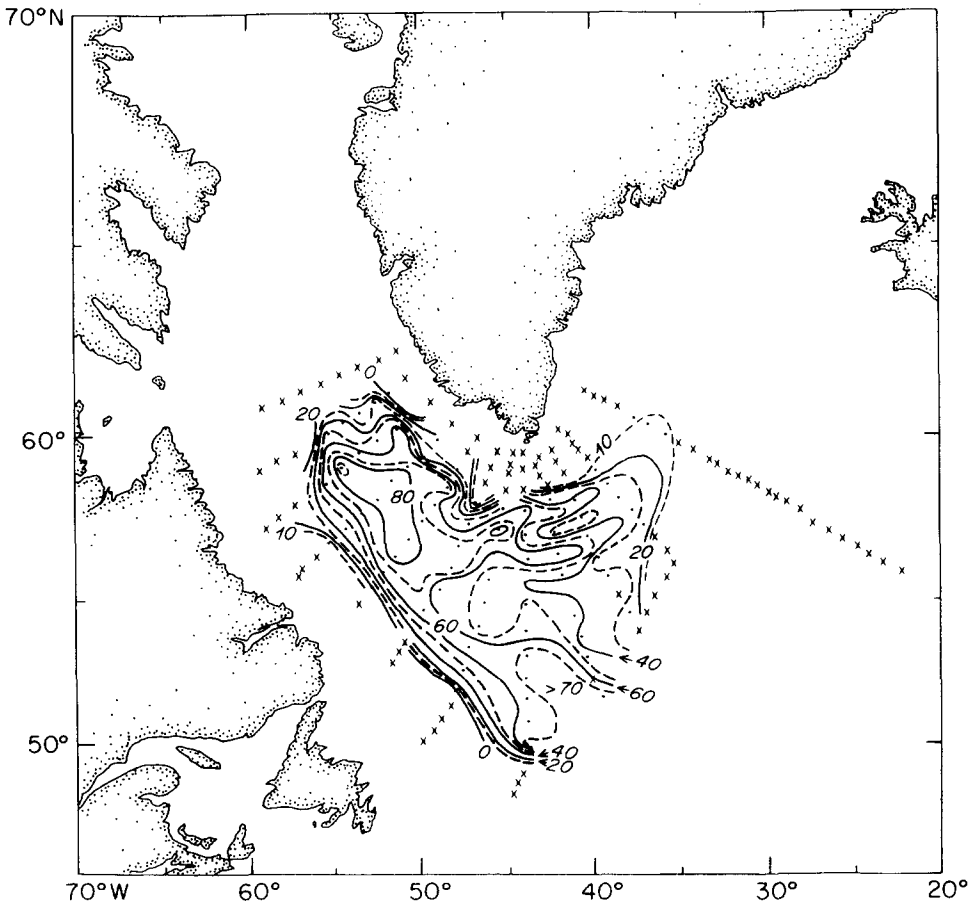


FIG.28b. As Fig.28a, for a different data set: the *Hudson* survey of the Labrador Basin, *Hudson Cruise* BI-0266, March-May 1966. (GRANT, 1968). Two sections from the southern Irminger Basin have been included to complete the sampling of that basin where it exceeds 3000db. These are from *Hudson Cruise* BI-0267, February-March 1967 (GRANT, 1968).

the 20°W section (Fig.12), across the West European Basin, a westward flow of $3.9 \times 10^6 \text{ m}^3 \text{ s}^{-1}$ is estimated below 27.8. This combines with the eastern overflows to give an estimated $6.6 \times 10^6 \text{ m}^3 \text{ s}^{-1}$ to flow west through the CGFZ, exclusive of any warm water entrainment downstream of the overflow measurements or LSW entrainment across the 27.8 isopycnal. The Denmark Strait Overflow (Fig.2) adds $2.9 \times 10^6 \text{ m}^3 \text{ s}^{-1}$, to raise the total DNBC flow to $9.5 \times 10^6 \text{ m}^3 \text{ s}^{-1}$. This total is less than the two DNBC measurements along the coast of Greenland in Fig.2 by $1.2 \times 10^6 \text{ m}^3 \text{ s}^{-1}$ (or $2.4 \times 10^6 \text{ m}^3 \text{ s}^{-1}$ using Dickson's final array transport) and $3.8 \times 10^6 \text{ m}^3 \text{ s}^{-1}$. In the schematic of Fig.8, these residues reflect three components. First is the net northward transport of western basin LDW into the Irminger Basin offshore of the DNBC measurements (or above the zero velocity surface defining the DNBC in the DICKSON, GMTROWICZ and WATSON (1990) estimates, where that surface is not vertical). Second is the northward flow of LSW offshore of the DNBC in the Irminger basin, that is entrained into the dense overflows and returned south in the DNBC. Third is the northward flow of LSW offshore of the DNBC in the Irminger Basin, that returns south

in the DNBC denser than $\sigma_\theta = 27.8$ but is still classified as LSW. At Cape Farewell the composition of the DNBC transport below $\sigma_\theta = 27.8$ is thus estimated as roughly 40% originating from northern dense overflows (with almost an equal split between western and eastern basin overflows) and 60% recirculating waters, including LSW, from the south (also with almost an equal split between western and eastern basins). DICKSON, GMITROWICZ and WATSON (1990) suggested that by the time it reaches the Flemish Cap of the northern Newfoundland Basin (heavy arrow with adjacent question mark, Fig.2) the DWBC might reach the expected magnitude, $15 \times 10^6 \text{m}^3 \text{s}^{-1}$, of the net meridional overturning. Given the probability of a cyclonic recirculation shown here, the magnitude is likely to be larger, since the DWBC will not reflect the net flow.

The downstream increase in the dense water transport of the DNBC apparent in Fig.2 has led me to examine successively the overlying LSW circulation in the subpolar gyre, the northward transport of LDW in the eastern basin, interbasin exchange through the CGFZ, and the northward transport of LDW in the western basin. All are found to contribute to the increase in DNBC transport. The following paragraphs highlight these circulations.

Like the dense overflows themselves, formed by cooling processes within the Nordic Seas, LSW is the product of warm-to-cold water conversion. LSW formation takes place in the western part of the subpolar gyre of the open North Atlantic. LSW participates in the recirculation of this gyre, with the eastward and northward flow of the interior circulation closed by westward flow at the northern boundary, and southward flow at the western boundary. The recirculating LSW in these boundary currents, to the extent that it is denser than $\sigma_\theta = 27.8$, contributes to the measured dense water transport of these currents.

A net production of LSW in the subpolar gyre exists, coupled to the loss of heat from the ocean to the atmosphere, acting on a net inflow of warm water across the boundary of the subtropical gyre, or more precisely the part of that inflow that does not pass into the Nordic Seas to be the source water for the production of dense overflow water. The net LSW production must, by mass conservation, be returned to mid-latitudes; this occurs in two ways. The DWBC carries LSW southward in its normal density range in relatively unaltered form. To the extent that this occurs at densities greater than $\sigma_\theta = 27.8$, it will be reflected in the measured transport of the dense water of the mid-latitude DWBC. In the subpolar gyre, entrainment from the recirculating LSW into the denser levels of the DNBC and DWBC occurs; this yields a mixed product denser than the LSW, but lighter than the overflow waters themselves and the LDW components that enter the subpolar basins from the south. Part of the net production of LSW thus returns to mid-latitude "disguised" in this mixed product.

The westward trending flow of the DNBC is found to begin in the West European Basin, initiated by a flow of LDW originating from the south rather than the northern overflows. A deep cyclonic gyre exists in the West European Basin, with a dynamic signature of a bowl in the deep isotherms. From mid-latitude in the eastern basin a northward flow of LDW towards this gyre is observed, which is western intensified within the basin south of 30°N , but becomes eastern intensified north of 32°N as it approaches the deep gyre. This flow appears both in the deep shear and the deep properties (silicate, salinity and oxygen) for temperatures below 2.5°C , and the coldest waters involved warm northwards from 2.0°C at 32°N to nearly 2.2°C in the West European Basin. In this Basin, the northward flow is diverted westward by the Rockall Plateau complex before turning back northward into the Iceland Basin. These flows augment the West European Basin deep gyre transport in its eastern and northern quadrants by the amount of southern originating LDW flowing northward from the Iberian Basin.

The deep gyre in the West European Basin acts laterally to homogenize the deep water to characteristics between the extremes provided by the southern originating LDW and the northern

overflows. In the west the gyre extends to the CGFZ, while in the north the gyre bulges into the Iceland Basin west of the Rockall Plateau. In the Iceland Basin the gyre's northward bulge intrudes cold higher silicate, and lower oxygen and salinity water into the Basin, and the net northward flow of LDW on the eastern side returns southward along the flank of the Reykjanes Ridge to the CGFZ, elevating the silicate and depressing the oxygen and salinity of the overflow components that have joined the DNBC in the northern Basin. The western extension of the gyre to the CGFZ brings relatively undiluted southern origin LDW near the CGFZ's sills with less interaction with the overflow waters than the waters looping more northward into the Iceland Basin.

The net flow of deep water through the CGFZ reflects the sum of the dense overflows, the southern originating LDW, and entrained LSW and warmer waters. Near the sills of the CGFZ these individual source water characteristics are blurred by the entrainment process, the action of the deep recirculating gyre, and some combination of vertical and lateral mixing within the CGFZ, to produce a relatively homogeneous product that transits to the western basin. This product has the classic slightly elevated salinity that contrasts with the western basin deep waters it penetrates, attributed to the high salinity of thermocline waters entrained into the northern overflows, but its silicate content is elevated and its oxygen depressed because of its component of southern originating LDW.

From mid-latitudes in the western basin, AABW and LDW penetrate northward into the deep recirculation system of the Gulf Stream southwest of the Grand Banks. A tongue of elevated silicate water emerges from this area to round the Southeast Newfoundland Rise and traverse the Newfoundland and Labrador Basins to the western side of the sills of the CGFZ. The tongue is concentrated on the eastern side of these Basins, and the fields of deep dynamic height show a corresponding shear signature. On the western sides of the Basins, lower silicate water is found near the bottom. Along with the shear, its distribution shows that this water originates as the overflow through the Denmark Strait, and evolves downstream along the western boundary through confluence of waters from the northward flow through the Basins from the Southeast Newfoundland Rise and from the eastward flow through the CGFZ.

These largest scale images are of a lateral counterflow system, a meridionally elongated cyclonic gyre receiving elevated silicate water in the southeast, intermediate silicate water from the CGFZ, and low-silicate water from the Denmark Strait Overflow, and returning (in the DWBC) to mid-latitude an intermediate silicate mixed product in the southwest. The large scale distribution of dynamic height confirms the overall structure of southward flow on the western side and northward flow on the eastern side of the western basin, and reveals superimposed on this, distinct recirculating gyre centers in the western Labrador Basin north of the Flemish-Milne Narrows, and in the Newfoundland Basin north of the Southeast Newfoundland Rise. These recirculation components are responsible for sharper transitions within the broad scale meridional gradients of silicate.

At the scale of the full ocean basin the overall system is a southward flowing DWBC whose transport is larger than that of the northward flowing warm source water that is cooled to deep water in the subpolar basins and the Nordic Seas because of the northward transport of LDW and LSW in the interior of the subpolar basins. For the LDW, this is the structure predicted by the most basic of abyssal circulation theories, the STOMMEL and ARONS (1960) theory. In that theory the upper bound for the transport of the recirculating component is 50% of the DWBC, that is, the source component and the recirculating component are equal in strength. In the observations discussed here rough equality of the northern source and recirculating components is indicated, although in the western basin the magnitude of the net northward flow of LDW from mid-latitude remains to be quantified, as it is masked by the deep cyclonic recirculation.

5. ACKNOWLEDGEMENTS

I would like to thank Val Worthington for getting me started on trying to understand the deep circulation of the North Atlantic, Ruth Gorski Curry, Mary Woodgate-Jones and Toshiko Turner for their help in collecting some of the data used in this study and for their diligence in preparation of the diverse analysis products needed for the project, the scientific teams and crews of *Oceanus* cruises 133 and 202, and *Knorr* cruise 104 for splendid performance under a heavy work load, Michel Arhan for providing the TOPOGULF data set, Ross Hendry for providing the *Hudson* data from 1982, Veta Green for preparing the manuscript, and Allyn Clarke, Greg Johnson, Ian McCave, Bob Pickart, Peter Saunders, Kevin Speer, Lynne Talley and Miki Tsuchiya for useful discussions of the data interpretations. The detailed text comments by the referees, and by Johnson, Pickart, Speer and Talley, were very useful. This work was supported by the National Science Foundation grants OCE 80-15789 (the *Oceanus* 133 data), OCE 78-22223 (the *Knorr* 104 data) and OCE 86-14486 (the *Oceanus* 202 data and the analysis reported in this paper) and by the Atlantic Climate Change Program of the National Oceanographic and Atmospheric Administration grant NA16RC0528-01 (the analysis reported in this paper). This paper is contribution number 7818 of the Woods Hole Oceanographic Institution.

6. REFERENCES

- ARMI, L. and R. WILLIAMS (1991) The deep western boundary undercurrent off the Newfoundland Ridge. *Deep-Sea Research*, **38**, 371-391.
- AUFFRET, G.A. and B. SICHLER (1982) Holocene sedimentary regime in two sites of the northeastern Atlantic slope.: *Bulletin de l'Institut de Geologie du Bassin d'Aquitaine*, **31**, 191-193.
- BORENÅS, K.M. and P.A. LUNDBERG (1988) On the deep-water flow through the Faroe Bank Channel. *Journal of Geophysical Research*, **93**, 1281-1292.
- BREWER, P.G., W.S. BROECKER, W.J. JENKINS, P.B. RHINES, C.G. ROOTH, J.H. SWIFT, T. TAKAHASHI and R.T. WILLIAMS (1983) A climatic freshening of the deep Atlantic north of 50°N over the past 20 years. *Science*, **222**, 1237-1239.
- BRYDEN, H.L. and M.M. HALL (1980) Heat transport by currents across 25°N latitude in the Atlantic Ocean. *Science*, **207**, 884-886.
- CLARKE, R.A. (1984) Transport through the Cape Farewell - Flemish Cap Section. *Rapports et Procès-Verbaux des Reunions Extrait du Journal du Conseil International Pour l'Exploration de la Mer*, **185**, 120-130.
- CLARKE, R.A., H.W. HILL, R.F. REINIGER and B.A. WARREN (1980) Current system south and east of the Grand Banks of Newfoundland. *Journal of Physical Oceanography*, **10**, 25-65.
- DICKSON, R.R. and I.N. McCAVE (1982) Properties of nepheloid layers on the upper slope west of Porcupine Bank. *International Council for the Exploration of the Sea*, **C:2**, 9pp.
- DICKSON, R.R., E.M. GMITROWICZ and A.J. WATSON (1990) Deep-water renewal in the northern North Atlantic. *Nature, London*, **344**, 848-850.
- DICKSON, R.R., P.A. GURBUTT and K.J. MEDLER (1980) Long-term water movements in the southern trough of the CGFZ. *Journal of Marine Research*, **38**, 571-583.
- DICKSON, R.R., J. GOULD, T.J. MÜLLER and C. MAILLARD (1985) Estimates of the mean circulation in the deep (>2000m) layer of the eastern North Atlantic. *Progress in Oceanography*, **14**, 103-127.
- DOOLEY, H.D. and J. MEINCKE (1981) Circulation and water masses in the Faroese Channels during Overflow '73. *Deutsche Hydrographische Zeitschrift*, **34**, 41-54.
- ELLETT, D.J. and A. EDWARDS (1978) A volume transport estimate for Norwegian Sea overflow across the Wyville-Thomson Ridge. *ICES CM 1978 C:19*, 11pp.
- ELLETT, D.J. and J.H.A. MARTIN (1973) The physical and chemical oceanography of the Rockall Channel. *Deep-Sea Research*, **20**, 585-625.
- ELLETT, D.J. and D.G. ROBERTS (1973) The overflow of Norwegian Sea deep water across the Wyville-Thomson Ridge. *Deep Sea Research*, **20**, 819-835.
- ELLETT, D.J., H.D. DOOLEY and H.W. HILL (1979) Is there a north-east Atlantic slope current? *ICES CM 1979, C:35*, 5pp (mimeo, unpublished manuscript)
- FOFONOFF, N.P. and R.M. HENDRY (1985) Current variability near the Southeast Newfoundland Ridge. *Journal*

- of *Physical Oceanography*, **15**, 963-984.
- FUGLISTER, F.C. (1960) Atlantic Ocean Atlas of Temperature and Salinity Profiles and Data from the International Geophysical Year of 1957-1958. *Woods Hole Oceanographic Institution Atlas Series*, **1**, 209pp.
- GARDNER, J.V. and R.B. KIDD (1987) Sedimentary processes in the northwestern Iberian continental margin viewed by long-range side-scan sonar and seismic data. *Journal of Sedimentary Petrology*, **57**, 397-407.
- GARNER, D.M. (1972) Flow through the Charlie-Gibbs Fracture Zone, Mid-Atlantic Ridge. *Canadian Journal of Earth Sciences*, **9**, 115-121.
- GRANT, A.B. (1968) Atlas of Oceanographic Sections: Temperature-salinity-dissolved oxygen-silica, Davis Strait-Labrador Basin-Denmark Strait-Newfoundland Basin, 1965-1967. *Atlantic Oceanographic Laboratory, Rep.A.O.L. 68-5*, Bedford Institute of Oceanography, Dartmouth, N.S., Canada.
- HALL, M.M. and H.L. BRYDEN (1982) Direct estimates and mechanisms of ocean heat transport. *Deep-Sea Research*, **29**, 339-359.
- HARVEY, J.G. (1980) Deep and bottom water in the Charlie-Gibbs Fracture Zone. *Journal of Marine Research*, **38**, 173-182.
- HARVEY, J.G. and M. ARHAN (1988) The water masses of the central North Atlantic in 1983-1984. *Journal of Physical Oceanography*, **18**, 1855-1875.
- HARVEY, J.G. and A. THEODOROU (1986) The circulation of Norwegian Sea overflow water in the eastern North Atlantic. *Oceanologica Acta*, **9**, 393-402.
- HENDRY, R.M. (1989) Hydrographic Measurements from C.S.S. *Hudson* Cruise 82-002. Bedford Institute of Oceanography. *Canadian Technical Report of Hydrography and Ocean Sciences*, **118**, 112pp.
- HOGG, N.G. (1983) A note on the deep circulation of the western North Atlantic: its nature and causes. *Deep-Sea Research*, **30**, 945-961.
- HOGG, N.G., R.S. PICKART, R.M. HENDRY and W.J. SMETHIE Jr (1986) The northern recirculation gyre of the Gulf Stream. *Deep-Sea Research*, **33**, 1139-1165.
- HURDLE, B.G. (1986) *The Nordic Seas*, Springer-Verlag, New York, 777pp.
- IVERS, W.D. (1975) *The deep circulation in the northern North Atlantic with special reference to the Labrador Sea*, PhD Thesis, University of California, San Diego, 179pp.
- KNAPP, G.P. and H.M. STOMMEL (1985) Hydrographic data from R.V. *Oceanus* Cruise 133, leg VII. *Woods Hole Oceanographic Institution Technical Report WHOI-85-38*, 107pp.
- LAUGHTON, A.S. and D. MONAHAN (1984) General bathymetric chart of the ocean, Chart 5.04. *International Hydrographic Organization*, Canadian Hydrographic Service, Ottawa, Canada.
- LAZIER, J.R.N. (1980) Oceanographic conditions at ocean water ship *Bravo*, 1964-1974. *Atmosphere-Ocean*, **18**, 227-238.
- LONSDALE, P. (1982) Sediment drifts of the northeast Atlantic and their relationship to the observed abyssal currents. *Bulletin de l'Institut Geologie du Bassin d'Aquitaine*, **31**, 141-149.
- LONSDALE, P.F. and C.D. HOLLISTER (1979) A near-bottom traverse of Rockall Trough: hydrographic and geologic inferences. *Oceanologica Acta*, **2**, 91-105.
- McCARTNEY, M.S. (1991) The system of deep western boundary currents and recirculations in the Atlantic Ocean. *Eos, Transactions, American Geophysical Union*, supplement, **72**, 31-32 (abstract).
- McCARTNEY, M.S. (1992) The transport of Antarctic Bottom Water at 4°N in the western basin of the North Atlantic Ocean. *Journal of Geophysical Research* **97**, (in press).
- McCARTNEY, M.S. and R. CURRY (1992) Trans-equatorial flow of Antarctic bottom water in the western Atlantic Ocean. *Journal of Physical Oceanography*, **22**, (in press).
- McCARTNEY, M.S. and L.D. TALLEY (1982) The subpolar mode water of the North Atlantic Ocean. *Journal of Physical Oceanography*, **12**, 1169-1188.
- McCARTNEY, M.S. and L.D. TALLEY (1984) Warm-to-cold water conversion in the northern North Atlantic Ocean. *Journal of Physical Oceanography*, **14**, 922-935.
- McCARTNEY, M.S., S.L. BENNETT and M.E. WOODGATE-JONES (1991) Eastward flow through the Mid-Atlantic Ridge at 11°N and its influence on the abyss of the eastern basin. *Journal of Physical Oceanography*, **21**, 1089-1121.
- McCAVE, I.N. and B.E. TUCHOLKE (1986) Deep current-controlled sedimentation in the western North Atlantic. In: *The geology of North America, Volume M, The western North Atlantic Region*, P.R. VOGT and B.E. TUCHOLKE, editors, Geological Society of America. Chapter 17, 451-468.
- McCAVE, I.N., P.F. LONSDALE, C.D. HOLLISTER and W.D. GARDNER (1980) Sediment transport over the

- Hatton and Gardar contourite drifts. *Journal of Sedimentary Petrology*, **50**, 1049-1062.
- MANN, C.R. (1969) Temperature and salinity characteristics of the Denmark Strait overflow. *Deep-Sea Research*, **16** (Suppl.), 125-137.
- MANN, C.R., A.R. COOTE and D.M. GARNER (1973) The meridional distribution of silicate in the western Atlantic Ocean. *Deep-Sea Research*, **20**, 791-801.
- MANN, C.R., A.B. GRANT and T.R. FOOTE (1965) Atlas of Oceanographic Sections: Temperature-salinity-dissolved oxygen. Northwest Atlantic Ocean, Newfoundland Basin and Gulf Stream, February 1962-July 1964. *Bedford Institute of Oceanography, Report BIO 65-16*, Dartmouth, N.S., Canada.
- MANTYLA, A.W. and J.L. REID (1983) Abyssal characteristics of the World Ocean waters. *Deep-Sea Research*, **30**, 805-833.
- MEINCKE, J. (1983) The modern current regime across the Greenland-Scotland ridge. In: *Structure and Development of the Greenland Scotland Ridge*, A. BOTT, B. SAKOV, C. TALWANI and D. THIODE, editors, Plenum Publishing Corporation, 637-650.
- MEINCKE, J., G. SIEDLER and W. ZENK (1975) Some current observations near the continental slope off Portugal. *Meteor Forschungen-Ergebnisse*, **A**, **16**, 15-22.
- METCALF, W.G. (1958) Oceanographic data from R.V. *Crawford* Cruise 16, 1 October-11 December 1957. International Geophysical Year. *Woods Hole Oceanographic Institution Technical Report*, **WHOI58-31**.
- METCALF, W.G. (1969) Dissolved silicate in the deep North Atlantic. *Deep-Sea Research*, **16** (Suppl.), 139-145.
- MÜLLER, T.J., J. MEINCKE and G.A. BECKER (1979) Overflow '73: the distribution of water masses on the Greenland-Scotland Ridge in August/September 1973 - A data report. *Berichte aus dem Institut für Meereskunde an der Christian-Albrechts-Universität, Kiel*, **62**, 172pp.
- ÖSTLUND, G.H. and C. GRALL (1987) Transient tracers in the ocean. North and tropical Atlantic tritium and radiocarbon. *Tritium Laboratory Data Report*, **No.16**, University of Miami, Rosenstiel School of Marine and Atmospheric Science, Miami, Florida, 277pp.
- ÖSTLUND, H.G. and C.G.H. ROTH (1990) The North Atlantic tritium and radiocarbon transients, 1972-1983. *Journal of Geophysical Research*, **95**(C11), 20147-20165.
- PROVOST, C. and R. SALMON (1986) A variational method for inverting hydrographic data. *Journal of Marine Research*, **44**, 1-34.
- REID, J.L. (1986) On the total geostrophic circulation of the South Pacific Ocean: Flow patterns, tracers and transport. *Progress in Oceanography*, **16**, 1-61.
- ROEMMICH, D.H. (1980) Estimation of meridional heat flux in the North Atlantic by inverse methods. *Journal of Physical Oceanography*, **10**, 1972-1983.
- ROEMMICH, D. and C. WUNSCH (1984) Apparent changes in the climatic state of the deep North Atlantic Ocean. *Nature, London*, **307**, 447-450.
- ROEMMICH, D. and C. WUNSCH (1985) Two transatlantic sections: Meridional circulation and heat flux in the subtropical North Atlantic Ocean. *Deep-Sea Research*, **32**, 619-664.
- ROSS, C.K. (1984) Temperature-salinity characteristics of the "overflow" water in Denmark Strait during "Overflow '73". *Rapports et Procès Verbaux des Reunions Extrait du Journal du Conseil International Pour l'Exploration de la Mer*, **185**, 111-119.
- SAUNDERS, P.M. (1987) Flow through Discovery Gap. *Journal of Physical Oceanography*, **17**, 631-643.
- SAUNDERS, P.M. (1990) Cold outflow from the Faroe Bank Channel. *Journal of Physical Oceanography*, **20**, 29-43.
- SAUNDERS, P.M. (1992) The flux of overflow water in the Charlie-Gibbs Fracture Zone. *Annales Geophysicae*, Supplement II to **10**, C166 (abstract).
- SCHMITZ, W.J. and N.G. HOGG (1978) Observations of energetic low-frequency current fluctuations in the Charlie-Gibbs Fracture Zone. *Journal of Marine Research*, **36**, 725-734.
- SCRIPPS INSTITUTION OF OCEANOGRAPHY (1986) Transient tracers in the ocean, North Atlantic Study, 1 April-19 October 1981. *Shipboard Physical Chemistry Data Report*, **86-15**, Scripps Institution of Oceanography, University of California, La Jolla, California.
- SEARLE, R.C., D. MONAHAN and G.L. JOHNSON (1982) General bathymetric chart of the oceans, Chart 5.08, *International Hydrographic Organization*, Canadian Hydrographic Service, Ottawa, Canada.
- SHOR, A., P. LONSDALE, C.D. HOLLISTER and D. SPENCER (1980) Charlie-Gibbs Fracture Zone: Bottom-water transport and its geological effects. *Deep-Sea Research*, **27**, 325-345.
- SMETHIE, W.M. and J.H. SWIFT (1989) The tritium:krypton-85 age of Denmark Strait Overflow Water and Gibbs Fracture Zone Water just south of Denmark Strait. *Journal of Geophysical Research*, **94**(C6), 8265-8275.

- SPEER, K.G. and M.S. McCARTNEY (1992) Bottom water circulation in the western North Atlantic. *Journal of Physical Oceanography*, **22**, 83-92.
- STEELE, J.H., J.R. BARRETT and L.V. WORTHINGTON (1962) Deep currents south of Iceland. *Deep-Sea Research*, **9**, 465-474.
- STOMMEL, H. and A.B. ARONS (1960) On the abyssal circulation of the World Ocean - I. Stationary planetary flow patterns on a sphere. *Deep-Sea Research*, **6**, 140-154.
- STOMMEL, H., P. NIELER and D. ANATI (1978) Dynamic topography and recirculation of the North Atlantic. *Journal of Marine Research*, **36**, 449-468.
- SWALLOW, J.C. and L.V. WORTHINGTON (1961) An observation of a deep counter-current in the western North Atlantic. *Deep-Sea Research*, **8**, 1-19.
- SWALLOW, J.C. and L.V. WORTHINGTON (1969) Deep currents in the Labrador Sea. *Deep-Sea Research*, **16**, 77-84.
- SWALLOW, J.C., W.J. GOULD and P.M. SAUNDERS (1977) Evidence for a poleward eastern boundary current in the North Atlantic Ocean. *ICES CM 1977, C:35*, 16pp. (mimeo, unpublished manuscript).
- SWIFT, J.H. (1984a) The circulation of the Denmark Strait and Iceland-Scotland overflow waters in the North Atlantic. *Deep-Sea Research*, **31**, 1339-1355.
- SWIFT, J.H. (1984b) A recent θ -S shift in the deep water of the northern North Atlantic. In: *Climate processes and climate sensitivity*, J.E. HANSEN and T. TAKAHASHI, editors, *Geophysical Monograph*, **29**, Maurice Ewing volume 5, American Geophysical Union, Washington DC, 39-47.
- TAIT, J.B., A.J. LEE, U. STEFANSSON and F. HERMAN (1967) Temperature and salinity distributions and water masses of the region. In: *The Iceland-Faroe Ridge International (ICES) "Overflow" Expedition, May-June 1960. An investigation of cold, deep water overspill into the northeastern Atlantic Ocean*. J.B. TAIT, editor, *Rapports et Procés Verbaux des Reunions Extrait du Journal du Conseil International Pour l'Exploration de la Mer*, **157**, 38-149.
- TALLEY, L.D. and M.S. McCARTNEY (1982) Distribution and circulation of Labrador Sea Water. *Journal of Physical Oceanography*, **12**, 1189-1205.
- TOPOGULF GROUP (1986) TOPOGULF data report Vol 1: CTD, O₂ and nutrients. *Berichte aus dem Institut für Meereskunde*, Nr **154**, Kiel, West Germany.
- TSUCHIYA, M., L.D. TALLEY and M.S. McCARTNEY (1992) An eastern Atlantic section from Iceland southward across the equator. *Deep-Sea Research*, **39**, (in press).
- WORTHINGTON, L.V. (1958) Oceanographic data from the RRS *Discovery II*. International Geophysical Year. Cruises 1 and 2. *National Institute of Oceanography and Woods Hole Oceanographic Institution*, **WHOI-58-30**.
- WORTHINGTON, L.V. (1959) Oceanographic data from the RRS *Discovery II*. International Geophysical Year. Cruise 3. *National Institute of Oceanography and Woods Hole Oceanographic Institution*, **WHOI-59-54**.
- WORTHINGTON, L.V. (1969) An attempt to measure the volume transport of Norwegian Sea overflow water through the Denmark Strait. *Deep-Sea Research*, **16** (Suppl.), 421-432.
- WORTHINGTON, L.V. (1970) The Norwegian Sea as a Mediterranean basin. *Deep-Sea Research*, **17**, 77-84.
- WORTHINGTON, L.V. (1976) On the North Atlantic circulation. *The John Hopkins Oceanographic Studies*, **6**, 110pp.
- WORTHINGTON, L.V. and W.G. METCALF (1961) The relationship between potential temperature and salinity in deep Atlantic water. *Rapports et Procés Verbaux des Reunions Extrait du Journal du Conseil International Pour l'Exploration de la Mer*, **149**, 122-128.
- WORTHINGTON, L.V. and G.H. VOLKMANN (1965) The volume of transport of the Norwegian Sea overflow water in the North Atlantic. *Deep-Sea Research*, **12**, 667-676.
- WORTHINGTON, L.V. and W.R. WRIGHT (1970) North Atlantic ocean atlas of potential temperature and salinity in the deep water including temperature, salinity and oxygen profiles from the *Erika Dan* Cruise of 1962. *Woods Hole Oceanographic Institution Atlas Series*, **2**, 24pp and 58 plates.
- WORTHINGTON, L.V. and W.R. WRIGHT (1971) Discussion of a paper by X. Le Pichon, S. Eitrem and J. Ewing. A sedimentary channel along Gibbs Fracture Zone. *Journal of Geophysical Research*, **76**, 6606-6608.
- WRIGHT, W.R. and L.V. WORTHINGTON (1970) The water masses of the North Atlantic Ocean; a volumetric census of temperature and salinity. *Serial Atlas of the Marine Environment*, Folio 19, American Geographical Society, 8pp, 7 plates.
- WUNSCH, C. (1980) Meridional heat flux of the North Atlantic Ocean. *Proceedings of the National Academy of*

- Sciences, USA, 77, 5043-5047.*
- WUNSCH, C. and B. GRANT (1982) Towards the general circulation of the North Atlantic Ocean. *Progress in Oceanography, 11, 1-59.*
- WÜST, G. (1933) Schichtung und Zirkulation des Atlantischen Ozeans. Das Bodenwasser und die Gliederung der Atlantischen Tiefsee. In: *Wissenschaftliche Ergebnisse der Deutschen Atlantischen Expedition auf dem Forschungs- und Vermessungsschiff "Meteor", 1925-1927, 6, 1st Part 1, 106pp. (Bottom Water and the Distribution of the Deep Water of the Atlantic, M. SLESSERS, translator, B.E. OLSON, editor, 1967. US Naval Oceanographic Office, Washington D.C., 145pp.)*
- WÜST, G. (1935) Schichtung und Zirkulation des Atlantischen Ozeans. Die Stratosphäre. In: *Wissenschaftliche Ergebnisse der Deutschen Atlantischen Expedition auf dem Forschungs- und Vermessungsschiff "Meteor", 1925-1927, 6 1st Part 2, 180pp. (The Stratosphere of the Atlantic Ocean, W.J. EMERY, editor, 1978, Amerind, New Delhi, 112pp).*

7. APPENDIX

ELLETT and ROBERTS (1973) discuss an overflow of cold dense water from the Faroe Bank Channel over the Wyville-Thomson Ridge into the Rockall Trough. The direct evidence for this is observations of cold water in a fissure that is the deepest pathway, silled near 600m. They found there a 15m thick layer of 1.57°C water overlaid by a sharp transition to thermocline waters. ELLETT and EDWARDS (1978) later estimated that this Overflow rarely exceeds $0.3 \times 10^6 \text{m}^3 \text{s}^{-1}$. DOOLEY and MEINCKE (1981) gave an estimate of $0.1 \times 10^6 \text{m}^3 \text{s}^{-1}$, and SAUNDERS (1990) gave two realizations, 0.35 and $0.3 \times 10^6 \text{m}^3 \text{s}^{-1}$.

The evidence for influence of this overflow down Trough is indirect: rather than observations of the cold water itself, it is based on distortions of the temperature salinity relation in the lower thermocline near 4.5°C, and their interpretation in the framework of end-member mixing. The existence of the overflow is inferred as a requirement to provide a saline influence to pull the relation from the mixing line between LSW and the main thermocline central water relation towards more saline values. It is a bit of a convoluted argument because the cold dense source water in the Faroe Bank Channel is actually fresher than the LSW in the Trough, but becomes more saline in the overflow process through entrainment of thermocline water. For example the aforementioned 1.57°C water near the sill is about 0.09×10^{-3} more saline than the source water. HARVEY and THEODOROU (1986) also use a three end-member mixing interpretation, but allow progressive variation of the end-members to reflect the changing environment following the flow, estimating that about 30% of the northern Trough Water mass is interpretable as this overflow water.

The focus of these treatments being on the lower thermocline rather than the cold water system ($\leq 4^\circ\text{C}$), the Wyville-Thomson Ridge Overflow will be ignored in the present study. ELLETT and MARTIN (1973) suggest that the higher salinity layer beneath the LSW, with temperatures near 3°C, also may reflect the overflow influence. In the present study that layer is interpreted as of mid-latitude origin rather than of northern origin, principally on the basis of its oxygen and silicate characteristics.